SIMULATION OF ESTUARY MIXING USING A TWO-DIMENSIONAL RANDOM WALK MODEL

by

KONSTANTINA DIMOU

Diploma in Civil Engineering
National Technical University of Athens, Greece
(1987)

SUBMITTED IN PARTIAL FULFILLMENT
OF THE REQUIREMENTS FOR
THE DEGREE OF

MASTER OF SCIENCE IN CIVIL ENGINEERING

at the

MASSACHUSETTS INSTITUTE OF TECHNOLOGY

September 1989

Signature of Author _____

Department of Civil Engineering
July 11, 1989

Certified by _____

E. Eric Adams
Principal Research Engineer, Civil Engineering
Thesis Supervisor

Accepted by ____ _____

Ole S. Madsen
Chairman, Department Graduate Committee
Department of Civil Engineering

SIMULATION OF ESTUARY MIXING USING A TWO-DIMENSIONAL RANDOM WALK MODEL

by

KONSTANTINA DIMOU

Submitted to the Department of Civil Engineering
on July 11 in partial fulfillment
of the requirements for the degree of
Master of Science in Civil Engineering

Abstract

The purpose of this study is the development and analysis of a two-dimensional particle tracking or random walk model for the simulation of transport in well-mixed estuaries. A "random walk model" is a model in which transported mass is represented by discrete particles which are advected and dispersed at each timestep. The mixing length approach was used according to which mass transport in estuaries can be modeled using a locally one-dimensional model where all mixing mechanisms are combined into a single longitudinal dispersion coefficient. The main assumption in this theory is that complete mixing is achieved on one tidal cycle over a fraction of the maximum tidal excursion. The model was tested by comparing simulated concentrations and residence times with corresponding analytical solutions for the one-dimensional case. Excellent agreement was obtained. The following questions were addressed: 1) the number of particles necessary to represent the dispersion, 2) the length of the timestep in order to obtain acceptable accuracy, and 3) a comparison with a concentration model. The model was applied in order to predict the entrainment effects resulting from the operation of a coastal nuclear power plant station at Millstone Point, Connecticut. Winter flounder larvae represented by particles were the species utilized in the model to simulate the effects of entrainment. In order to explain the inconsistencies between the actual larvae length distribution of entrained larvae and the one predicted by the model two dye studies were conducted and salinity data were collected.

Thesis supervisor: E. Eric Adams
Title: Principal Research Engineer

ACKNOWLEDGMENTS

Support for this research was provided by Northeast Utilities Environmental Laboratory.

I wish to thank my advisor, Dr. Eric Adams, for his support and guidance. His patience and insight throughout my work has been irreplaceable. I am grateful for his kindness, the enthusiasm he displayed toward my results, and the long hours he spent reading my thesis.

I wish to thank Read Schusky who efficiently typed this work without complaining about my handwriting.

I wish to thank all students of the Environmental Engineering group for listening to my presentations during the group seminars (pizza meetings). I wish to thank Mr. and Mrs. Harleman for their kindness and hospitality.

Finally I wish to thank my parents, Xenophon and Athanassia, and my sister Christina for their love, support, and encouragement.

Contents

List of Figures

List of Tables

1 INTRODUCTION

1.1 Purpose and Scope

The purpose of this study is the development and analysis of a two dimensional particle tracking or "random walk" transport model. The scope of this study is the application of this model for the simulation of transport in well-mixed estuaries. The motivation of this study was a project for the prediction of entrainment rates of winter flounder larvae through the cooling station of the Millstone Nuclear Power Station (MNPS). Larvae are born in the Niantic River (Figure 1) and their behavior depends on age, tidal phase and time of day. According to this the entrainment rates of the larvae at the power plant are dependent on their residence time in the estuary.

A "random walk" model is a model in which mass is transported as discrete particles. At each timestep the displacement of each particle consists of an advective, deterministic component and an independent, random Markovian component. A "random walk" model can be used as an alternative for modeling mass transport to concentration models, where the dependent variable of concentration is advected and diffused.

The reasons for using a particle tracking/random walk model instead of a concentration/diffusivity model for simulating mixing in estuaries are the following:

1) The dispersion coefficient in estuaries is not a constant, but varies as a function of the tidal velocity. This variation in dispersivity is more easily modeled by a random walk process.

2) Random walk models appear to be a natural choice, where transport processes are best described by attributes of the individual particles rather than their aggregation (i.e., concentration). As mentioned above this was the case in the MNPS Case Study,

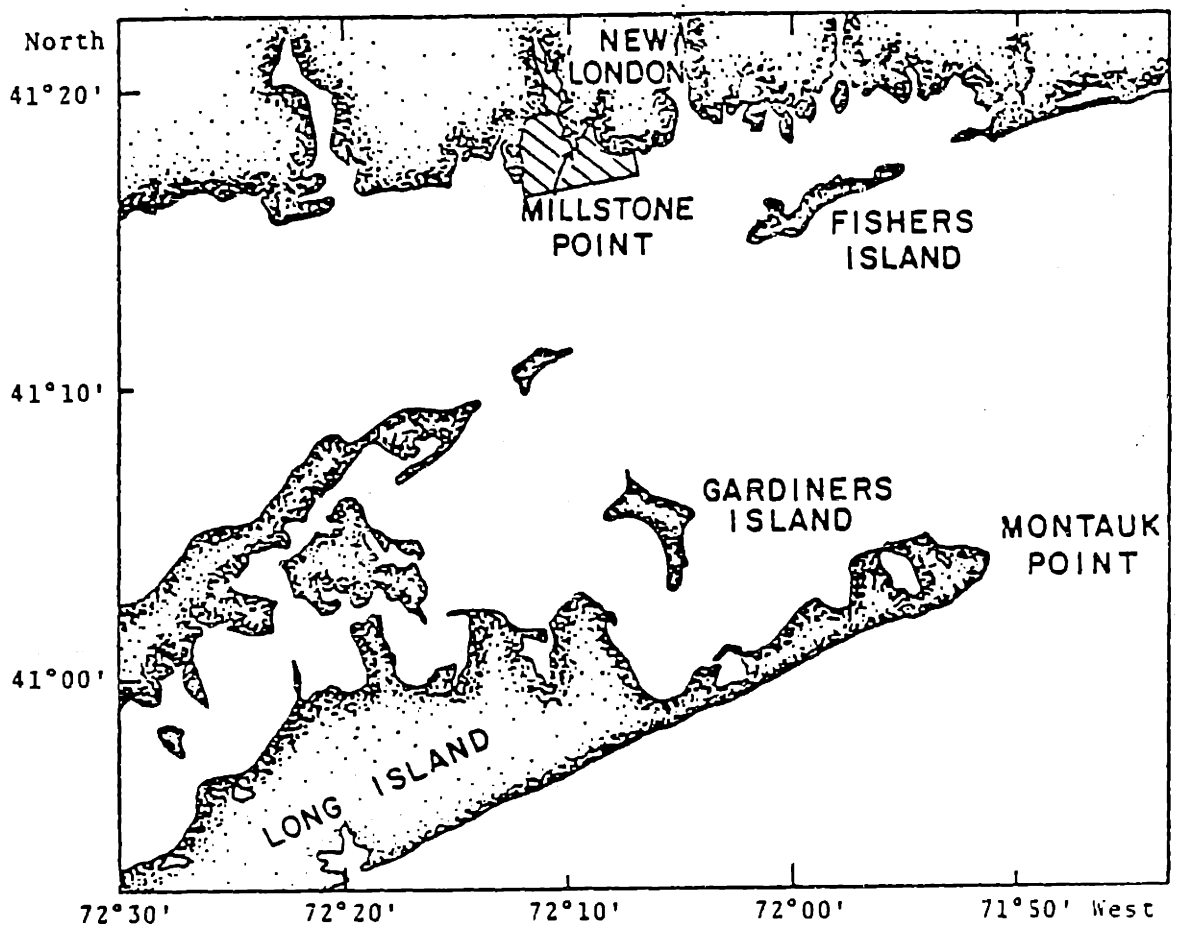

Figure 1 Location of Millstone Nuclear Power Station (from Saila, 1976, Figure 1)

where particles represented winter flounder larvae that show distinct behavioral patterns.

3) The source representation is simple in a random walk model (i.e., introduction of particles) whereas in concentration models the representation of point sources creates difficulties since a model is unable to resolve concentration fields, whose spatial extent is small compared to the spatial scale of discretization.

4) In random walk models the computational effort is concentrated in regions where most particles are located, i.e., regions with highest concentrations, whereas in concentration models all regions of the domain are treated equally in terms of computational effort.

1.2 Organization of Study

In Chapter 2 different models for simulating mixing in estuaries are presented. In particular the mixing length theory is analyzed and models based on this theory are described.

Chapter 3 includes a discussion about the distinctions between concentration and random walk models, the development of a random walk model and a thorough analysis of the two dimensional random walk model used in this study and its relation to the equivalent two dimensional depth averaged transport equation.

Chapter 4 includes the verification of the two dimensional random walk model developed in Chapter 3. A one dimensional test case simulating mass transport on an estuary of uniform cross section is used. The results of the random walk simulations are compared to the results of the analytical solution of the equivalent concentration model. The sensitivity of the random walk model on the size of the timestep, the

number of the particles and the size of the volume V_s over which concentration of particles is measured is analyzed.

Chapter 5 includes the analysis and the results of the application of the two dimensional random walk model MILL in the MNPS Case Study. The purpose of this study was the prediction of the entrainment effects from the operation of MNPS located in Niantic Bay on winter flounder larvae spawned in Niantic River (Figure 1). Spatial variations in mixing within the river is simulated according to a mixing length theory (consistent with Ketchum's modified tidal prism model, 1951) and mixing in the bay is simulated in a manner consistent with a constant diffusion coefficient. The mixing model for the river is compared with the results of Ketchum's model and with observed larval concentrations in the river and the station intake. In order to understand inconsistencies between model predictions for entrainment rates and actual field data the results of two dye studies and salinity data are analyzed and conclusions are drawn.

Chapter 6 includes a summary of the study and conclusions.

2 ESTUARIES

2.1 Definition and Classification

According to Pritchard (1967) and Cameron and Pritchard (1965) an estuary is defined as a semi-enclosed body of water having a free connection with the open sea and within which sea water is measurably diluted with fresh water derived from land drainage. This definition is very restrictive and does not include water bodies as Niantic River, where the fresh water inflow is negligible. So we will make the definition of an estuary broader as to include all water bodies where the flow is primarily driven by the slope of the tidal wave.

Various attempts have been made to classify estuaries by type. The classification of Hansen and Rattray (1966) will be mentioned here because it is based on simple observable quantities and describes a continuum. They classified estuaries in terms of two dimensionless parameters: the stratification parameter $\delta S/S_0$ and the circulation parameter U_s/U_f where

δS is the difference in salinity between surface and bottom
S_0 is the sectional mean salinity
U_s is the longitudinal time-mean velocity at the surface $z = 0$
U_f is the integral mean velocity (river discharge rate divided by the cross-sectional area of the estuary)

According to this classification seven types of estuaries are identified (Figure 2). In Type 1 the net flow is seaward at all depths and the upstream salt transfer is primarily due to diffusion. For Type 2 the net flow reverses at depth and both advection and diffusion contribute importantly to the upstream salt flux. The distinction between category a and b in the first two types is that between a well-mixed and a stratified

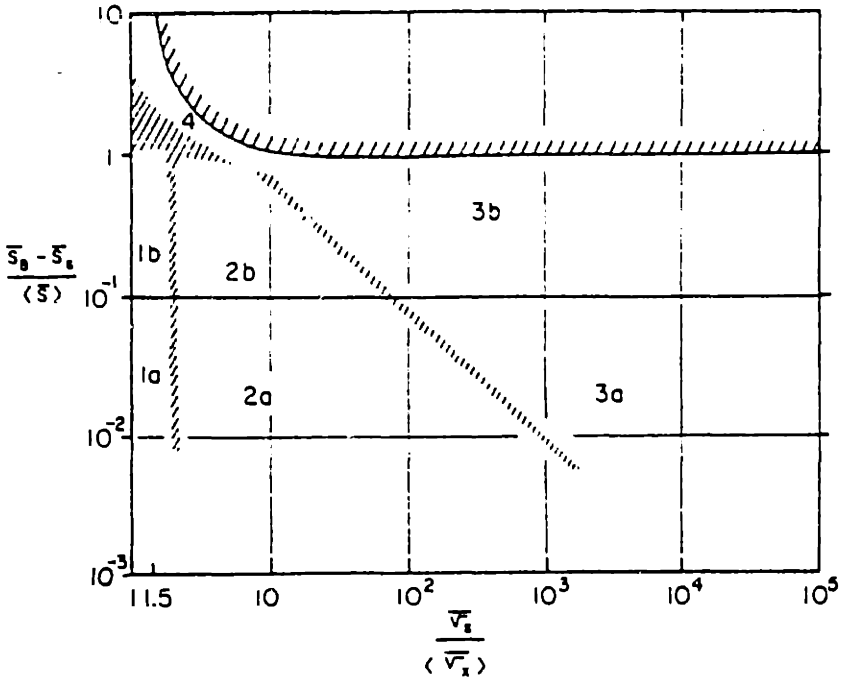

Figure 2 Classification of estuaries (from Hansen and Rattray, 1966)

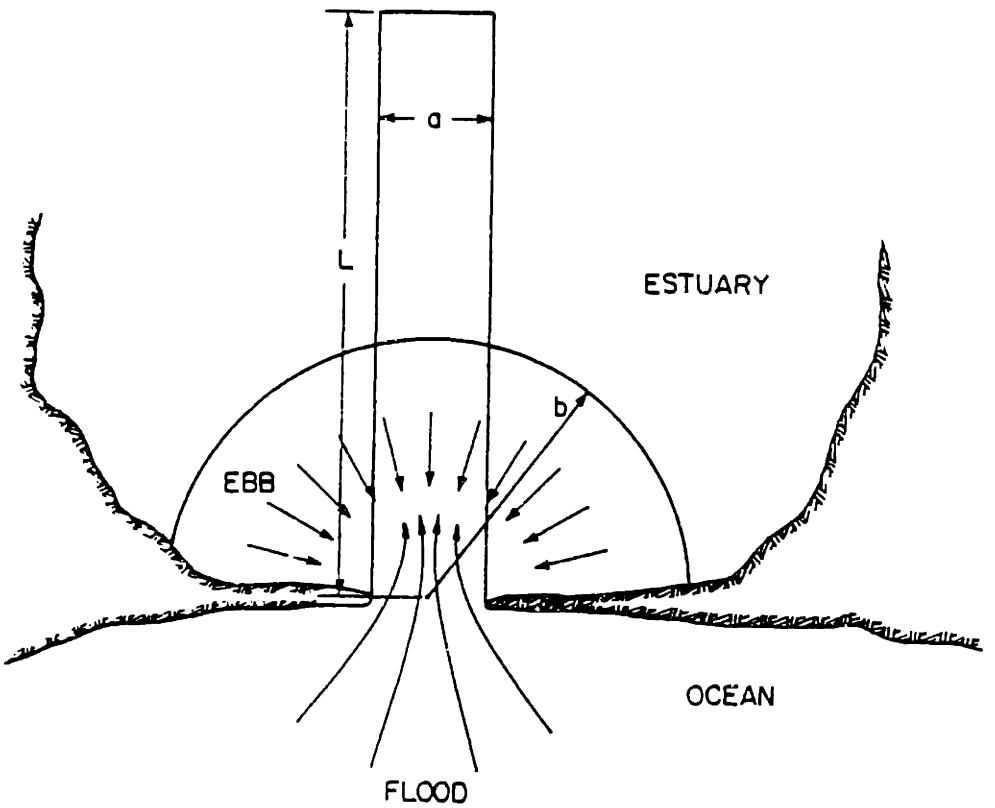

Figure 3 "Pumping" (from Stommel and Farmer, 1956)

condition. In Type 3 the upstream salt transfer is due to advection. In Type 3b estuaries, the lower layer is so deep that in effect the salinity gradient and the circulation do not extend to the bottom, an important qualitative difference from other types of estuaries. In Type 4 estuaries (salt-wedge) the stratification is still greater and the flow grades from a thick upper layer flowing over and little influenced by a thin lower layer, to a shallow surface layer flowing with little influence over a deep lower layer. In Niantic River the fresh water inflow is negligible and the stratification parameter $\delta S/S_0$ according to salinity data (Chapter 5) is less than 0.1. According to this Niantic River belongs to Type 1a, i.e., it is a vertically well mixed estuary.

2.2 Causes of Mixing in Estuaries

Mixing in estuaries is related to the following: 1) the tide, 2) the wind, and 3) the river (Fisher et al., 1979). Each mixing mechanism is described below and the relative importance of each mechanism in the case of Niantic River Niantic Bay is estimated.

2.2.1 Mixing Caused by the Tide

Mixing generated by the tide is caused by the following two basic mechanisms: 1) Dispersion that is generated by the interaction of the tidal wave with the bathymetry creating non-uniform flow. The effects of dispersion include shear flow dispersion, "pumping" and "trapping." 2) Turbulent diffusion that is generated from the friction between the tide flow and the channel bottom.

The longitudinal dispersion coefficient due to shear effects is given by the expression (Fisher et al, 1979)

$$K = 0.1\overline{u'^2}T[(1/T')f(T')] \qquad (2.1)$$

where

$T' = T/T_c$

T is the tidal period

T_c is the cross sectional mixing time estimated by the expression $T_c = w^2/\epsilon_t$

w is the width of the estuary

ϵ_t is the tranverse mixing coefficient that can be estimated from the expression

$\epsilon_t = 0.6du^*$

d is the mean depth

u^* is the shear velocity $\sqrt{\tau_0/\rho}$ (u^* can be taken to be equal to $0.1\bar{u}$ (Fischer et al., 1979))

$u'(y) = \bar{u}^z(y) - \bar{u}$

$\bar{u}$ is the time averaged velocity that is calculated from the expression $\bar{u} = \frac{2}{T}\int_0^{T/2} u_0 \sin\omega t dt = \frac{2}{\pi}u_0$ or equivalently $\bar{u} = \frac{2\xi_0}{T/2}$ (see Equations (2.6)-(2.8) later in the text)

u_0 is the amplitude of the tidal velocity

$\bar{u}^z(y)$ is the depth averaged velocity

$\overline{u'^2}$ can be approximated by $0.2\bar{u}^2$

$f(T')$ is a function

The axis x and y are defined in Figure 4

According to the above we see that the dispersion coefficient K is proportional to the amplitude of the tidal velocity u_0 squared.

Niantic River is approximately 6.5 km long and 500 m wide on the average. The averaged depth is 2 m and the tidal range is approximately 0.8 m. Since the tidal range is 2/5 of the mean depth the tidal excursion at the mouth will be approximately 2/5 of the length or approximately 2.6 km. The mean tidal velocity is $\bar{u}$ = 2.6 km/6.2 h =

0.12m/sec. Using Equation (2.1) and the diagram of $\frac{1}{T'}f(T')$ versus T' from Fischer et al., 1979 ($\frac{1}{T'}f(T') = 0.1$), we end up with $K = 1.2\ m^2/sec$.

As tidal "pumping" we mean net, steady circulation (residual circulation) that results from the superposition on the back-and-forth tidal flow. A first cause of the residual circulation is the earth's rotation, which deflects currents to the right in the Northern hemisphere and to the left in the southern hemisphere. A second cause is the interaction of the tidal flow with the irregular bathymetry found in most estuaries.

One form of this circulation is shown in Figure 3. In flood the water comes as a jet while in the ebb the water comes from all around the mouth in the form of potential flow to a sink. This results in a residual circulation (an inward flow in the area of the jet and an outward flow elsewhere). In our case this circulation is expected to play an important role as a mixing mechanism because of the shape of Niantic River.

"Trapping" results from trapping of low-velocity water along the sides of an estuary. Okubo (1973) includes the effects of "trapping" in his expression of the effective longitudinal dispersion coefficient in an estuary where the main channel has a uniform velocity $u = u_0 \sin\omega t$ and the traps are uniformly distributed along the sides.

$$K = \frac{K'}{1+r} + \frac{r u_0^{\,2}}{2k(1+r)^2(1+r+w/k)} \qquad (2.2a)$$

where

K' is the longitudinal diffusivity in the main channel

r is the ratio of trap volume to channel volume

k^{-1} is a characteristic exchange time between traps and main flow

By rearranging Equation (2.2a) and neglecting the first term we end up with the following expression for K

$$K = \frac{ru_0^2}{2(1+r)^2(k+rk+\omega)} \tag{2.2b}$$

K becomes maximum for r = 1 k = 0

$$K_{max} = 890u_0^2 \tag{2.2c}$$

Equation (2.2c) indicates as Equation (2.1) that the dispersion coefficient due to trapping is proportional to the amplitude of the tidal velocity squared.

In the case of Niantic River the trap volume consists of Keeney Cove and Smith Cove (Figure 17) The ratio of trap volume to channel volume r is equal to 0.08. If we take a characteristic exchange time $k^{-1} = 10^4$sec (Fisher et al.) we get $K = 0.93K' + 140u_0^2$. By taking $u_0 = \frac{\omega a_0 x}{h}$ where a_0 is the amplitude of the tide elevation and setting x = 6500 km we get $K = 0.93K' + 4.7\ m^2/sec \approx 4.7\ m^2/sec$.

Turbulence generated by bottom shear stress causes vertical and transverse mixing. In the case of constant-density tidal flow the vertical mixing coefficient ϵ_v is given by the expression (Bowden, 1967)

$$\epsilon_v = 0.0025dU_a \tag{2.3}$$

where

d is the depth

U_a is the depth mean amplitude of the current

and the tranverse mixing coefficient as mentioned before is $\epsilon_t = 0.6du^* = 0.06d\bar{u}$.

By taking $U_a = u_0 = 0.19$ m/sec we get $\epsilon_v = 0.0009$ m^2/sec for Niantic River and $\epsilon_t = 0.0132$ m^2/sec. Comparing the values of K resulting from Equations (2.1) and (2.2) to ϵ_v and ϵ_v we see that ϵ_v, $\epsilon_t \ll K$ which means, as expected, that dispersion is a much more important mixing mechanism than turbulent diffusion.

2.2.2 Mixing Caused by the Wind

Wind may or may not play a significant role in estuary mixing depending on the shape of the estuary. In a long, narrow estuary the tide is the dominant mechanism and wind has little chance to generate currents. In a wide estuary or in an estuary consisting of a series of bays, wind stress can generate currents of considerable importance. According to this wind is more likely to be important in Niantic Bay and less likely to be important in Niantic River. In the case of a floating object wind exerts a drag on the water surface and moves the object in the wind direction. In the case of a substance that is well mixed in the vertical direction the important mechanisms are the currents induced by the wind that cause the mean motion of the water column.

2.2.3 Mixing Caused by the River

The river delivers a discharge of fresh water Q_f and thus becomes a source of buoyancy of magnitude $\Delta\rho g Q_f$ where $\Delta\rho$ is the difference in density between the river and the ocean water. In a nearly tideless sea the fresh water forms an upper layer and flows as a nearly undiluted layer into the sea. The salt water layer is underneath the fresh water layer and forms a wedge. In the case of a tidal sea, the tide moves the wedge back and forth and this motion is a source of kinetic energy available to break down the interface and turbulently mix the fresh and the saline layers. The ratio of the

input of buoyancy per unit width of channel delivered by the river to the mixing power available from the tide is given by the dimensionless "Estuarine Richardson Number" (Fisher, 1979)

$$Ri = (\Delta\rho/\rho)gQ_f/wU_t^3 \qquad (2.4)$$

where

U_t is the rms tidal velocity

w is the channel width

Several attempts have been made to analyze density-driven circulation theoretically as well as by laboratory studies. Since we are interested in vertically well mixed estuaries we will not go into detail and present these studies.

2.3 Mixing Length Theory

2.3.1 General

In Section 2.2 the various mechanisms that cause mixing have been described qualitatively. Various transport models have been used for modeling mass transport in estuaries. Since we are interested in modeling mass transport in well mixed estuaries (i.e., Niantic River) the estuary mixing models based on the mixing length theory, a method for modeling mass transport in well mixed estuaries, will be presented here. The reason is that this theory is very simple and yet efficient in representing the physics of mixing in well-mixed estuaries. However, it uses many simplified assumptions and so it should be seen only as an "attempt to model" mixing and not as a tool for "predicting" mass transport in any estuary.

According to the mixing length theory mass transport in estuaries can be modeled using a model, where all mixing mechanisms are combined into a single longitudinal dispersion coefficient D_x. The main assumption in this theory is that complete mixing is achieved in one tidal cycle over a certain length that is proportional to the local tidal excursion. The Coriolis forces are neglected. A steady state distribution of fresh and salt water within the estuary is assumed. This is true over long periods of time. However over short periods of time an increase in river flow will produce an increase in the fraction of freshwater throughout the estuary and the steady state distribution cannot be assumed. This theory was developed by Arons and Stommel (1951) and was based on Ketchum's idea, that the element of mixing volume is bounded by the length of the tidal excursion.

The theory of mixing length by Arons and Stommel will be presented in Section 2.3.2. The tidal prism method by Ketchum and modifications to this model will be presented in Section 2.3.3

2.3.2 Model of Arons and Stommel

We consider an estuary of uniform width (w) and of uniform depth (h) (Figure 4). If we make the assumption that the length of the estuary is small compared to the wavelength of the tidal co-oscillation, the tide is simultaneous and elevations are uniform over the entire estuary. The tidal amplitude η, the tidal velocity u_{xt} and the horizontal tidal displacement ξ are then given by the expressions:

$$\eta = a_0 \cos\omega t \tag{2.6}$$

$$u_{xt} = \frac{\omega a_0 x}{h} \sin\omega t = u_0 \sin\omega t \tag{2.7}$$

$$\xi = -\frac{a_0 x}{h} \cos\omega t \tag{2.8}$$

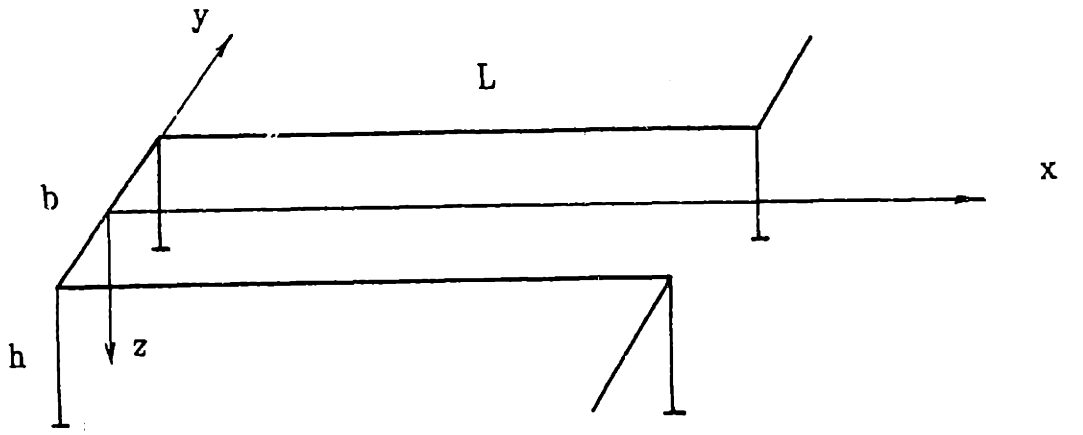

Figure 4 Uniform estuary

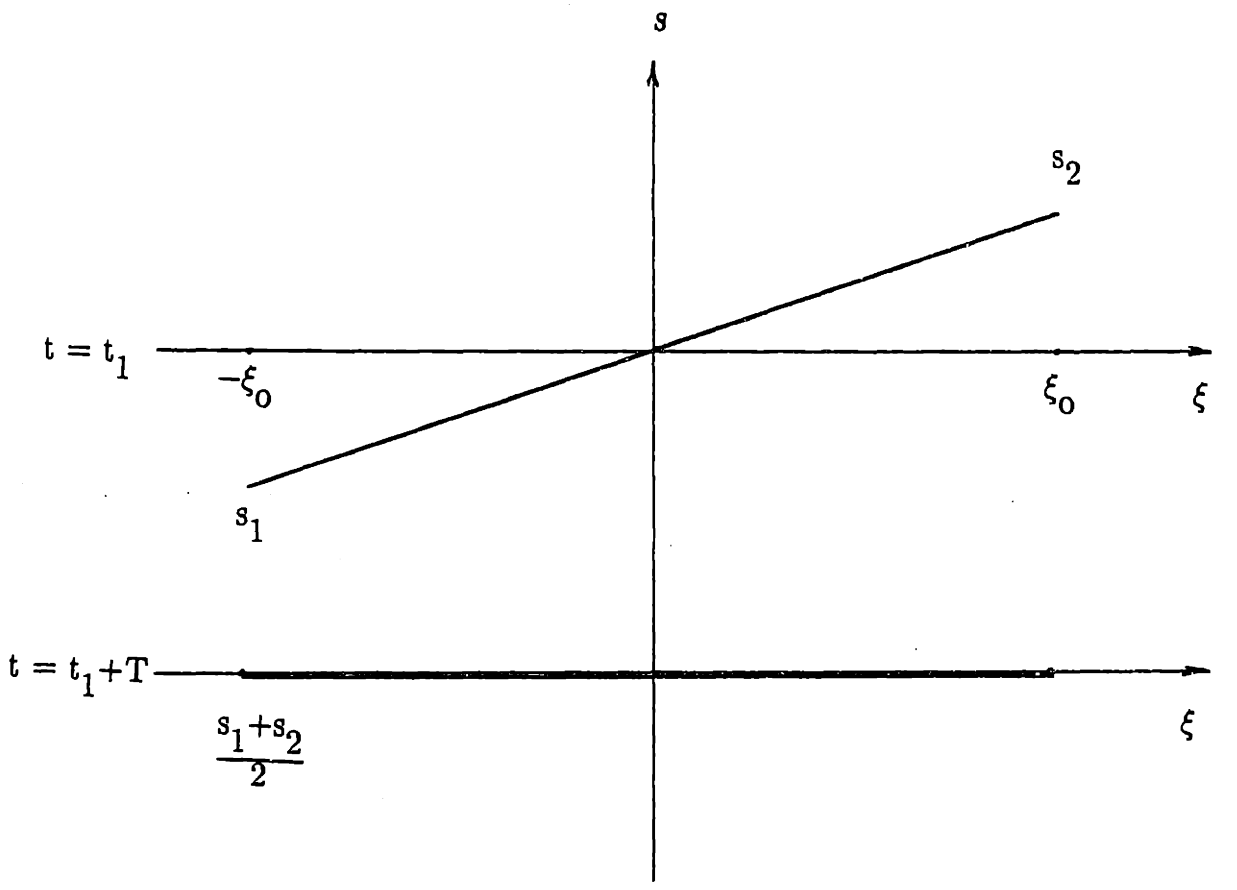

Figure 5 Model of Arons and Stommel

where

a_0 is the amplitude of the vertical tidal movement

u_0 is the amplitude of the tidal velocity $u_0 = \omega a_0 x/h$

The governing equation describing the mass balance for tidal average salinity for this one dimensional model is the following

$$\frac{\partial s}{\partial t} + u\frac{\partial s}{\partial x} = \frac{\partial}{\partial x}\left[D_x \frac{\partial s}{\partial x}\right] \tag{2.9}$$

where

s is the mean point salinity at any point x

u is the time mean velocity at x which we take equal to the river velocity

D_x is the longitudinal dispersion coefficient

In order to define D_x Officer (1976) made the assumption of complete mixing in one tidal cycle over the maximum tidal excursion $2\xi_0$ (Figure 5).

According to Figure 5 at the beginning of the tidal cycle the salinity distribution is given by the expression

$$s(x) = s_1 + \frac{s_2 - s_1}{2\xi_0} x \tag{2.10}$$

If the salinity distribution were uniform at the end of the cycle, the salt flux S during the cycle would be given by the integral

$$S = -\frac{2}{T}\int_0^{\xi} \frac{s_2 - s_1}{2\xi_0} x \, dx = -\frac{(s_2 - s_1)\xi_0}{2T} \tag{2.11}$$

The salt flux is also given by the expression

$$S = -D_x \frac{\partial s}{\partial x} = -D_x \frac{s_2 - s_1}{2\xi_0} \tag{2.12}$$

Equating Equations (2.11) and (2.12) we get the following expression for the longitudinal dispersion coefficient D_x

$$D_x = \frac{\xi_0^2}{T} = \frac{\omega a_0^2 x^2}{2\pi h^2} \tag{2.13}$$

If we make the assumption of complete mixing over a fraction B_1 of the maximum tidal excursion $2\xi_0$ (i.e., over $2B_1\xi_0$), Equation (2.13) becomes

$$D_x = \frac{B_1^2 \omega a_0^2 x^2}{2\pi h^2} = \frac{B_1^2 T}{4\pi^2} u_0^2 = \beta u_0^2 \tag{2.14}$$

where

$$\beta = \frac{B_1^2 T}{4\pi^2}$$

From Equation (2.13) we can see that D_x is proportional to distance squared and from Equation (2.14) we see it is proportional to the amplitude of the tidal velocity squared which agrees with the expressions for the dispersion coefficient K due to shear flow and to trapping in Section 2.2.1.

Equation (2.13) can be used in the case of "pumping" (Section 2.2.1) since the mixing length there is equal to the maximum tidal excursion. In the case of Niantic River the value of the dispersion coefficient due to "pumping" is equal to 150 m^2/sec. We can see that this value outweighs the values of the dispersion coefficient due to

shear effects (= 1.2 m^2/sec) and due to trapping (= 4.7 m^2/sec). From that we can conclude that "pumping" is the most important mixing mechanism in Niantic River.

We could also arrive at Equation (2.13) using dimensional analysis (Arons and Stammel, 1951). According to this approach the dispersion coefficient D_x can be expressed as the product of a characteristic velocity, which is taken to be equal to the amplitude of the tidal velocity, and a characteristic length, which is taken to be equal to the total excursion of a particle $2\xi_0$. Hence

$$D_x = 2B_2\xi_0 u_0 = 2B_2\frac{a_0 x}{h}\frac{\omega a_0 x}{h} = \frac{2B_2 a_0^2 \omega}{h^2}x^2 \qquad (2.15)$$

According to Equation (2.14) the factor of proportionality B_2 is equal to $B_1^2/4\pi$.

The steady state form of Equation (2.9), applicable to tidal average concentration with steady river input and tidal conditions, is:

$$u\frac{ds}{dx} = \frac{d}{dx}\left[D_x\frac{ds}{dx}\right] \qquad (2.16)$$

The boundary conditions for Equation (2.16) are:

at $x = 0$ $s = 0$

at $x = L$ $s = \sigma$

where

σ is the ocean salinity

Equation (2.16) has the following solution

$$s/\sigma = e^{F(1-1/\lambda)} \tag{2.17}$$

where

$\lambda = \frac{x}{L}$

$F = \frac{uh^2}{2B_2 a_0^2 \omega L}$ is called the flushing number

The family of curves on the relation of λ to s/σ is shown in Figure 6 for various values of the flushing number F (Arons and Stommel, 1951). From this Figure we see that the curves are most sensitive to F in the region $0.1 < F < 10$

Arons and Stommel calculated the values of the constant B_2 for the Raritan River, New Jersey, and the Alberni Inlet, Vancouver. There was an order of magnitude difference in the results that according to them might be due partly to the rather unnatural assumptions of the analysis (uniform geometry) and to the form of the longitudinal dispersion coefficient. On the other hand the shape of the theoretical curves appeared to be in good agreement with the observations at hand. This leads to the conclusion that the flushing number may be a convenient concept to characterize estuaries but, without calibration, it cannot be used to predict salinity distributions. However, the model of Arons and Stommel can be viewed as semi-empirical, where the constant B_2 in Equation (2.15) is the empirical coefficient. B_2 depends on the different mixing mechanisms that are caused by the tide (Section 2.2.1). Since their magnitude varies from site to site, B_2 should be established using field data. This suggests why, although the shape of the salinity distributions were well predicted by the model, the values of F could be an order of magnitude different.

From Equation (2.17) we can also estimate the flushing time of an estuary, which is defined as the time required to replace the existing fresh water in an estuary at a rate

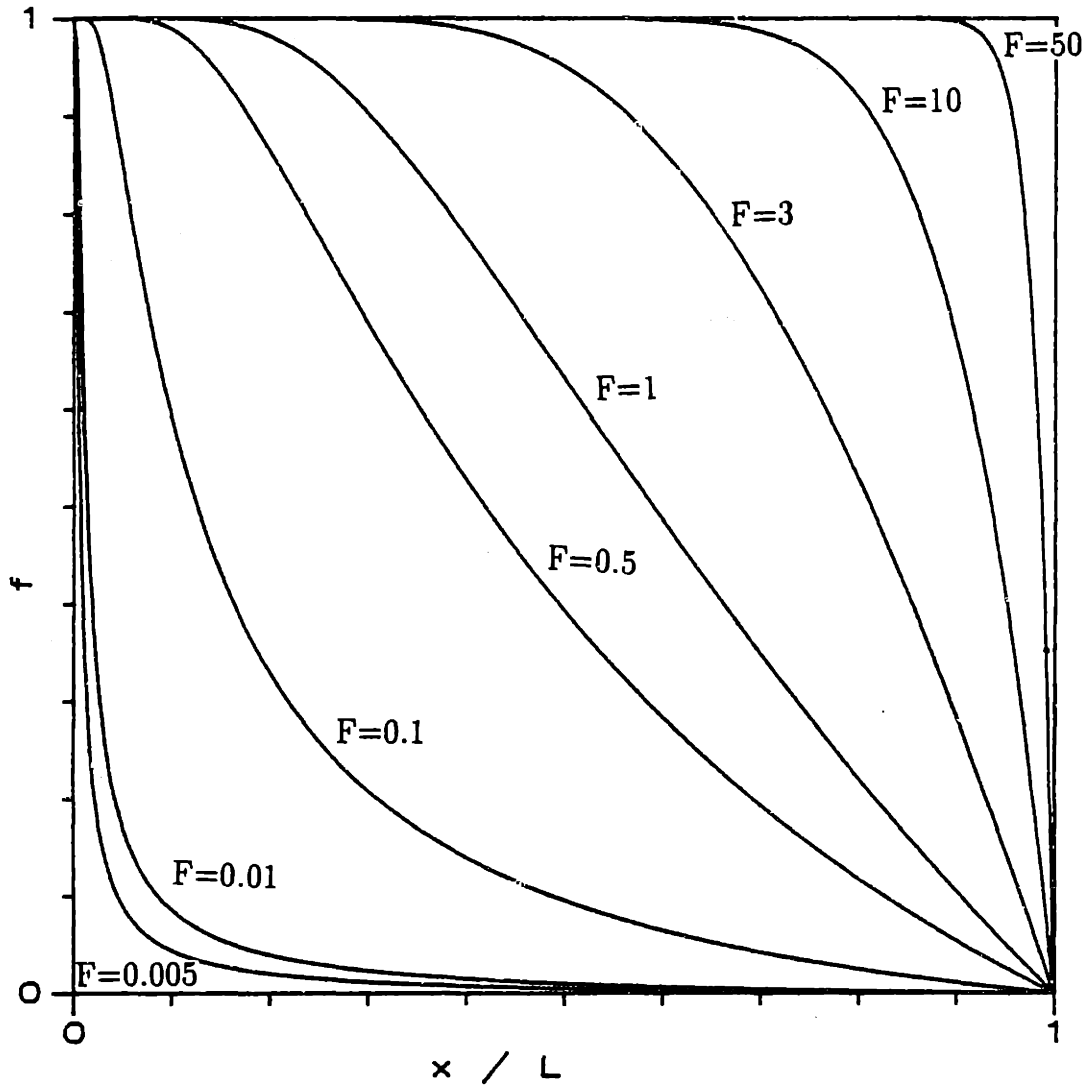

Figure 6 Family of curves showing relation of λ to s/σ

equal to the river discharge. According to this definition the flushing time t_{res} of an estuary is given by the expression:

$$t_{res} = \frac{V_f}{R} \tag{2.18}$$

where

V_f is the total freshwater volume of the estuary

R is the river runoff flow = u/A

A is the crossectional area of the estuary

The total freshwater volume V_f of an estuary is given by the integral over the volume of the estuary

$$V_f = \int f dV \tag{2.19}$$

where

f is the freshwater fraction $f = \frac{\sigma - s}{\sigma}$

According to Equation (2.17) the fresh water fraction along the estuary is given by:

$$f = 1 - e^{F(1-1/\lambda)} \tag{2.20}$$

According to Equations (2.18), (2.19), and (2.20) the flushing time is given by

$$t_{res} = \frac{A}{R} \int_0^L \left[1 - e^{F(1-1/\lambda)}\right] dx \tag{2.21}$$

Equation (2.20) can be used for estimating the distribution of a conservative pollutant in an estuary where the outfall of the pollutant is located at $x = 0$. At $x = 0$ the concentration of the pollutant is equal to c_0

$$c_0 = \frac{W}{R} \tag{2.22}$$

where

W is the rate of supply of the pollutant in mass of pollutant per unit time

At $x = L$ the concentration of the pollutant is taken to be equal to $c = 0$. At any location x ($0 < x < L$) the concentration of the pollutant will be given by the equation

$$c(x) = f(x)\frac{W}{R} \tag{2.23}$$

According to Equations (2.21), (2.22), and (2.23) we have

$$c(x) = c_0\left[1-e^{F(1-1/\lambda)}\right] \tag{2.24}$$

2.3.3 Ketchum's Model

Ketchum's model (1951) describes the exchanges between various parts of an estuary as a result of tidal oscillations. It calculates the average distribution of fresh and salt water within the estuary. It is a modification of the tidal prism method.

According to Ketchum the estuary is divided into volume segments. In every segment the tidal prism volume will be designated as P and is equal to the volume entering into the segment on a flood time. The low tide volume of every segment will be designated as V. The innermost volume segment, called segment 0, is defined as

that for which the entire intertidal volume P_0 is supplied by the river flow over a tidal cycle

$$P_0 = V_R \tag{2.25}$$

Consecutive volume segments are defined so that the distance between their inner and outer boundaries is equal to the average excursion of a particle of water on the flooding tide. The average excursion is found as follows. If the assumption is made that the entire volume of the seaward segment acts like a piston, displacing and pushing its volume of water to fill the high-tide volume of the landward segment, the distance moved would be the average excursion of a particle of water on the flood tide in that part of the estuary. According to this each segment is so defined that the high-tide volume in the landward segment is equal to the low-tide volume in the adjacent seaward segment. So we have

$$\begin{aligned} V_1 &= V_0 + P_0 \\ V_2 &= V_1 + P_1 = V_0 + P_0 + P_1 \\ &\vdots \\ V_n &= V_0 + \sum_{n=1}^{n-1} P_n = V_0 + V_R + \sum_{n=1}^{n-1} P_n \end{aligned} \tag{2.26}$$

The exchange ratio r_n for each segment n is defined as

$$r_n = \frac{P_n}{P_n + V_n} \tag{2.27}$$

The tidal flushing time t_n for segment n is given by

$$t_n = \frac{T}{r_n} \tag{2.28}$$

The accumulated fresh water in each volume segment V_{fn} is given by

$$V_{fn} = t_n \cdot R = \frac{T}{r_n}\frac{V_R}{T} = \frac{V_R}{r_n} \tag{2.29}$$

where R is the discharge rate of the river $R = \frac{V_R}{T}$. The freshwater fraction f_n of each segment, at high tide, is then equal to

$$f_n = \frac{V_{fn}}{P_n + V_n} = \frac{V_R}{r_n(P_n + V_n)} = \frac{V_R}{r_n V_{n+1}} = \frac{V_R}{P_n} \tag{2.30}$$

The salinity s_n of each segment is given by

$$s_n = \sigma(1 - f_n) = \sigma\left[1 - \frac{V_R}{P_n}\right] \tag{2.31}$$

where σ is the ocean salinity.

Ketchum (1955) extended these mixing concepts to estimate the distribution of both conservative and non-conservative pollutants in an estuary, where the outfall for the pollutant may be at any given location along the estuary.

At the location of the outfall, a conservative pollutant will become mixed and its average concentration c_0 after steady-state conditions are reached is given by

$$c_0 = \frac{W}{R} f_0 \tag{2.32}$$

where

W is the rate of supply of the pollutant

R is the rate of the river flow

f_0 is the average fraction of fresh water in the complete cross section of the estuary which passes through the outfall location

The down-estuary distribution of a conservative pollutant is given by

$$c_n = c_0 \frac{f_n}{f_0} = \frac{W}{R} f_n \tag{2.33}$$

The up-estuary distribution of a conservative pollutant is given by

$$c_n = c_0 \frac{s_n}{s_0} \tag{2.34}$$

In order to account for vertical stratification effects Dyer and Taylor (1973) used a modification of Ketchum's model. They consider the vertical stratification effects in terms of a parameter M which represents, physically, the fraction of the low tide volume that is "active." This parameter ($0 < M < 1$) is related to mixing processes in the estuary and approaches unity for a well mixed estuary.

So Equations (2.26) change to:

$$\begin{aligned} V_1 &= V_0 + P_0 \\ MV_2 &= P_1 + MV_1 \\ &\vdots \\ MV_n &= P_n + MV_n \end{aligned} \tag{2.35}$$

Thus the exchange ratio r_n for each segment n is

$$r_n = \frac{P_n}{P_n + MV_n} \tag{2.36}$$

Since M accounts for vertical stratification effects it should decrease as the vertical salinity differences increase. Wang et al. (1985) adopt a linear relationship between M and local stratification dS for the Bay. They propose the following expression for M

$$M = 1 - \frac{dS}{S_0} \tag{2.37}$$

where

S_0 is a constant

dS is a characteristic vertical salinity difference at some location of the Bay.

Procedures such as these predict that tidal flushing improves as the vertical stratification increases, which is consistent with observations. However, the additional mixing is simulated to take place entirely through increased mixing ($M < 1$) without the density-driven circulation known to occur in real estuaries.

2.3.4 Comparison between Arons and Stommel's Model and Ketchum's Model

In order to find the longitudinal dispersion coefficient that corresponds to Ketchum's model we make the following assumption. We consider an estuary with rectangular sides of uniform cross sectional area. The tidal prism volume P_i of section i is equal to

$$P_i = (2\xi_0)(2a_0)w \tag{2.38}$$

According to Equations (2.30), (2.33), and (2.38) the down-estuary concentration of the pollutant at section n is given by the expression

$$c_n = \frac{WT}{P_n} = \frac{WT}{(2\xi_0)\,(2a_0)w} = \frac{(W/A)h^2T}{4a_0^2}\frac{1}{x} \tag{2.39}$$

For steady state the diffusive flux $-D_x\frac{dc}{dx}$ is equal to the rate of supply of the pollutant

$$-D_x\frac{dc}{dx} = \frac{W}{A} \tag{2.40}$$

According to Equations (2.39) and (2.40) we have

$$D_x\frac{(W/A)h^2T}{4a_0^2}\frac{1}{x^2} = \frac{W}{A} \tag{2.42}$$

Solving Equation (2.42) for D_x we get

$$D_x = \frac{4a_0x^2}{Th^2} = \frac{T}{\pi^2}u_0^2 \tag{2.43}$$

Comparing Equation (2.43) with Equation (2.14) we see that in Ketchum's model $B_2 = 1/\pi$ which means that *in the case of a rectangular channel* Ketchum's model makes the assumption of complete mixing over twice the length of the maximum tidal excursion.

3 DEVELOPMENT OF RANDOM WALK MODEL

3.1 Diffusivity/Concentration Models

Diffusion is a microscopically observed phenomenon, attributed to the Brownian motion of microscopic particles. It accomplishes a net transport of a macroscopic property such as concentration, heat, or vorticity through a material continuum without a coherent displacement of that continuum (Ghoniem et al., 1985). From now on we will refer to concentration as the macroscopic property.

In order to simulate diffusion we make use of the diffusivity D, which is the factor of proportionality between the diffusive flux $\underline{F}$ and the concentration gradient $\underline{\nabla}c$.

$$\underline{F} = -\underline{\underline{D}}\underline{\nabla}\rho c \tag{3.1}$$

where $\underline{\underline{D}} = \begin{bmatrix} D & 0 & 0 \\ 0 & D & 0 \\ 0 & 0 & D \end{bmatrix}$

Equation (3.1) is known as Fick's Law. The diffusivity D is proportional to the product wl_m where l_m is the mean free path of the molecules and w is a representative velocity. Under certain conditions, Fick's law can also be used to describe mixing due to bulk fluid motion (Fischer et al., 1979). For example, three-dimensional mass flux due to turbulent diffusion and depth-averaged mass flux due to horizontal dispersion can be simulated using the same approach if $\underline{\underline{D}}$ in Equation (3.1) is replaced by the turbulent diffusion tensor $\underline{\underline{E}}$ and the dispersion tensor $\underline{\underline{K}}$ respectively where $\underline{\underline{E}} = \begin{bmatrix} E^{xx} & E^{xy} & E^{xz} \\ E^{yx} & E^{yy} & E^{yz} \\ E^{zx} & E^{zy} & E^{zz} \end{bmatrix}$ and $K = \begin{bmatrix} K^{xx} & K^{xy} \\ K^{yx} & K^{yy} \end{bmatrix}$. Recognizing the fundamental difference in the nature and magnitude of the various processes, we will from now on use the symbol D to represent molecular diffusion, turbulent diffusion, and dispersion coefficient, and we will simply refer to "diffusion" in order to describe all these mechanisms.

When diffusion is the only transport mechanism the conservation of mass is given by the following equation:

$$\frac{\partial c}{\partial t} = \underline{\nabla} \cdot \underline{\underline{D}} \cdot \underline{\nabla} c \tag{3.2}$$

Equation (3.2) is well known in mathematical physics and a large body of analytical and numerical methods exists for its solution. We will call models based on Equation (3.2) diffusivity/concentration models

When other transport mechanisms besides diffusion are involved, and domains are irregular, analytical methods have limited applications and standard numerical algorithms suffer from problems associated with the use of grids and the discretization of gradients. Good examples are convection dominated problems, where the convective displacements by far exceed displacements due to diffusion everywhere in the fluid except in regions close to the boundaries, where diffusion becomes the dominating mechanism. In these cases a fixed Eulerian grid runs into difficulties because: 1) it is hard to provide sufficient grid refinement, where it is needed because that increases the computational effort per timestep and the storage requirements and 2) the proper direction of discretization of the convective derivative may result in excessive numerical diffusion. In these cases the following alternatives are used:

- use of Lagrangian grid schemes, where the computational grid follows the motion of the flow
- use of Eurerian-Lagrangian schemes, where the mass transport equation is decoupled into a pure-advection component that is solved using a Lagrangian scheme and a pure-diffusion component that is solved using an Eulerian scheme

- use of adaptive-grid techniques, where the computational grid adapts itself to the evolving distribution of gradients

- use of particle tracking methods (random walk models), where the computational effort and the storage requirements are proportional to the number of particles

A second problem with concentration models arises when the diffusivity varies over spatial scales too small to be accurately resolved in a discretized numerical model. A usual procedure in these situations is to consider a number of homogeneous layers or zones and assign different values of diffusivity to each element or node in a traditional finite element or finite difference grid. Using this approach fine variations of the diffusivity within the elements or between the nodes are ignored. The alternative in this case is the use of a particle tracking model, which accounts for these small-scale variabilities without any grid resolution expense.

A third limitation of concentration models arises when we are more interested in the behavior of individual particles in a transport problem rather than their aggregation (concentration). In these cases particle tracking models are a better choice. This was the case in the MNPS Case Study where particles represented winter flounder larvae which show distinct behavioral patterns.

A fourth limitation of concentration models is the representation of point sources since a model is unable to resolve concentration fields whose spatial extent is small compared to the spatial scale of discretization. In order to resolve this problem some hybrid models have been developed (e.g., Pinder and Cooper, 1970; Konikow and Bredehoft, 1978; Neuman, 1981) where, near sources or zones of high spatial gradient, mass is represented by a large collection of particles, each of which is assigned a "value" of concentration. This procedure is somewhat awkward and suffers from mass

conservation problems that arise from the translation of particle concentrations to node concentrations and in the case of the models of Pinder and Cooper, 1970, and Konikow and Bredehoft, 1978, the use of particles to represent concentration rather than mass. Particle tracking models are the best choice in this case.

A fifth limitation of concentration models is the fact that all regions of the domain are treated equally in terms of computational effort. In particle tracking models the computational effort is concentrated in regions where most particles are located.

3.2 Particle Tracking/Random Walk Models

3.2.1 General

From now on the terms random walk model and particle tracking model will be used interchangeably. In random walk models mass is represented by a large amount of particles. Each particle represents a constant mass (total mass released divided by the total number of particles). These particles are moving in the domain according to the following general rule: The displacement Δx of each particle in a time-step Δt is decomposed into two components: the deterministic advection component and the probabilistic diffusion component (random displacement). The random component has an associated probability density function. The positions of the particles are found at every timestep. The concentration at a certain point x at a time t is found by dividing the number of particles in the interval V_s around point x by the volume V_s. In the case of a two dimensional model the volume V_s is replaced by an area A_s and in the case of a one dimensional model by a length l_s.

An interesting aspect of random walk models has to be mentioned at this point. Instead of using particles representing the property whose distribution we are interested in, we can use particles representing the gradient of this property, and afterwards

perform the integration. These models are called Gradient Random Walk Models. Such a model has been used by Chorin (1973) for the solution of the incompressible Navier-Stokes equation. In this model particles are used to transport elements of vorticity—a derivative of the velocity—and an integration process is performed to evaluate the latter. The advantage of this method is that the process of integration diminishes most of the statistical error introduced in the random displacements.

3.2.2 Applications of Random Walk Models in Environmental Engineering

A short and by no means complete review of random walk models in Environmental Engineering is given below.

Subsurface Waters. Random walk models have been extensively used in modeling one-, two-, and three-dimensional solute transport in groundwater (e.g., Ahlstrom et al., 1977; Prickett et al., 1981, Ackerer and Kinzelbach, 1985; Uffink, 1987; Tompson et al., 1988). The motivation for using random walk models instead of diffusivity models can be summarized in the following reasons.

- Avoidance of amplitude and phase errors
- In groundwater problems we encounter small scale variabilities. Using a random walk model this variability can be modeled without grid resolution expense.

Surface Waters. In surface water the following applications of random walk models can be mentioned. Bugliarcello and Jackson (1964) used a random walk model to simulate neutrally buoyant solute in a laminar shear flow. Sullivan (1977) simulated the same problem in a turbulent shear flow. The random displacement is allowed in vertical direction only and is related to the turbulent length scale. The results of the model are in agreement with open channel experiments.

Jeng et al. (1987) applied a two-dimensional depth averaged random walk model in a natural river with variable curvature, depth, and velocity, and constant mixing coefficients. The motivation for using a random walk model versus a diffusivity model was to avoid amplitude and phase errors produced by fixed grid numerical methods in the case of advection dominated problems. The initial conditions considered in this work are restricted to a slug-type release of inert, neutrally buoyant pollutant into a steady natural river. A three-point probability density function is used for the random walk component. Concentration distributions at different locations as a function of time are compared with experimental data from dye studies in a straight channel, a straight natural river and a meandering laboratory channel.

3.3 Random Walk Model

3.3.1 Development of Random Walk Model

The procedure for proving the equivalence between a random walk model and a diffusivity model is shown below. For simplicity the one-dimensional analysis is presented. Using the exact same procedure we could show the analogy for the three-dimensional case. At the end of this section only the results for the three-dimensional case are presented. For a more thorough analysis the reader is referred to Gardiner (1985).

Let's consider a system that is described by a state variable x(t), where x(t) represents the position of a particle in a one dimensional space. The position of the particle x(t) is modeled by the nonlinear Langevin equation

$$\frac{dx}{dt} = a(x,t) + b(x,t)\xi(t) \tag{3.3}$$

where

$a(x,t)$ is a known function representing the deterministic forces that act to change $x(t)$

$b(x,t)$ is a known function that characterizes the random forces

$\xi(t)$ is a random number that represents the rapidly changing forces, that act to change $x(t)$. $\xi(t)$ must satisfy the following conditions:

$$<\xi(t)> = 0 \tag{3.4}$$

$$<\xi(t)\ \xi(t')> = \delta(t-t') \tag{3.5}$$

which means that for $t \neq t'$ $\xi(t)$ and $\xi(t')$ are statistically independent.

Integrating Equation (3.3) we get the following equation

$$x(t) - x(0) = \int_0^t a(x(s),s)ds + \int_0^t b(x(s),s)\xi(s)ds \tag{3.6}$$

The quantity

$$W(t) \equiv \int_0^t \xi(s)ds \tag{3.7}$$

is known as a Wiener process.

According to Equation (3.7) we have

$$dW(t) = W(t+dt) - W(t) = \xi(t)dt \tag{3.8}$$

and Equation (3.6) can be written in the following form:

$$x(t+dt) - x(t) = a(x(t),t)dt + \int_t^{t+dt} b(x(s),s)\xi(s)ds \tag{3.9}$$

In order to derive Equation (3.9) we made the assumption that a(x,t) is a smooth function so its integral can be estimated as adt. In order to estimate the integral in Equation (3.9) we use the so called Ito assumption:

$$\int_t^{t+dt} b(x(s),s)\xi(s)ds = b(x(t),t)\int_t^{t+dt} \xi(s)ds = b(x(t),t)dW(t) \tag{3.10}$$

According to the Ito assumption Equation (3.9) becomes:

$$dx = x(t+dt)-x(t) = a(x(t),t)dt + b(x(t),t)dW(t) \tag{3.11}$$

Equation (3.11) shows that the displacement of a particle consists of a deterministic component a(x(t),t)dt and a random component b(x(t),t)dW(t). The random Wiener process can be shown to have the following properties (Gardiner, 1985)

$<dW> = 0$:mean zero

$<dWdW> = dt$:mean square proportional to dt

The second property shows that dW(t) is approximately $O(dt^{1/2})$

Let's consider now an arbitrary function f(x), that does not explicitly depend on t. Expanding df(x) to second order in dW(t) and discarding higher order terms $O(dtdW,dt^2)$ we get the following expression:

$$
\begin{aligned}
df[x(t)] &= f[x(t)+dx(t)]-f[x(t)] \\
&= f'[x(t)]dx(t)+\tfrac{1}{2}f''[x(t)]dx(t)^2+ \ldots \\
&= f'[x(t)]\{a[x(t),t]dt+b[x(t),t]dW(t)\} \\
&\quad +\tfrac{1}{2}f''[x(t)]b[x(t),t]^2[dW(t)]^2 + \ldots
\end{aligned} \tag{3.12}
$$

Using $<dWdW> = dt$ Equation (3.12) becomes

$$
\begin{aligned}
df[x(t)] &= \{a[x(t),t]f'[x(t)]+\tfrac{1}{2}b[x(t),t]^2f''[x(t)]\}dt \\
&\quad +b[x(t),t]f'[x(t)]dW(t)
\end{aligned} \tag{3.13}
$$

Equation (3.13) is known as Ito's formula. Let's consider now the time development of $f[x(t)]$

$$
\begin{aligned}
\frac{<df[x(t)]>}{dt} &= \frac{0}{1}\frac{df[x(t)]}{dt}\frac{1}{0} = \frac{d}{dt}<f[x(t)]> \\
&= \frac{0}{1}a[x(t),t]\frac{\partial f}{\partial x} + \tfrac{1}{2}b[x(t),t]^2\,\frac{\partial^2 f}{\partial x^2}\frac{1}{0}
\end{aligned} \tag{3.14}
$$

If $p(x,t\,|\,x_0,t_0)$ is the conditional probability density for $x(t)$ we have:

$$
\begin{aligned}
\frac{d}{dt}<f[x(t)]> &= \int dx f(x)\,\frac{\partial p(x,t\,|\,x_0,t_0)}{\partial t} \\
&= \int dx\left[a(x,t)\frac{\partial f}{\partial x} + \tfrac{1}{2}b^2(x,t)\frac{\partial^2 f}{\partial x^2}\right]p(x,t\,|\,x_0,t_0)
\end{aligned} \tag{3.15}
$$

Integrating Equation (3.15) by parts and discarding surface terms we obtain:

$$
\int dx f(x)\frac{\partial p}{\partial t} = \int dx f(x)\left\{\frac{-\partial[a(x,t)p]}{\partial x} + \frac{1}{2}\,\frac{\partial^2[b^2(x,t)p]}{\partial x^2}\right\}
$$

or

$$
\int dx f(x)\left\{\frac{\partial p}{\partial t}+\frac{\partial[a(x,t)p]}{\partial x} - \frac{1}{2}\,\frac{\partial^2[b^2(x,t)p]}{\partial x^2}\right\} = 0 \tag{3.16}
$$

Since f(x) is arbitrary we get:

$$\frac{\partial p}{\partial t} = - \frac{\partial [a(x,t)p]}{\partial x} + \frac{1}{2} \frac{\partial^2 [b(x,t)^2 p]}{\partial x^2} \tag{3.17}$$

Equation (3.17) is known as the Fokker-Planck equation. The above analysis shows that the stochastic process described by a conditional probability satisfying the Fokker-Planck equation is equivalent to the Ito stochastic differential Equation (3.11). In other words the distribution of particles that move according to an equation such as Equation (3.11) satisfies a diffusive type conservation law (3.17) similar in form to the conservative form of the mass transport equation:

$$\frac{\partial c}{\partial t} = - \frac{\partial (uc)}{\partial x} + \frac{\partial}{\partial x} \left[D \frac{\partial c}{\partial x} \right] \tag{3.18}$$

A thorough analysis for the analogy between the Fokker-Planck equation and the three dimensional form of Equation (3.18) is given by Tompson et al. (1988). A summary of this analysis for the one dimensional case is presented below

In a discrete sense Equation (3.11) can be written as:

$$\Delta x_n = x_n - x_{n-1} = a(x_{n-1},t_{n-1})\Delta t + b(x_{n-1},t_{n-1})\Delta W(t_n) \tag{3.19}$$

Let us identify the position $x(t_n) = x_n$ of a particle at time $t_n = T$, that at time t_0 is located at x_0 and that moves according to Equation (3.19), i.e., its displacement at every timestep consists of a deterministic component $a(x_{n-1},t_{n-1})\Delta t$ and an independent, random Markovian component $b(x_{n-1},t_{n-1})\Delta W(t_n)$. If we repeat this experiment with the same initial condition N times the spatial density of these N particles at time $t = T$ will be a function $p(x,t)$ which satisfies Equation (3.17) according to a zero boundary

condition $f(\infty,t) = 0$ on the infinite domain and a "point source" initial condition $p(x,t_0) = N\delta(x-x_0)$. The equivalence of the particle spread and the "ideal" nature of the function $p(x,t)$ will be exact only in the limit as $N \to \infty$ and $\Delta t \to 0$. The same analysis can be applied when instead of repeating the same experiment N times we take N particles at the same initial location x_0 at t_0 and move each of them according to Equation (3.19) up to the same time $t = T$. Again the equivalence between the "ideal" nature of the function $p(x,t)$ in Equation (3.17) and the particle spatial distribution function will be exact in the limit as $N \to \infty$ and $\Delta t \to 0$.

The expected number of particles N_e located in a (infinitesimal) length l_s centered at x at time t is approximately

$$N_e \approx N\, p(x,t)\, l_s \tag{3.20}$$

If these particles represent a fixed amount of total solute mass M in the domain then each particle represents a mass $m = \frac{M}{N}$ and the expected mass M_e in l_s is equal to:

$$M_e = mN_e = MN_e/N \tag{3.21}$$

using the particle approach. Using the continuum approach the amount of mass M_t in the infinitesimal length l_s is

$$M_t = \rho c l_s \tag{3.22}$$

Setting $M_e = M_t$ we get

$$Mp(x,t) = \rho c \tag{3.23}$$

Substituting Equation (3.23) into the Fokker-Planck Equation (3.17) and assuming that the mass M and the density ρ are constant we get the following equation:

$$\frac{\partial c}{\partial t} = - \frac{\partial}{\partial x} \left[\left[a - \frac{1}{2} \frac{\partial b^2}{\partial x} \right] c \right] + \frac{\partial}{\partial x} \left[\frac{1}{2} b^2 \frac{\partial c}{\partial x} \right] \tag{3.24}$$

In order to have a complete analogy between Equation (3.19) and the mass transport equation (3.18) we have to choose the terms a(x,t), b(x,t) and $\Delta W(t)$

By comaring Equations (3.18) and (3.24) we get the following expressions for a(x,t) and b(x,t)

$$a = u + \frac{\partial D}{\partial x} \tag{3.25}$$

$$b = \sqrt{2D} \tag{3.26}$$

According to the properties of the Wiener process $\Delta W(t)$ the normalized random displacement $\Delta W(t_n)$ in Equation (3.19) is given by the expression:

$$\Delta W(t_n) = Z_n \sqrt{\Delta t} \tag{3.27}$$

where

Z_n is a random number with the following properties (Tompson et al., 1988)

$\langle Z \rangle = 0$

$\langle Z\ Z \rangle = 1$

Figures 7 and 8 show the equivalence between the Ito differential equation, the Fokker-Planck equation, and the mass transport equation for the one-dimensional and the three-dimensional case respectively.

One-dimensional Case

Ito Stochastic Differential Equation

$$dx = a(x(t),t)dt + b(x(t),t)dW(t)$$

$$\Updownarrow \begin{matrix} N \to \infty \\ \Delta t \to 0 \end{matrix}$$

Fokker-Planck Equation

$$\frac{\partial f(x,t)}{\partial t} = -\frac{\partial}{\partial x}[a(x,t)f(x,t)] + \frac{1}{2}\frac{\partial^2}{\partial x^2}[b(x,t)f(x,t)]$$

$$\Updownarrow \begin{matrix} u = a - \frac{1}{2}\frac{\partial b^2}{\partial x} \\ D = \frac{1}{2}b^2 \end{matrix}$$

Transport Equation

$$\frac{\partial c}{\partial t} = -\frac{\partial}{\partial x}(u \cdot c) + \frac{\partial}{\partial x}\left[D\frac{\partial c}{\partial x}\right]$$

Figure 7 Equivalence between the Ito Differenetial Equation, the Fokker-Planck Equation, and the Transport Equation for the one-dimensional case

Three-dimensional Case

Ito Stochastic Differential Equation

$$d\underline{x} = \underline{A}(\underline{x}(t),t)dt + \underline{\underline{B}}(\underline{x}(t),t)d\underline{W}(t)$$

$$\Updownarrow \begin{matrix} N \to \infty \\ \Delta t \to 0 \end{matrix}$$

Fokker-Planck Equation

$$\frac{\partial f}{\partial t} + \frac{\partial}{\partial x}(A_i f) - \frac{\partial^2}{\partial x_i x_j}(\tfrac{1}{2}B_{ik}B_{jk}f) = 0$$

$$\Updownarrow \begin{matrix} \underline{v} = \underline{A} - \nabla\cdot(\tfrac{1}{2}\underline{\underline{B}}\cdot\underline{\underline{B}}^T) \\ \underline{\underline{D}} = \tfrac{1}{2}\underline{\underline{B}}\cdot\underline{\underline{B}}^T \end{matrix}$$

Transport Equation

$$\frac{\partial c}{\partial t}(\rho c) + \nabla\cdot(\rho\underline{v}) - \nabla\cdot\underline{\underline{D}}\cdot\nabla(\rho c) = 0$$

Figure 8 Equivalence between the Ito Differenetial Equation, the Fokker-Planck Equation, and the Transport Equation for the three-dimensional case

3.3.2 Application in the Two-Dimensional Depth-Averaged Transport Equation

The conservative form of the two-dimensional depth-averaged mass transport equation is given by the following expression (Daily and Harleman, 1966)

$$\frac{\partial(ch)}{\partial t} + \frac{\partial(uch)}{\partial x} + \frac{\partial(vch)}{\partial y} = \frac{\partial}{\partial x}\left[hD_{xx}\frac{\partial c}{\partial x} + hD_{xy}\frac{\partial c}{\partial y}\right] + \frac{\partial}{\partial y}\left[hD_{yx}\frac{\partial c}{\partial x} + hD_{yy}\frac{\partial c}{\partial y}\right] + Q \qquad (3.28)$$

where

c(x,y,t) is the depth-averaged concentration

u(x,y,t) is the x-component of the depth-averaged velocity

v(x,y,t) is the y-component of the depth-averaged velocity

h(x,y) is the depth (mean sea level)

D_{xx}, D_{xy}, D_{yx}, D_{yy} are dispersion coefficients

Q represents sources, sinks and vertical boundary fluxes

For a coordinate system along the principal axes (i.e., $D_{xy} = D_{yx} = 0$) and assuming that there are no sources or sinks ($Q = 0$) Equation (3.28) takes the form:

$$\frac{\partial(ch)}{\partial t} + \frac{\partial(uch)}{\partial x} + \frac{\partial(vch)}{\partial y} = \frac{\partial}{\partial x}\left[hD_{xx}\frac{\partial c}{\partial x}\right] + \frac{\partial}{\partial y}\left[hD_{yy}\frac{\partial c}{\partial y}\right] \qquad (3.29a)$$

which can also be written (see Appendix A) as

$$\frac{\partial}{\partial t}(ch) + \frac{\partial}{\partial x}\left[\left[\frac{D_{xx}}{h}\frac{\partial h}{\partial x} + \frac{\partial}{\partial x}D_{xx} + u\right]ch\right] + \frac{\partial}{\partial y}\left[\left[\frac{D_{yy}}{h}\frac{\partial h}{\partial y} + \frac{\partial}{\partial y}D_{yy} + v\right]ch\right] = \frac{\partial^2}{\partial x^2}(D_{xx}ch) + \frac{\partial^2}{\partial y^2}(D_{yy}ch) \qquad (3.29b)$$

Following Section 3.3.1 the random walk analog to Equation (3.29) is:

$$dx = \left[\frac{D_{xx}}{h}\frac{\partial h}{\partial x} + \frac{\partial}{\partial x}D_{xx} + u\right]dt + \sqrt{2}\sqrt{D_{xx}}\sqrt{\Delta t}\,Z_n \tag{3.30}$$

$$dy = \left[\frac{D_{yy}}{h}\frac{\partial h}{\partial y} + \frac{\partial}{\partial y}D_{yy} + v\right]dt + \sqrt{2}\sqrt{D_{yy}}\sqrt{\Delta t}\,Z_n \tag{3.31}$$

Looking at Equation (3.30) (the same applies for Equation 3.31) we see that the deterministic or "advective" velocity of a particle in the x direction a_x is given by the relation

$$a_x = \left[\frac{D_{xx}}{h}\frac{\partial h}{\partial x} + \frac{\partial}{\partial x}D_{xx} + u\right] \tag{3.32}$$

which consists of three components:

- the component u that is due to the advective velocity u
- the component $\frac{\partial}{\partial x}D_{xx}$ that is due to the spatial variation of the diffusion coefficient D_{xx}
- the component $\frac{D_{xx}}{h}\frac{\partial h}{\partial x}$ that is due to the spatial variation of the water depth

The significance of the second two components can be analyzed using the general moment analysis. For simplicity we will neglect the advection terms and the y-component of the diffusion terms such that Equation (3.29) reduces to:

$$\frac{\partial(ch)}{\partial t} = \frac{\partial}{\partial x}\left[hD_{xx}\frac{\partial c}{\partial x}\right] \tag{3.33}$$

The spatial moments of the distribution of the depth integrated concentration ch, in a laterally unbounded domain, are defined as:

$$\text{zeroth moment} = M_0 = \int_{-\infty}^{\infty} c(x,t)\, h(x)\, dx \tag{3.34}$$

$$\text{first moment} = M_1 = \int_{-\infty}^{\infty} x\, c(x,t)\, h(x)\, dx \tag{3.35}$$

$$\text{second moment} = M_2 = \int_{-\infty}^{\infty} x^2\, c(x,t)\, h(x)\, dx \tag{3.36}$$

The mean μ and the variance σ^2 of a distribution are found from the moments by the equations:

$$\mu = \frac{M_1}{M_0} \tag{3.37}$$

$$\sigma^2 = \int_{-\infty}^{\infty} (x-\mu)^2\, c(x,t) h(x)\, dx / M_0 = \frac{M_2}{M_0} - \mu^2 \tag{3.38}$$

Multiplying Equation (3.35) by x, integrating over x, and using Equations (3.34)-(3.38) we get the following set of equations:

$$\int_{-\infty}^{\infty} \frac{\partial (ch)}{\partial t} x\, dx = \frac{\partial}{\partial t} \int_{-\infty}^{\infty} ch\, x\, dx = \frac{dM_1}{dt} = M_0 \frac{d\mu}{dt} \tag{3.39}$$

$$\int_{-\infty}^{\infty} \frac{\partial}{\partial x}\left[hD_{xx} \frac{\partial c}{\partial x}\right] x dx = \int_{-\infty}^{\infty} x \frac{\partial}{\partial x}\left[hD_{xx} \frac{\partial c}{\partial x}\right] dx = \int_{-\infty}^{\infty} D_{xx} \frac{\partial h}{\partial x} c dx + \int_{-\infty}^{\infty} \frac{\partial D_{xx}}{\partial x} h c dx \tag{3.40}$$

Equating Equations (3.39) and (3.40) we get:

$$\frac{d\mu}{dt} = \frac{\int_{-\infty}^{\infty} D_{xx} \frac{\partial h}{\partial x} c dx + \int_{-\infty}^{\infty} \frac{\partial D_{xx}}{\partial x} h c dx}{M_0} \tag{3.41}$$

In Equation (3.41) $\frac{d\mu}{dt}$ represents the velocity of the center of mass of the ch distribution. Comparing Equations (3.41) and (3.30) we see that the center of mass moves with a velocity equal to the average value of the deterministic velocity a_x of particles in the domain $-\infty < x < \infty$.

In the case where the depth h is constant Equation (3.32) becomes:

$$a = \frac{\partial}{\partial x} D_{xx} + u \tag{3.42}$$

If the diffusion coefficient D_{xx} is also constant then the deterministic velocity of a particle becomes equal to the advection velocity u.

Following the same procedure we can also find an expression for $\frac{d\sigma^2}{dt}$. Multiplying Equation (3.33) by x^2, integrating over x and using Equations (3.34)-(3.38) we get the following set of equations:

$$\int_{-\infty}^{\infty} \frac{\partial (ch)}{\partial t} x^2 \, dx = \frac{\partial}{\partial t} \int_{-\infty}^{\infty} ch \, x^2 dx = \frac{dM_2}{dt} = M_0 \frac{d\sigma^2}{dt} + M_0 \frac{d\mu^2}{dt} \tag{3.43}$$

$$\int_{-\infty}^{\infty} \frac{\partial}{\partial x} \left[h D_{xx} \frac{\partial c}{\partial x} \right] x^2 dx = 2 \int_{-\infty}^{\infty} D_{xx} ch dx + 2 \int_{-\infty}^{\infty} D_{xx} \frac{\partial h}{\partial x} cx dx + 2 \int_{-\infty}^{\infty} \frac{\partial D_{xx}}{\partial x} chx dx \tag{3.44}$$

From Equation (3.41) we have

$$\frac{d\mu^2}{dt} = 2\mu \frac{d\mu}{dt} = \frac{2\mu \int_{-\infty}^{\infty} D_{xx} \frac{\partial h}{\partial x} c \, dx + \int_{-\infty}^{\infty} \frac{\partial D_{xx}}{\partial x} hc dx}{M_0} \tag{3.45}$$

Equating Equations (3.43) and (3.44) and using Equation (3.45) we get:

$$\frac{d\sigma^2}{dt} = \frac{2}{M_0}\left[\int_{-\infty}^{\infty}(x-\mu)\frac{\partial D_{xx}}{\partial x}hc + (x-\mu)D_{xx}\frac{\partial h}{\partial x}c + D_{xx}hc\right]dx \qquad (3.46)$$

If h is constant Equation (3.46) reduces to

$$\frac{d\sigma^2}{dt} = \frac{2}{M_0}\left[\int_{-\infty}^{\infty}(x-\mu)\frac{\partial D_{xx}}{\partial x}hc + D_{xx}hc\right]dx \qquad (3.46)$$

If the diffusion coefficient D_{xx} is also constant we get the familiar expression:

$$\frac{d\sigma^2}{dt} = 2D_{xx} \qquad (3.47)$$

3.3.3 Implementation of Boundary Conditions

A transport problem described by Equation (3.18) requires an initial condition for c in the domain Ω_c as well as boundary conditions on the domain boundary $\partial\Omega_c$ (Figure 9). The boundary conditions are usually a combination of Dirichlet conditions (specified c) on a part $\partial\Omega_{c1}$ of $\partial\Omega_c$ and Neuman conditions or normal flux conditions (specified $\underline{n}\cdot\underline{F}$), $\underline{n}$ being an outward normal vector to $\partial\Omega_c$ on the complementary part of $\partial\Omega_c$, and $\underline{F}$ being the mass flux.

A thorough analysis for the implementation of boundary conditions in random walk models is given by Csanady (1972), Ghoniem et al. (1985), and Tompson et al (1988). Here the implementation of Dirichlet boundary conditions, zero flux boundary conditions, and inflow flux boundary conditions is presented, since these are used in the case of estuary mixing.

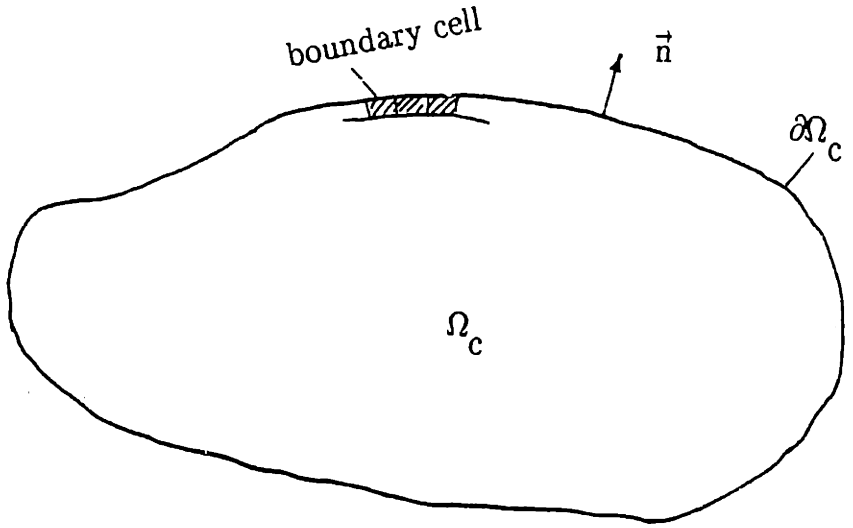

Figure 9 Implementation of boundary conditions in a random walk model

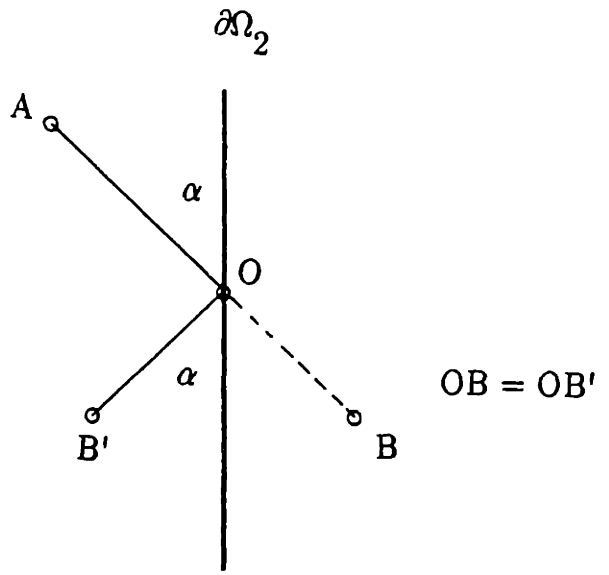

Figure 10 Representation of a zero flux boundary condition in a random walk model

Dirichlet Boundary Conditions on the boundary $\partial\Omega_1$: $c = c_0$ $\underline{x} \in \partial\Omega_1$. In the one dimensional case we have $c = c_0$ at $x = x_0$, where x_0 is a boundary node. Let's say that the concentration of particles is measured over cells of volume V_s in the three-dimensional case or over cells of area A_s or over cells of length l_s in the two- and one-dimensional cases respectively (see Section 3.3.1). To each cell in $\partial\Omega_1$ a number of particles that represent the concentration c_0 in the cell is assigned. These particles are randomly distributed over the boundary cells. At the beginning of a new timestep the particles that remain in the boundary cells are removed and the boundary condition is reinstated as before. In the case of $c_0 = 0$ the particles that reach these boundary cells are removed from the domain. According to the above the implementation of the first type boundary condition is very sensitive to the size of the boundary cell and the timestep Δt.

Zero-Flux Boundary Conditions on the boundary $\partial\Omega_2$: $\underline{n}\cdot\underline{F} = 0$ $\underline{x} \in \partial\Omega_2$. In the one-dimensional case we have $\frac{\partial c}{\partial x} = 0$ at $x = x_0$, where x_0 is a boundary node. A zero-flux boundary is a boundary across which no mass can cross. Particles may be "forced" to move across such a boundary due to their diffusive displacement. Any particles moving across a zero-flux boundary cell will be reflected back into the domain as shown in Figure 10. In the case of highly irregular boundaries (e.g., the area around the mouth of Niantic River in Figure 18) the implementation of a zero-flux boundary condition may cause problems because of the many particle reflections.

Inflow-Flux Boundary Condition on the boundary $\partial\Omega_3$: $\underline{n}\cdot\underline{F} = \underline{F}_n$. This boundary condition involves specifying a certain amount of mass (i.e., number of particles) that must flow into the system through a certain area over some span of time (Tompson et al., 1988). It is implemented by introducing the corresponding particles on the

boundary cells in $\partial\Omega_3$ every timestep, distributing them randomly over these cells and letting them advect and diffuse.

From the above we can conclude that the implementation of flux boundary conditions in a random walk model is easier than the implementation of first type boundary condition because it is not sensitive to cell size.

4 TEST CASE VERIFICATION OF RANDOM WALK MODEL IN 1-D ESTUARY

A one-dimensional random walk model developed for the simulation of mixing of a conservative pollutant in an estuary is presented in this chapter. The one-dimensional model is a limiting case of the two-dimensional random walk model presented in the following chapter and is used for verification purposes since there exists an analytical solution for the one-dimensional concentration model to which the results from the random walk model could be compared. The longitudinal concentration distributions and the flushing time that results from the integration of the concentration distribution (Equation 2.21) were compared. The model was also used in order to investigate the sensitivity of the random walk model to parameters such as the timestep Δt, the number of particles, and the size of the length l_s over which the concentration of particles are measured. The physics of the model are based on the mixing length theory described in Section 2.3.2 and the numerical aspects are based on the random walk theory described in Chapter 3.

According to Section 2.3.2 the concentration (mass of pollutant per unit length) of a conservative pollutant discharged at a constant rate W (mass of pollutant per unit time) at $x = 0$ along an estuary of uniform crossection with unit crossectional area and length L is given by the following governing equation

$$\frac{\partial c}{\partial t} + u\frac{\partial c}{\partial x} = \frac{\partial}{\partial x}\left[D_x\frac{\partial c}{\partial x}\right] \tag{4.1}$$

where

u is the river velocity and

$D_x = \frac{\omega a_0{}^2 x^2}{2\pi h^2}$ (see Equation 2.13) is the longitudinal dispersion coefficient.

Boundary conditions are

$$c = c_0 = \frac{W}{u} \quad \text{at} \quad x = 0 \tag{4.2}$$

$$c = 0 \quad \text{at} \quad x = L \tag{4.3}$$

Since the injection is continuous we may assume steady-state tidal averaged conditions at a certain time after the beginning of the injection. In this case Equation (4.1) reduces to

$$u\frac{\partial c}{\partial x} = \frac{\partial}{\partial x}\left[D_x\frac{\partial c}{\partial x}\right] \tag{4.4}$$

The analytical solution to Equation (4.4) is given by Equation (2.24)

$$c = c_0\left[1 - e^{F(1-1/\lambda)}\right] \tag{4.5}$$

The flushing time of the estuary is given according to Equation (2.21) given by

$$t = \frac{\left[1-e^{F(1-1/\lambda)}\right]dx}{u} \tag{4.6}$$

The integral in Equation (4.6) was estimated using Gaussian quadrature.

Comparison between the concentration distributions of the two models was made using normalized concentration of the two models, i.e.,

- for the concentration model (analytical solution) c(x) was normalized by dividing by the injection concentration, c_0
- for the random walk model, particle concentration (particles/distance) was normalized by dividing by the particle injection rate (particles/time) and multiplying by the river velocity u (distance/time)

The flushing time using the random walk model was estimated by adding the number of particles in the estuary after steady state was reached and dividing by the particle injection rate.

For all runs the following parameters were used

$$L = 7000 \text{ m}$$
$$\frac{a_0}{h} = \frac{1}{2}$$
$$h = 10 \text{ m}$$

In order to simulate the longitudinal distribution of a conservative pollutant given by the governing Equation (4.4) and satisfying the boundary condition given by Equations (4.2) and (4.3) using a random walk model the following aspects have to be resolved

- random walk algorithm
- simulation of continuous release using particles reaching steady state
- implementation of boundary conditions
- volume over which the concentration of particles will be measured
- time stepping method
- number of particles necessary for expected accuracy
- dependence of accuracy on the flushing number

4.1 Random Walk Algorithm

According to the analysis in Section 3.3.1 Equation (4.1) is equivalent to the Fokker-Planck equation (Equation 3.17) if a(x,t) and b(x,t) are chosen so that

$$u = a - \frac{\partial}{\partial x}[\tfrac{1}{2}b^2] \tag{4.6}$$

$$D_x = \tfrac{1}{2}b^2 \tag{4.7}$$

According to Equations (4.6) and (4.7) a(x,t) and b(x,t) are given by the expressions

$$b = \sqrt{2D_x} = \sqrt{\frac{2}{T}}\frac{a_0}{h}x = \sqrt{\frac{2\omega}{2\pi}}\frac{a_0}{h}x = \sqrt{\frac{\omega}{\pi}}\frac{a_0}{h}x \tag{4.8}$$

$$a = u + \frac{\omega a_0^2}{\pi h^2}x \tag{4.9}$$

According to the above equations and Equation (3.19) the particles move according to the following step equation

$$x(t_n) = x(t_{n-1}) + \left[u + \frac{\omega a_0^2}{\pi h^2}x\right]\Delta t + \sqrt{\frac{\omega}{\pi}}\frac{a_0}{h}x\sqrt{\Delta t}\,p_i \tag{4.10}$$

where p_i is a random number that must satisfy the conditions: $\langle p_i \rangle = 0$ and $\langle p_i p_i \rangle = 1$. We chose p_i to have a normal N(0,1) distribution.

4.2 Convergence to Steady State for a Continuous Release

In order to simulate a continuous release a certain number of particles are released at $x = 0$ every timestep.

Steady state is reached when the concentration c does not change appreciably as a function of time. Since the concentration c at a position $x = x_s$ in a random walk model is equal to the number of particles over some length l_s, c depends on l_s (see Section 4.4) and might fluctuate over time more or less according to whether l_s is "small" or "large" respectively. So instead of comparing concentrations we chose to estimate the spatial integral of concentration, (i.e., the number of particles over the

entire estuary) as a function of time for testing convergence to steady state. Figure 11 shows how the number of particles N in the domain changes as a function of time (u = 0.005 m/sec, Δt = 3h, 6 particles per timestep). If we define as Δt_s the flushing time of the estuary due to the advection velocity u, i.e.,

$$\Delta t_s = \frac{L}{u} \tag{4.11}$$

from Figure 11 we see that steady state is reached before time $t = \Delta t_s$. In order to guarantee convergence the simulation time was set equal to $2\Delta t_s$.

In order to show the significance of the second term of the advective displacement ($\frac{\partial}{\partial x}D_x = \frac{\omega a_0^2}{\pi h^2}x$; see Equation (4.9)) we neglected this term in one run. Figure 12 shows that the average concentration in the estuary continues to increase; i.e., steady state is never reached. The physical interpretation is that, for this run, an additional velocity equal to $-\frac{\omega a_0^2 x}{\pi h^2}$ has been added to the mean velocity u, tending to prevent flushing.

4.3 Implementation of Boundary Conditions

According to Equations (4.4) and (4.5) we have two first-type (Dirichilet) boundary conditions at x = 0 and x = L. The flux $F_{x=0}$ at x = 0 is given by

$$F_{x=0} = uc_0 - D_x\frac{dc}{dx} \tag{4.12}$$

From Equations (4.7) and (4.8) we can see that $D_x = 0$ at x = 0, so $F_{x=0}$ simplifies to

$$F_{x=0} = uc_0 \tag{4.13}$$

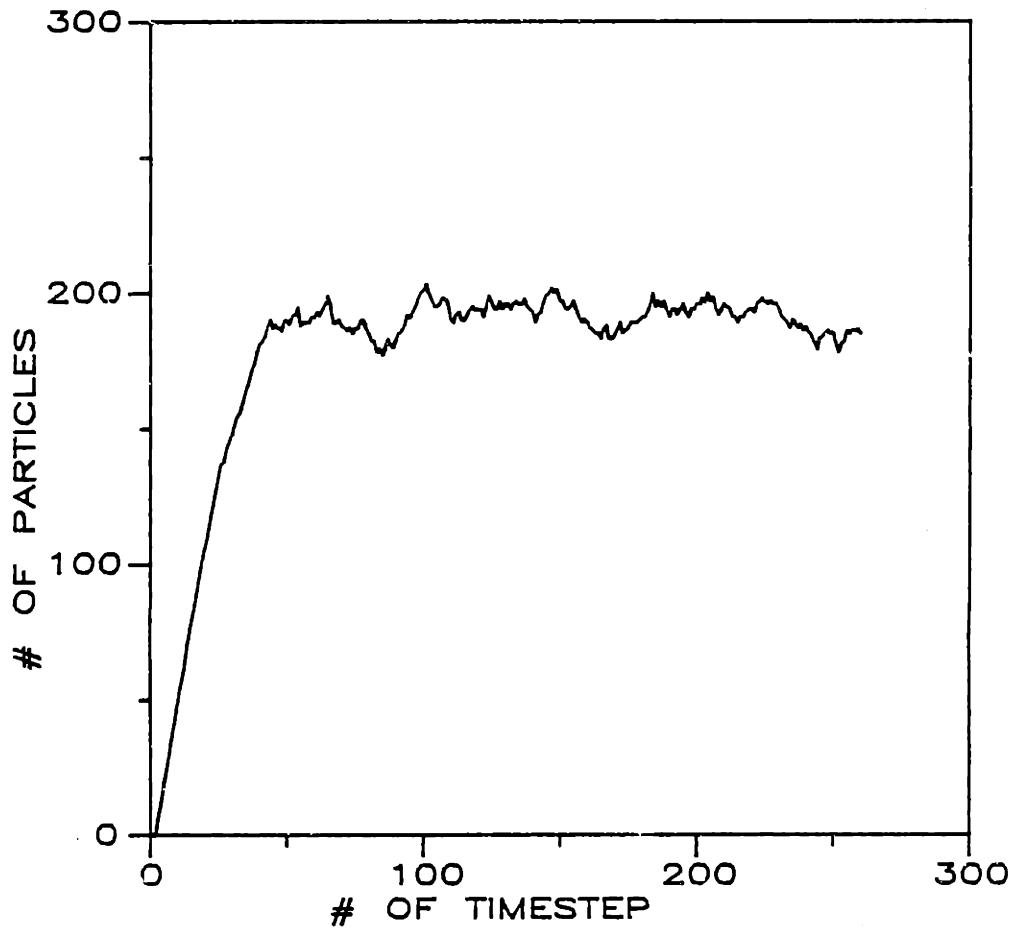

Figure 11 Number of particles in the domain as a function of time for $\Delta t = 3h$, injection rate 6 particles per timestep, u = 0.005 m/sec

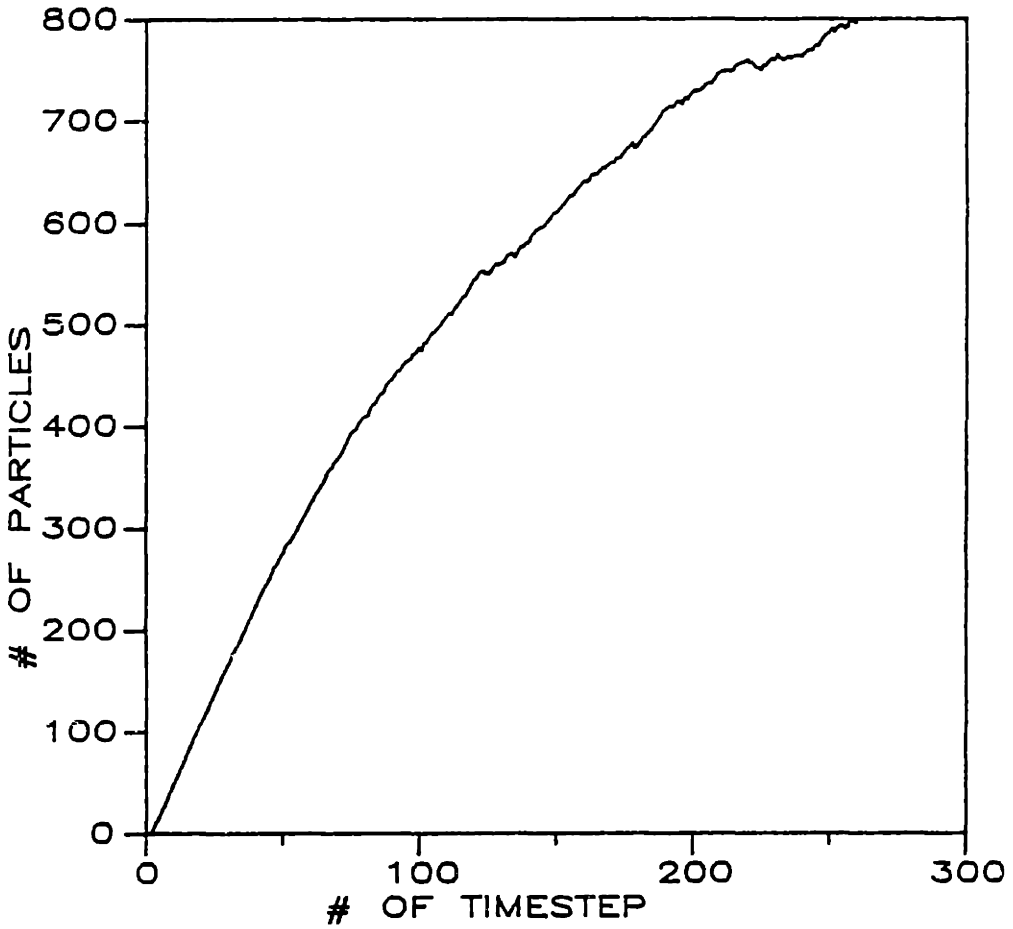

Figure 12 Number of particles in the domain as a function of time for $\Delta t = 3h$, injection rate 6 particles per timestep, $u = 0.005$ m/sec in the case where the advection step is taken to be equal to $u\Delta t$

Equation (4.13) implies that we can implement the first type boundary condition $c = c_0$ at $x = 0$ by specifying a constant flux and implementing the inflow flux boundary condition. As mentioned in Section 3.3.3 flux boundary conditions are easier to implement than first type boundary conditions. So the first-type boundary condition $c = c_0$ at $x = 0$ is simulated by introducing a certain number of particles every timestep at $x = 0$. The first-type boundary condition $c = 0$ at $x = L$ is implemented by removing from consideration particles that exceed $x = L$ during a timestep. In case particles are forced to move across $x = 0$ due to their diffusive displacement they are reflected back since $x = 0$ is a zero diffusive flux boundary.

4.4 Length over which Concentration of Particles will be Measured

In a random walk model a fixed amount of mass M of the pollutant is represented by N particles. So each particle represents a mass $m = \frac{M}{N}$. The concentration c of the pollutant per unit length (1-D model) at a point x is represented in a random walk model as the number of particles in a length l_s centered at x. The larger l_s is, the larger the number of particles found within it will be and so the more smoothly varying the concentration will be. However if l_s is too large, all the mass will be found within it and so little sense of its spatial distribution will be discerned. Figure 13 shows a comparison between the concentration distributions for $l_s = L/100$, $L/20$, and $L/10$, for $u = .005$ m/s, $\Delta t = 0.5$h and 8 particles released every timestep. We see that, as l_s becomes smaller, the solutions become more "noisy."

4.5 Time Stepping Method

Ideally a particle should follow a streamline in a steady-flow pure-advection problem. If finite time steps are used then small spatial overshoot errors will occur due to the incremental nature of the timestep. Since the dispersion displacements are a

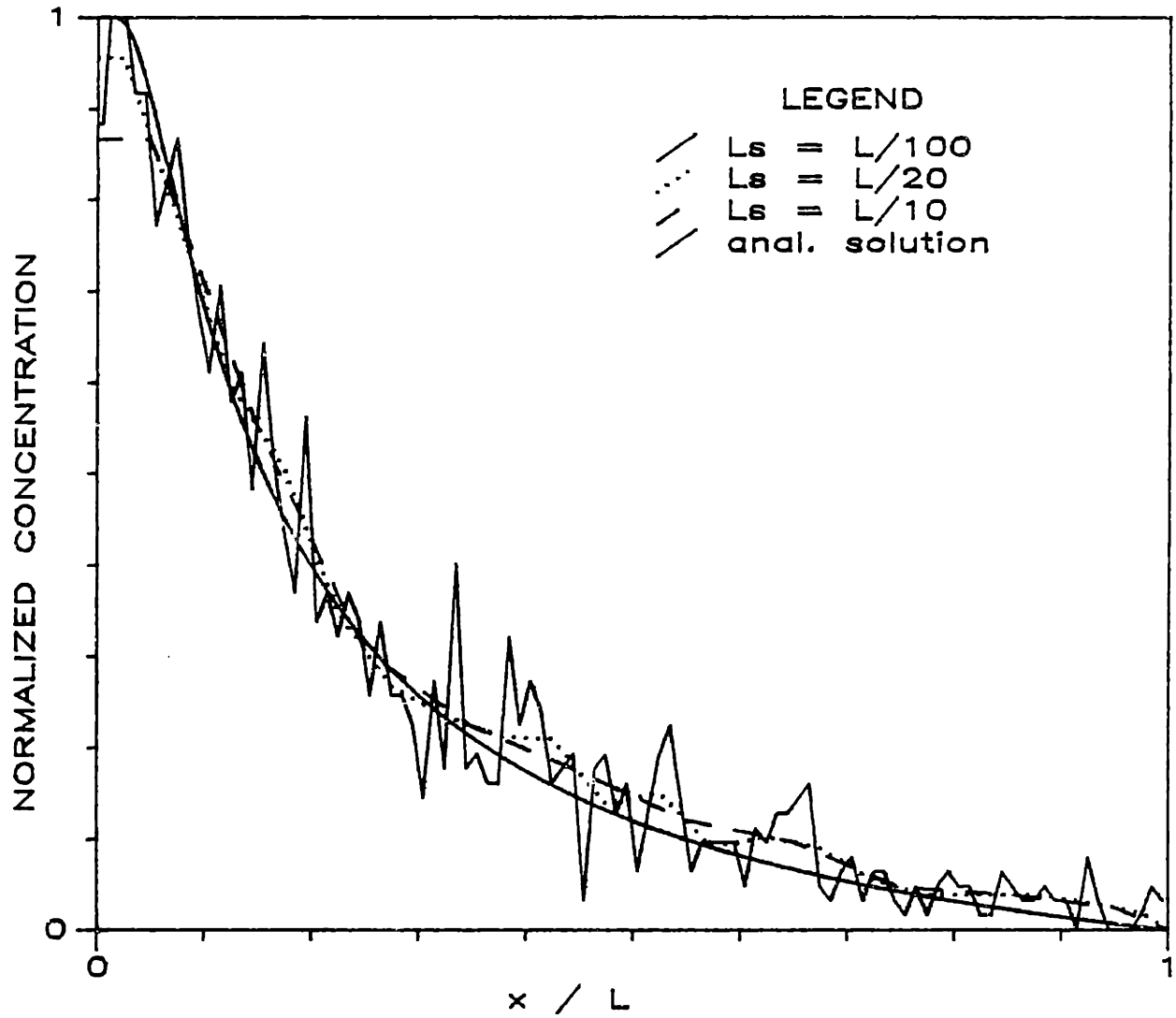

Figure 13 Sensitivity on l_s u = 0.005 m/sec, Δt = 0.5 h, injection rate 16 particles per hour

function of a dispersive velocity that varies spatially the same considerations are made for the dispersive displacements as for the advective displacements.

The magnitude of this problem can be reduced by using infinitely small time steps or adopting an improved integration (particle tracking) scheme, such as a Runge-Kutta method. For this example a single first-order integration scheme (i.e., constant velocity over the interval Δt) was used.

Figure 14 shows the comparison between the concentration distribution for Δt = 3 h, 1.5 h, and 0.5 h in the case where u = .005 m/s $l_s = L/10$ and two particles are released every hour; i.e., 6 particles per timestep for Δt = 3h, 3 particles per timestep for Δt = 1.5h, and 1 particle per timestep for Δt = 0.5h. We see that as Δt becomes smaller the curve becomes smoother and resembles in shape the analytical solution. Also the flushing time approaches the flushing time resulting from the analytical solution.

4.6 Number of Particles

As mentioned in Section 3.3.1 the random walk algorithm becomes equivalent to the mass transport equation as the number of particles $N \to \infty$. So the more particles we use the more accurate our solution becomes. In Figure 15 a comparison is made between solutions for u = .005 m/s, Δt = 0.5 h, and $l_s = L/10$ in the cases where one, two, and eight particles per timestep are released. We see that as the number of particles increases the distribution becomes smoother, so the statistical error is decreased. In terms of flushing times there is no difference between the three cases which implies that the error in the flushing time evaluation is more related to time discretization than the number of particles.

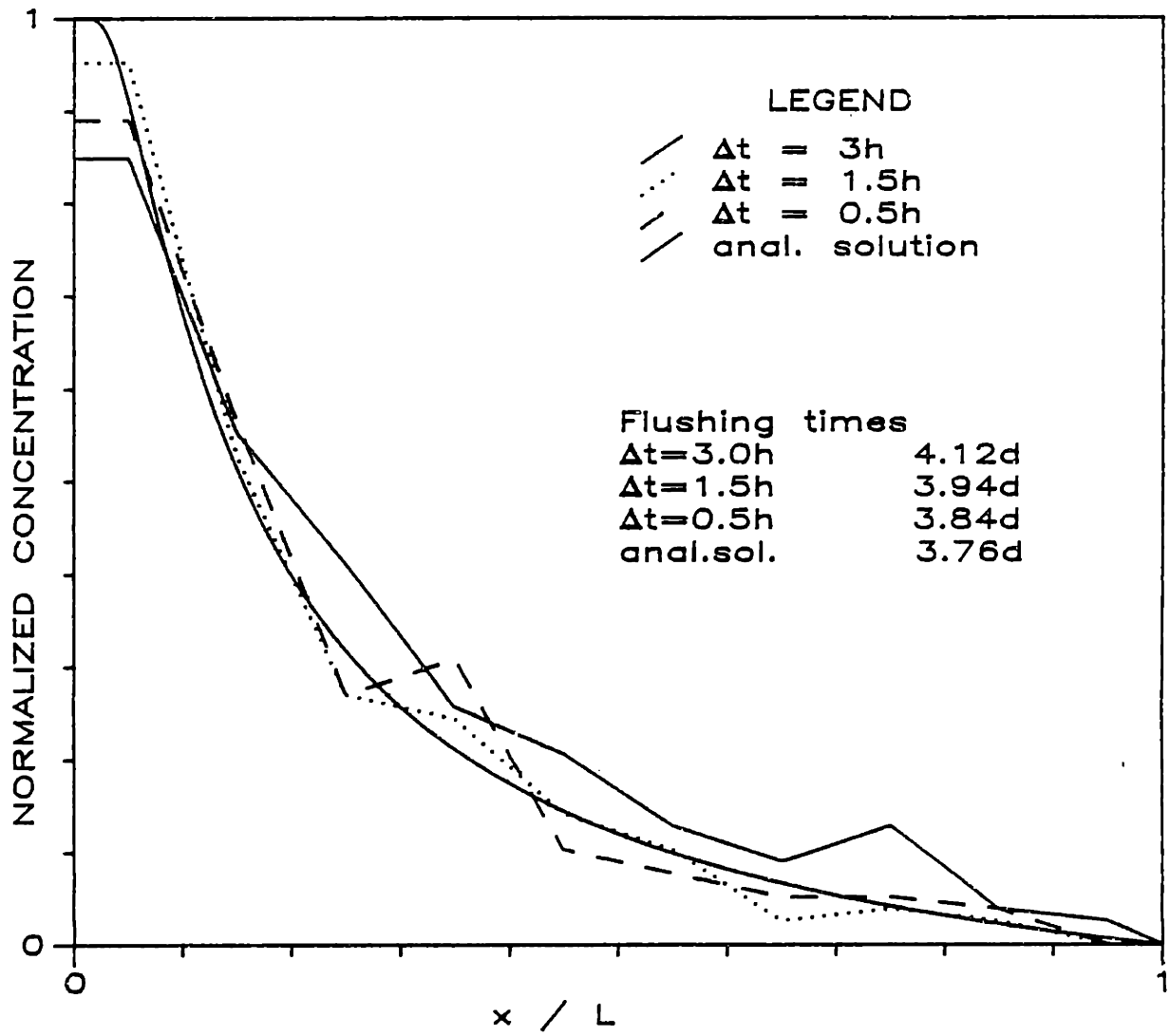

Figure 14 Sensitivity on Δt u = 0.005 m/sec, injection rate 2 particles per hour, l_s = L/10

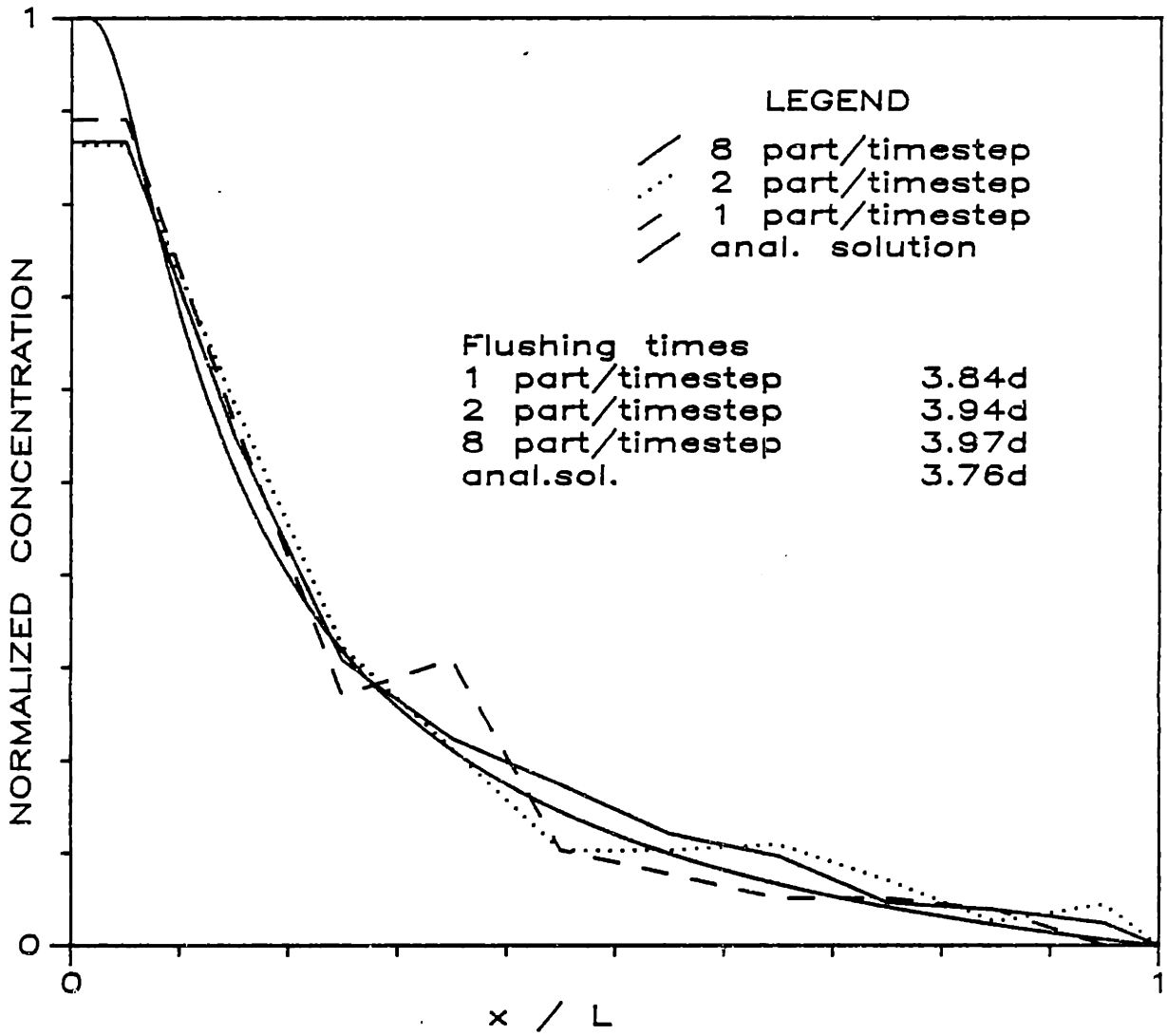

Figure 15 Sensitivity on the number of particles released per time u = 0.005 m/sec, Δt = 0.5 h, l_s = L/10

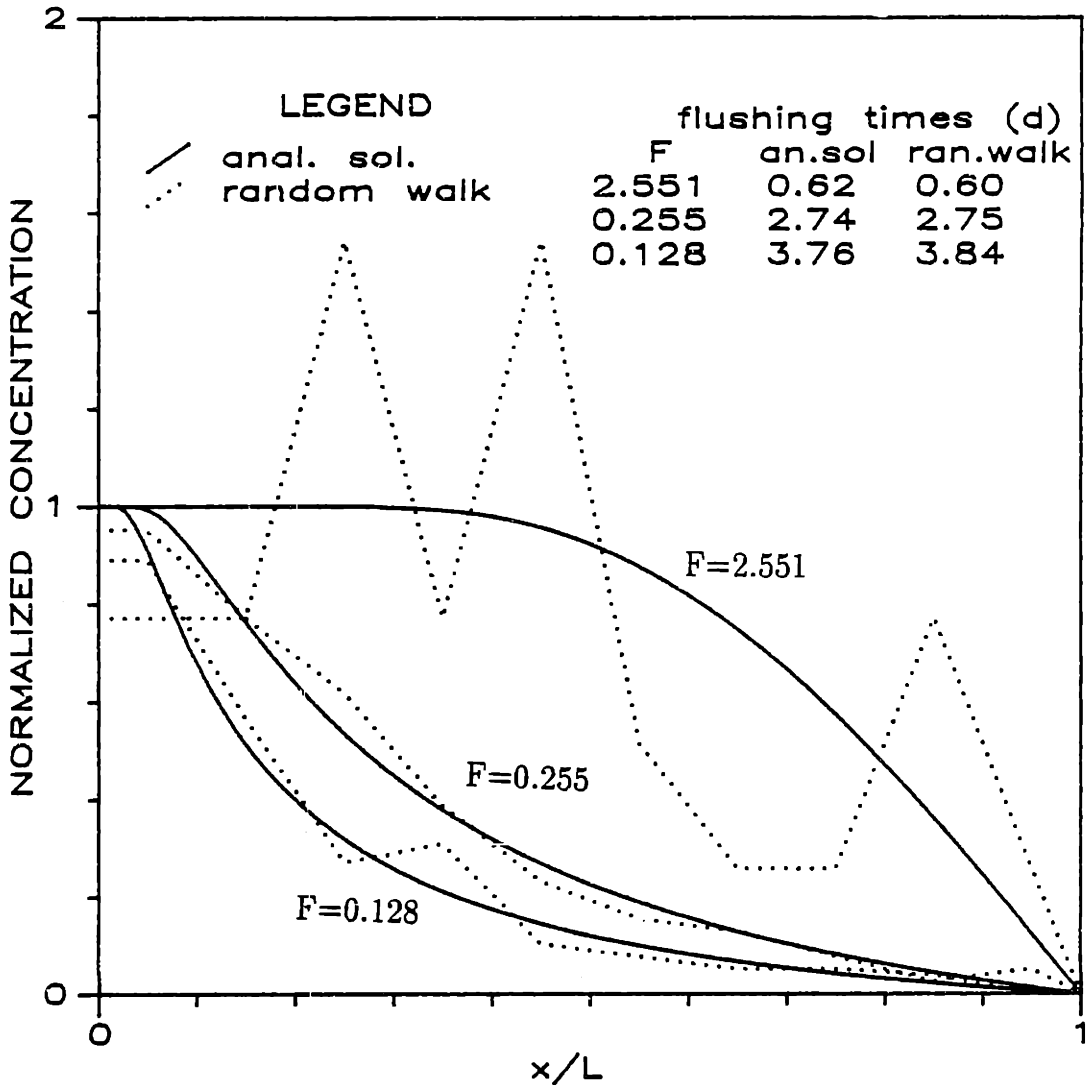

Figure 16 Dependence of accuracy on flushing number $\Delta t = 0.5$ h, $l_s = L/10$, injection rate 1 particle per timestep

4.7 Dependence of Accuracy on the Flushing Number

The flushing number F is a measure of the relative importance between the advective and the diffusive displacement. As F increases, advection becomes more important. Figure 16 shows a comparison between three runs with u = 0.1 (F = 2.551), 0.01 (F = 0.255), and 0.005 m/sec (F = 0.128) where Δt = 0.5 h and one particle was introduced every timestep. We can see that as F increases, the distribution becomes noisy because there are fewer particles are in the domain. (As before, however, the flushing time, which is proportional to the spatial integration of concentration, is less affected.) To maintain accuracy of the concentration distribution, we must therefore increase the number of particles introduced per time step in proportion to u such that the average particle density remains constant. As a conclusion we can say that the important factor governing accuracy of the concentration distribution is the number of particles per "cell" or $N_t \ell_s / u$ where N_t is the number of particles released per time.

5 MILLSTONE POINT CASE STUDY

5.1 Purpose and Scope

A major objective of this project was to develop the model MILL, based on the two-dimensional random walk model described in Section 3.3.2, to simulate the entrainment effects from the operation of MNPS (Figure 1). A study of regionally important species subject to entrainment in the Millstone Point area identified winter flounder as the species to be modeled. Several shallow areas in the vicinity of MNPS (including Niantic River and Outer Jordan Cove) serve as spawning areas for winter flounder. A fraction of larvae, hatched in these areas, is expected to be entrained, and hence killed, through entrainment at the station.

5.2 Background

The large effort devoted to winter flounder studies is related to its importance for the Connecticut sport and commercial fisheries. It is the most valuable commercial finfish in Connecticut and on average makes up about 20% of the total finfish landings. The winter flounder is also one of the most popular marine sport fishes in the state with an estimated annual catch in 1979 of almost 1.4 million fish with a total weight of 412,243 kg. Its particular life history also makes it potentially susceptible to various types of impacts (NUEL Annual Report 1988).

The MNPS is located on the north shore of Long Island Sound in Waterford, Connecticut (Figure 1). The station consists of three operating units: Millstone Unit 1 commenced commercial operation in 1970, Unit 2 in 1975, and Unit 3 in 1986. Extensive studies of the potential impacts of MNPS on local marine flora and fauna have been conducted since 1968. During this period studies have consistently been reviewed and updated to assure that the best available methods were used. Preliminary field

studies to estimate abundance of the winter flounder population in 1973-74 were expanded in scope in 1975, when surveys using mark and recapture techniques were initiated. An adult abundance survey was completed each year through the present. In many years, studies of age structure, reproductive activity, growth, survival, movements, early life history, and stock identification were conducted. For plant impact, impingement and entrainment estimates are available for each year (NUEL Annual Report 1988). Data from many of these studies have been used in a predictive mathematical population dynamics model developed by the University of Rhode Island (Saila, 1976). This model formed the basis for earlier MNPS impact assessments, including that for Unit 3. The present analysis is based on the MIT model MILL. Model MILL is a two-dimensional random walk model based on the Eulerian-Lagrangian finite element transport model ELA (Baptista et al., 1984). This circulation model the harmonic finite element model TEA (Westerink et al., 1984; Westerink et al., 1985; Westerink, 1986) is used. The input of the model consists of the continuous distribution of larvae hatching over time, the larval behavior as a function of age, tidal and diurnal phase, and natural mortality. The output of the model gives the locations and fate of the larvae at a specific time after the start of the simulation. As described in more detail, MILL is similar in many ways to Saila's model (1976) but also includes some major differences. The major differences between the model MILL and the model used by Saila (1976) are the following:

1) Differences in grid used: MILL is a finite element model and uses irregular, triangular grid elements whereas Saila's model is a finite difference model and uses regular, square grid elements. This configuration allows for easy grid refinement in critical regions, such as the Niantic River and the plant intake area (Figure 19).

2) Differences in larval distribution: In Saila's analysis larvae were hatched instantaneously over a prescribed spatial distribution whereas in MILL larvae are

hatched over a 2-month period in three stations A, B, C (Figure 18) according to temporal and spatial distributions provided by NUEL.

3) Differences in larval behavior: In Saila's analysis larvae were passive (i.e., they follow the motion of the water) throughout their development. However according to studies larvae show a specific tidal and diurnal behavior that is a function of their age. This behavior is simulated in model MILL.

4) Difference in model: Saila uses an Eulerian model, where larvae are simulated as mass of larvae and concentration is found at every grid point. This model uses a Lagrangian approach, where larvae are simulated by particles and followed around the waterway. The location of these particles is found at every timestep. Saila (1973) admits that the Lagrangian approach is preferable for describing larvae, but he does not follow this approach because of the long computer times required. MILL takes advantage of newly developed computational methods, which provide higher speed for extended simulations.

5.3 Grid

The Millstone grid used to study the thermal plume at Millstone (Adams and Cosler, 1987) was extended to include the northern reaches of Niantic River where larvae are spawned (Station A) (Figure 18). It was also extended further south and east in Niantic Bay to enlarge the domain, thus reducing the frequency of simulated larval losses at the open boundaries. Figure 17 shows the domains covered by the different grids used in the Millstone area: 1) the grid used by Saila (1976), 2) the grid used by Adams and Cosler (1987), and 3) the grid used in this study. Figures 18, 19 show the grid used in this study and the locations of:

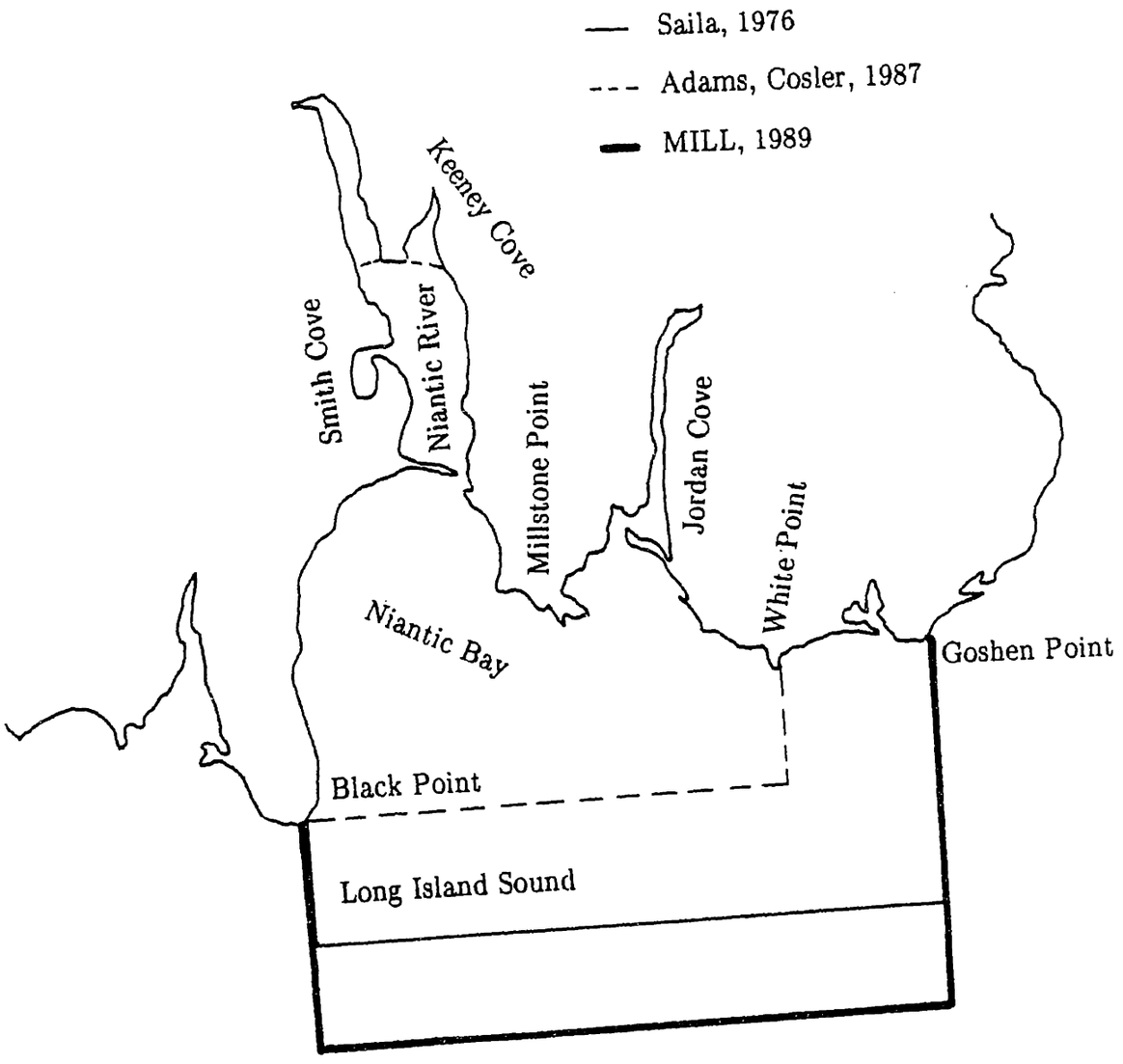

Figure 17 Comparison between the three grids

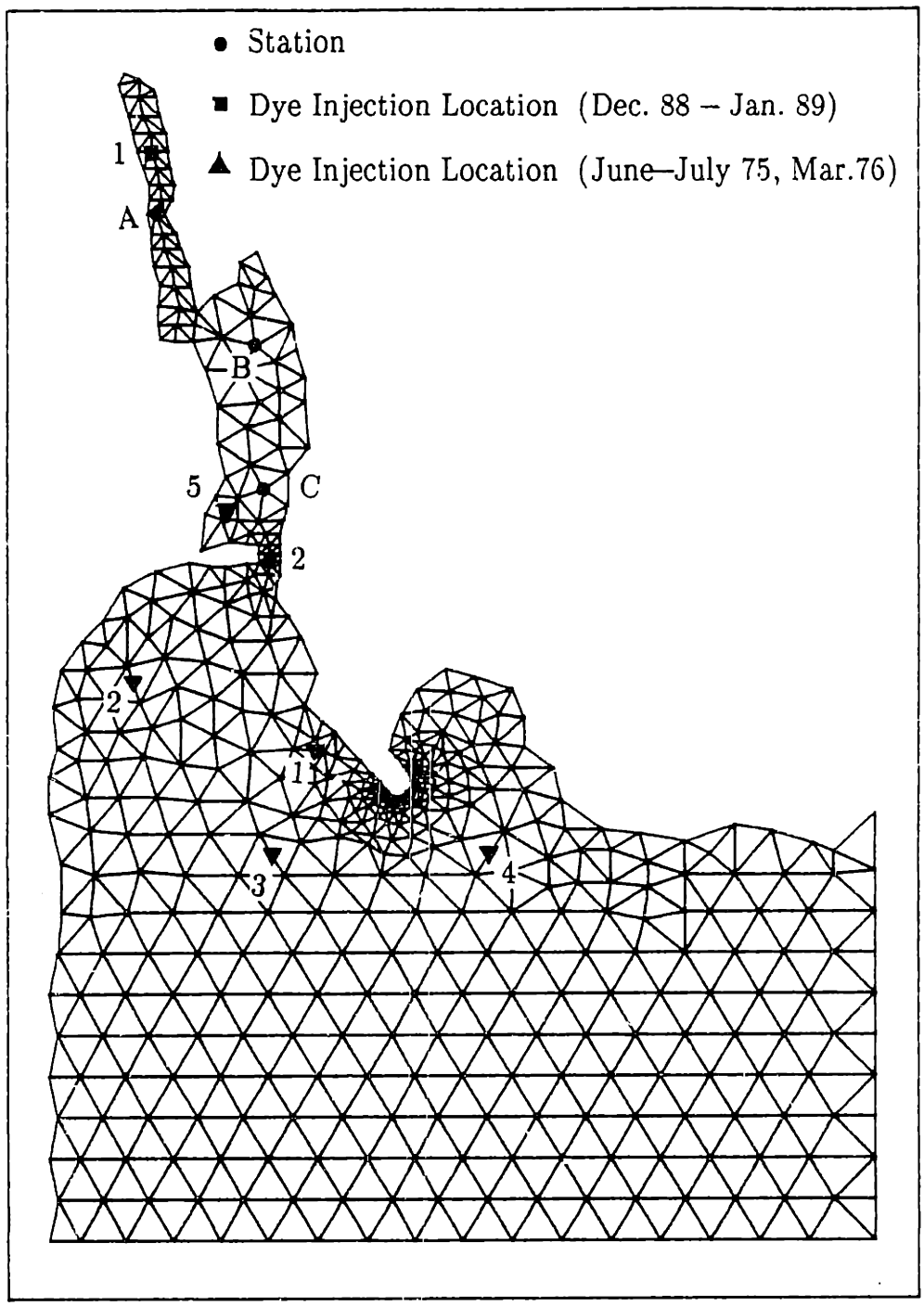

Figure 18 Locations of Stations A, B, C. Dye injection locations for dye studies conducted in December 1988 - January 1989 and June-July 1975, March 1976

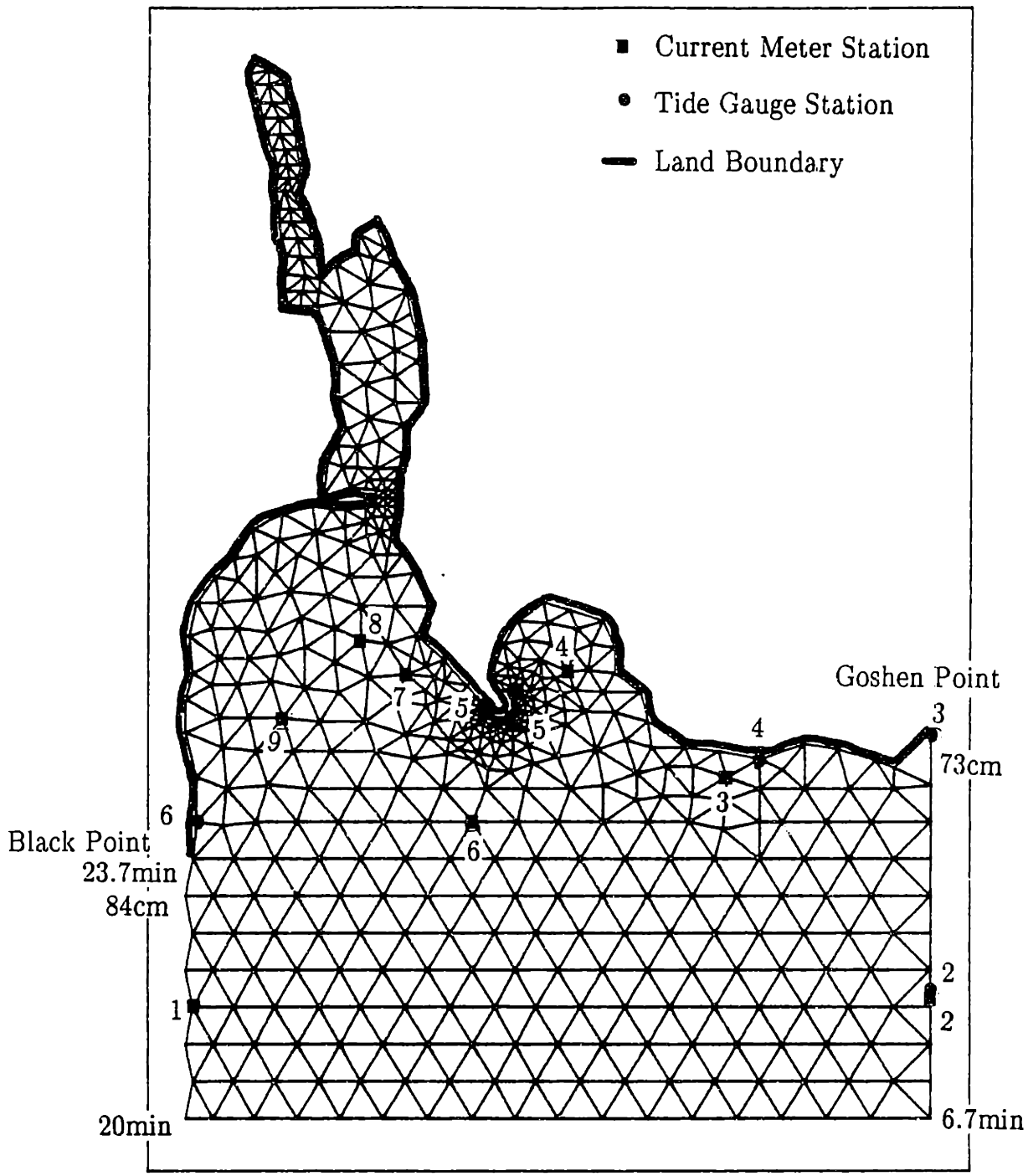

Figure 19 Current meter locations, tidal current meter locations, tide gauge locations

- Larvae hatching stations A, B, C (see Section 5.6.2)
- Current water stations, tidal meter stations, tide gauge stations (see Section 5.4)
- Dye injection locations for studies in 1975-1976 (see Section 5.4.2)
- Dye injection locations for studies in 1988-1989 (see Section 5.8)

5.4 Flow Model

5.4.1 General

The linear version of the two-dimensional (depth-averaged) harmonic finite element circulation model TEA was used. The equations to be solved are the depth-averaged continuity and Navier Stokes equations under the assumption of constant fluid density, small tidal amplitude, hydrostatic pressure distribution, negligible convective acceleration and momentum dispersion, and constant pressure at the air-water interface (Westerink et al., 1984). These equations are

$$\eta_t + (uh)_x + (vh)_y = 0 \tag{5.1}$$

$$u_t + gn_x - fv - \frac{1}{\rho h}(\tau_x^s - \tau_x^{b,lin}) = 0 \tag{5.2}$$

$$v_t + gn_y - fu - \frac{1}{\rho h}(\tau_y^s - \tau_y^{b,lin}) = 0 \tag{5.3}$$

where

u,v are the depth-averaged velocities in the x and y directions respectively

η is the surface elevation above the mean water level

h is the mean water depth

t is the time

g is the acceleration due to gravity

ρ is the density of water

f is the Coriolis parameter

τ_x^s and τ_y^s are the surface stresses in the x and y directions respectively

$\tau_x^{b,lin}$ and $\tau_y^{b,lin}$ are the linearized bottom stresses in the x and y directions respectively

The bottom friction has been linearized as

$$\frac{T_x^{b,lin}}{\rho} = \lambda u \quad \text{and} \quad \frac{T_y^{b,lin}}{\rho} = \lambda v \tag{5.4}$$

λ is the linearized friction coefficient and has the form

$$\lambda = u_{max} \frac{8}{3\pi} c_f \tag{5.5}$$

where

u_{max} is the representative maximum velocity during a tidal cycle

c_f is the friction factor.

The following assumptions were made:

- No tributary inflows. Average freshwater inflow from Lattimer Brook and Jordan Brook are about 10 cfs and 2 cfs respectively and generally have a negligible effect on circulation compared to tidal currents.

- Circulation induced by winds was ignored because they generally have only a secondary influence on the circulation (Saila, 1976). Furthermore, the effects of extreme winds are manifest in vertical as well as horizontal gradients of velocity; the former are not properly represented in a depth-averaged model. To the extent

they are important, both freshwater inflow and wind-driven circulation must be accounted for by mixing in the transport model.

For the simulation of the flow in Niantic River and Bay two runs of TEA were necessary. In the first run the tidally induced circulation was simulated. In the second run the steady-state depth-averaged circulation due to the operation of the three units was simulated following Adams and Cosler (1987). The result of the two runs were superimposed.

5.4.2 Boundary Conditions

For specifying the boundary conditions, data from two hydrographic surveys, conducted during summer (8 Aug to 10 Sept, 1973) and winter (6 to 20 Feb, 1974), were used. The data from the tide elevations were used to specify tide amplitude and phase lag at the boundary nodes and velocity current data were used to check the accuracy of the model. In Figure 19 the configurations of shoreline tide gauging stations and current meters for the winter survey are shown.

As shown in Figure 19 there are not enough tide elevation data in order to specify boundary conditions for the present domain. So the boundary conditions were chosen to achieve a reasonable fit in terms of flood and ebb current speed and direction.

The tide range was taken to increase linearly across the boundary from the value $R_1 = 73$ cm at Goshen Point to the value $R_2 = 84$ cm at Black Point (Figure 19); i.e., $\eta = R_1 + x(R_2-R_1)$ where x is the dimensionless distance from Black Point to Goshen Point.

The phase lag ϕ was also chosen to vary linearly from Goshen Point to Black Point with the phase at Goshen Point occurring 23.2 min later than Black Point (Figure 19), ϕ (min) = 23.7 min.

A constant friction factor of f = 0.0001 was used.

In Figure 20 the flow field due to tidal currents at time t = 3.1 h after high tide is plotted.

5.4.3 Intake and Discharge Flux Conditions

The condenser water intake flow for three units is about 118 m^3/sec. This flux was evenly distributed among four nodes (Figure 21). Adams and Cosler (1987) calculated that the near field volumetric dilution due to the surface discharge is about 3. Therefore the plume entrainment rate is twice the intake flow rate and is evenly distributed among three entrainment nodes on the left and three entrainment nodes on the right of the discharge. The discharge is distributed among four nodes (Figure 23). In Figure 21 the flow field due to the steady-state operation of the three units is plotted.

In Figure 23 the flow field from the superposition of the flow fields of Figures 20, 22 is plotted.

5.5 Transport Model

A two-dimensional depth-averaged random walk transport model was used. The governing equation is given by Equation (3.29) and the random walk algorithm is given by Equations (3.30) and (3.31). It remains to specify the dispersion coefficients D_{xx}

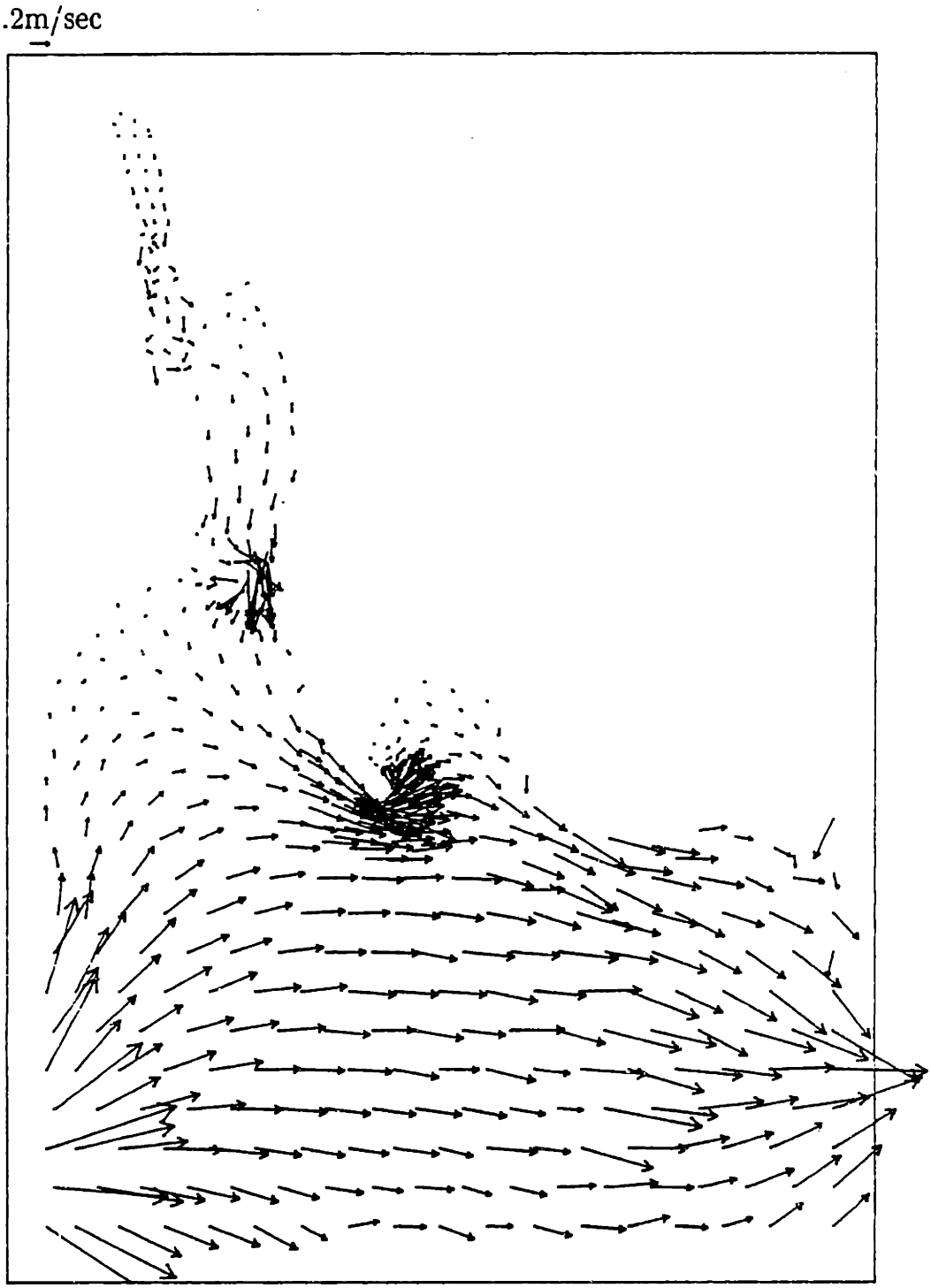

Figure 20 Flow field due to tidal currents at time t = 3.1 h after high tide

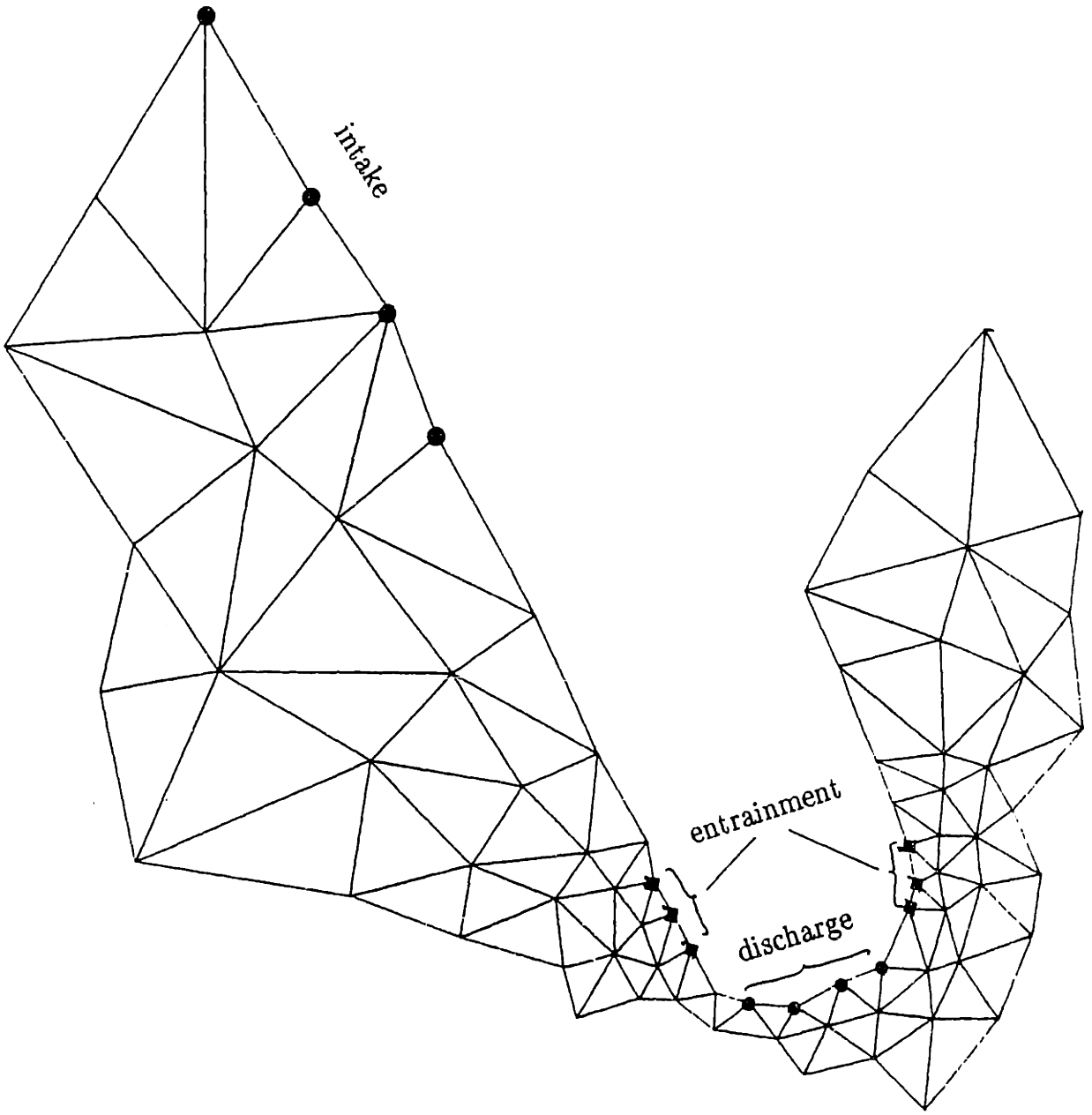

Figure 21 Intake and discharge

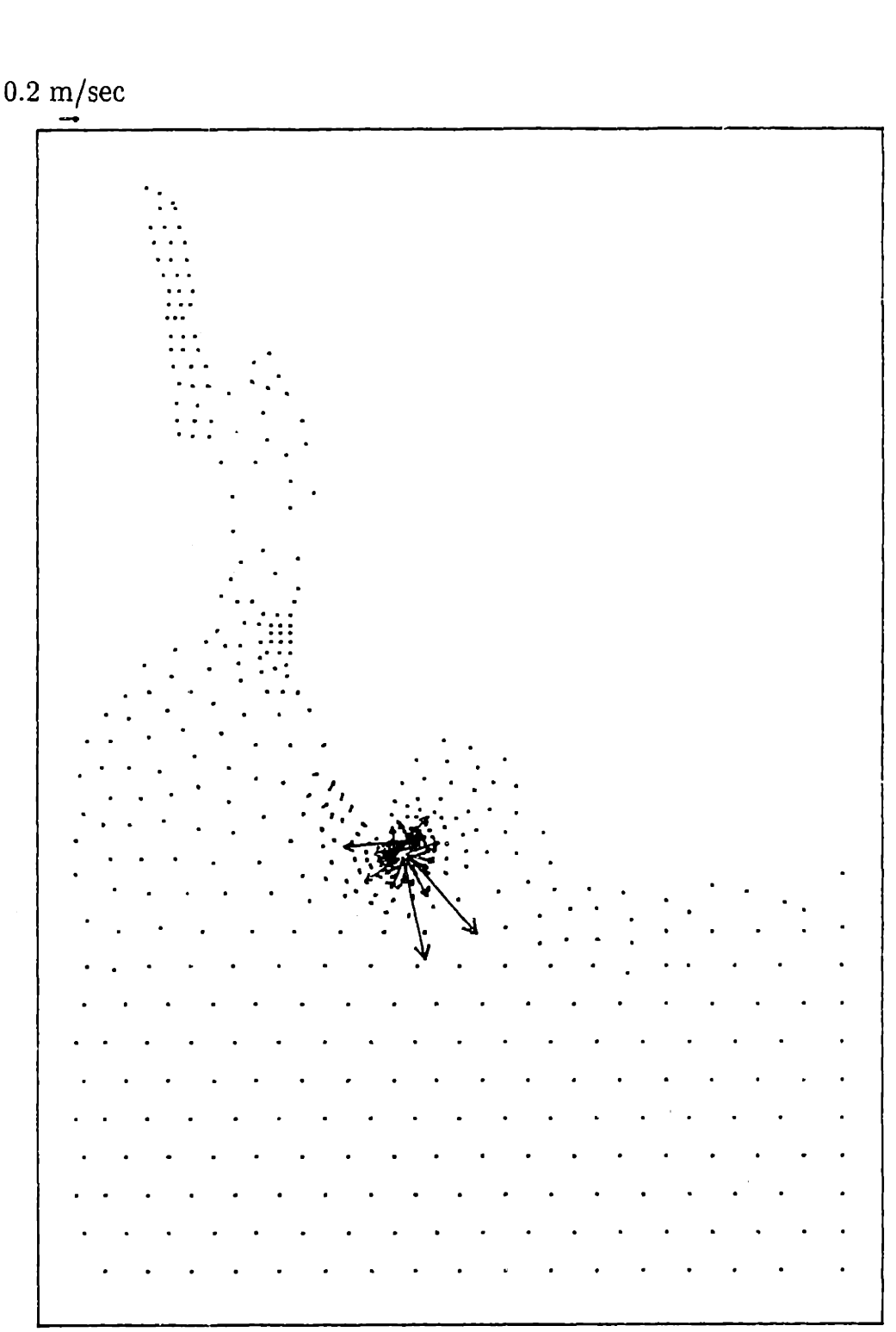

Figure 22 Flow field due to steady-state operation of the three units

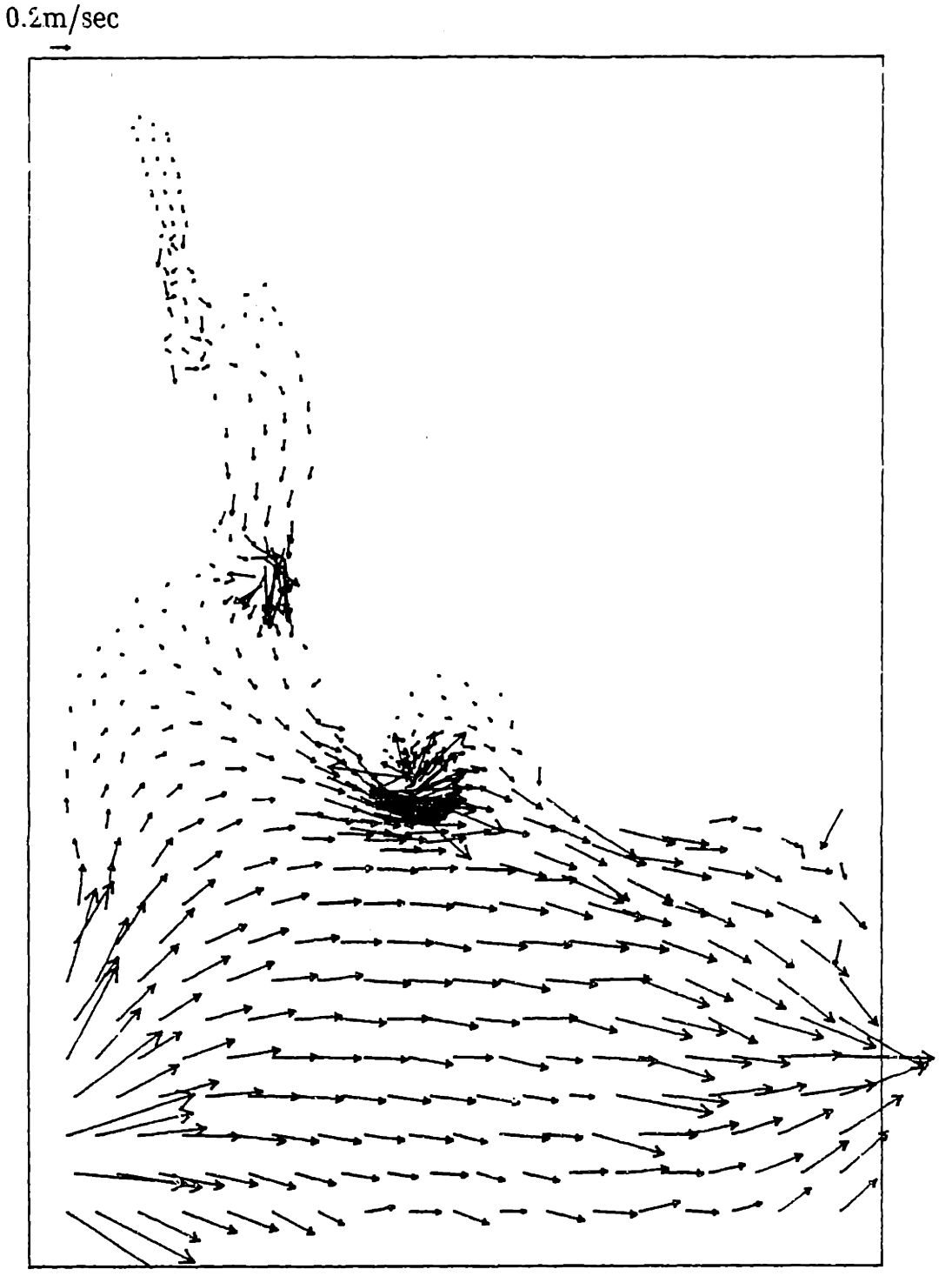

Figure 23 Flow field from superposition of flow fields of Figures 20 and 22

and D_{yy}. In order to do that the domain was divided into two regions: Niantic River and Niantic Bay.

Niantic River was treated as an estuary using the mixing length theory. According to this tidal mixing is represented by a longitudinal dispersion coefficient given by

$$D = \beta u_0^2 \tag{5.8}$$

In the case of irregular geometry we make the assumption that Equation (5.8) still holds. Since the dispersivity tensor $\underline{\underline{D}}$ is diagonal we can evaluate D_{xx} and D_{yy} using the expressions

$$D_{xx} = \beta u_0^2 \tag{5.9}$$

$$D_{yy} = \beta v_0^2 \tag{5.10}$$

where

u_0 and v_0 are the maximum tidal velocities in the x and y direction respectively

Thus the random walk algorithm is given by

$$dx = \left[u + \beta \frac{u_0^2 \partial h}{h \partial x} + \frac{\partial(\beta u_0^2)}{\partial x}\right] dt + \sqrt{2\beta}\, u_0 \sqrt{\Delta t}\, p_i \tag{5.11}$$

$$dy = \left[v + \beta \frac{v_0^2 \partial h}{h \partial y} + \frac{\partial(\beta v_0^2)}{\partial x}\right] dt + \sqrt{2\beta}\, v_0 \sqrt{\Delta t}\, p_i \tag{5.12}$$

u and v in Equations (5.11) and (5.12) are the steady state velocities from the plant operation

The gradients $\frac{\partial h}{\partial x}$, $\frac{\partial h}{\partial y}$, $\frac{\partial(\beta u_0^2)}{\partial x}$, $\frac{\partial(\beta v_0^2)}{\partial y}$ are estimated at every node using a finite element code. For estimating these gradients at intermediate points in the domain, quadratic interpolation functions are used. The deterministic component of the random walk algorithm is estimated using the fifth-order Runge-Kutta method used in ELA (Baptista et al., 1987).

The mixing parameter β in our model for Niantic River was computed using Ketchum's theoretical model. The reason for using Ketchum's model is that it can be used for estimating longitudinal concentration distributions and flushing times in estuaries of irregular geometry and bathymetry. Ketchum's model has been previously used for the prediction of flushing times and longitudinal salinity distributions in Niantic River (Kollmeyer, 1972), but without any field verification. According to Equation (2.43), which was developed for estuaries of uniform crossection, $\beta = T/\pi^2$.

Because β was computed from Ketchum's theoretical model, it was useful to compare modeled residence times with those computed with Ketchum's model. Accordingly, Ketchum's expression (Equation 2.28) was used to compute residence times corresponding to the location of dye injection from Study 1 conducted in Niantic River in 1988 (Figure 18). (Bathymetric data were obtained from Kollemyer, 1977; see Section 5.8.1 for a detailed description of the dye study.) The computed residence time was 15 days and the model segmentation is shown in Figure 24.

This theoretical estimate can be compared with our model flushing time in the following way. Several particles are released at the injection point. For each of these particles a residence time is recorded. By residence time we mean the time it takes for a particle to leave the estuary (pass south of Mijoy Dock). As flushing time of the estuary we designate the mean of the resulting residence time distribution. The flushing time from the model MILL (calibrated by using Ketchum's model) is equal to

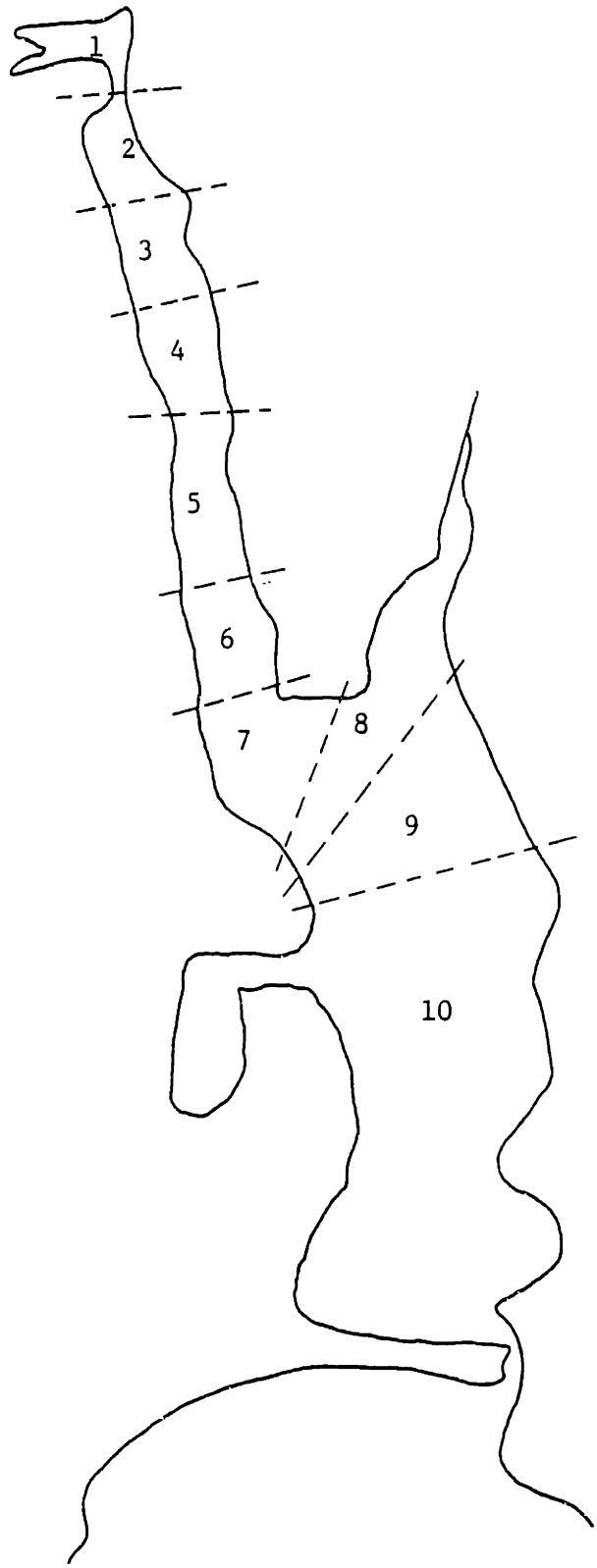

Figure 24 Estuary segmentation using Ketchum's model

14 days. The small difference may be due to the fact that we are using an ideal geometry for calibrating the parameter β, while for estimating the flushing time we are using the actual irregular geometry and bathymetry.

Niantic Bay was assumed to have a constant dispersion coefficient $D_{xx} = D_{yy} = D$. The value of 21.9 ft^2/sec from Saila's model was used. The advective velocities u and v were obtained from the superposition of the tidal velocities and the velocities from the power plant operation.

Accordingly this the random walk algorithm is given by

$$dx = udt + \sqrt{2D}\sqrt{\Delta t}\, p_i \tag{5.13}$$

$$dy = vdt + \sqrt{2D}\sqrt{\Delta t}\, p_i \tag{5.14}$$

5.6 Modeling Larval Behavior

5.6.1 General

Larval growth and behavior are modeled according to data provided by NUEL. This information is based on field data collected from Niantic River and Bay and includes

- estimates of the temporal and spatial distribution of yolk-sac larvae from which hatching rates may be estimated
- daily growth rates as a function of temperature
- average weekly water temperature
- daily larval survival rates as a function of age
- diel and tidal behavioral responses as a function of larval size

- mortality due to entrainment as a function of larval size

The general approach followed in the simulations is the following. Particles are released at a fixed rate from several points in space that approximate a spatial distribution of hatching of winter flounder larvae. Each particle represents a certain number of larvae corresponding to the temporal distribution of hatching winter flounder larvae. The larvae in each "larval cohort" represented in one particle may have one of the following fates:

- Die because of natural mortality.
- Go through the intake. In this case, if the length of the larvae in the cohort is less than 7 mm we have 100% mortality so we stop tracking the particle. Otherwise we have 20% mortality so the particle is placed in the discharge plume and we continue tracking the particle that now represents 20% fewer larvae than in the timestep before entrainment.
- Go out of the model boundary (i.e., are flushed out) in which case tracking stops.
- Reach the length of 8 mm. In this case larvae are considered juveniles and we stop tracking them.

According to the above, if we designate the survival factor SF(i,t) as the fraction of larvae in cohort i which are alive and in the domain at time t after they were born, then SF(i,t) is given by the expression

$$SF(i,t) = NSF \cdot ESF \cdot FSF \cdot JSF \tag{5.15}$$

where

NSF is the fraction not dead due to natural mortality

ESF is the entrainment survival rate. It can take the following values:

ESF = 1 if the particle representing the larvae cohort did not go through the intake

ESF = 0 if the particle representing the larvae cohort goes through the intake and the length of the larvae is less than 7 mm

ESF = $(0.8)^n$ if the particle representing the larvae went through the intake n times and the length of the larvae was more than 7 mm the first time it was entrained

FSF is "flushing" survival rate that takes the values 0 or 1 if the particle has or has not been flushed out of the domain

JSF is the "juvenile" survival factor that takes the value 0 if the larvae reach the length of 8 mm; otherwise it is equal to 1

5.6.2 Larval Hatching Distribution

Estimated larval hatching was based on the abundance of yolk-sac larvae (larvae less than ten days old) in the Niantic River in Stations A, B, C (Figure 18) during 1984-87. Abundance is expressed as density/500m^3. Figure 25 shows the average temporal abundance of yolk-sac larvae for the four-year period for Stations A, B, and C.

Daily larval hatching rates were estimated from daily abundance data according to the following procedure. If we call N(i,10) the cumulative number of larvae born per 500 m^3 on the days j where i-10 < j < i and alive on day i then

$$N(i,10) = \sum_{ll=1}^{10} B(i - ll)e^{-kll} \qquad (5.16)$$

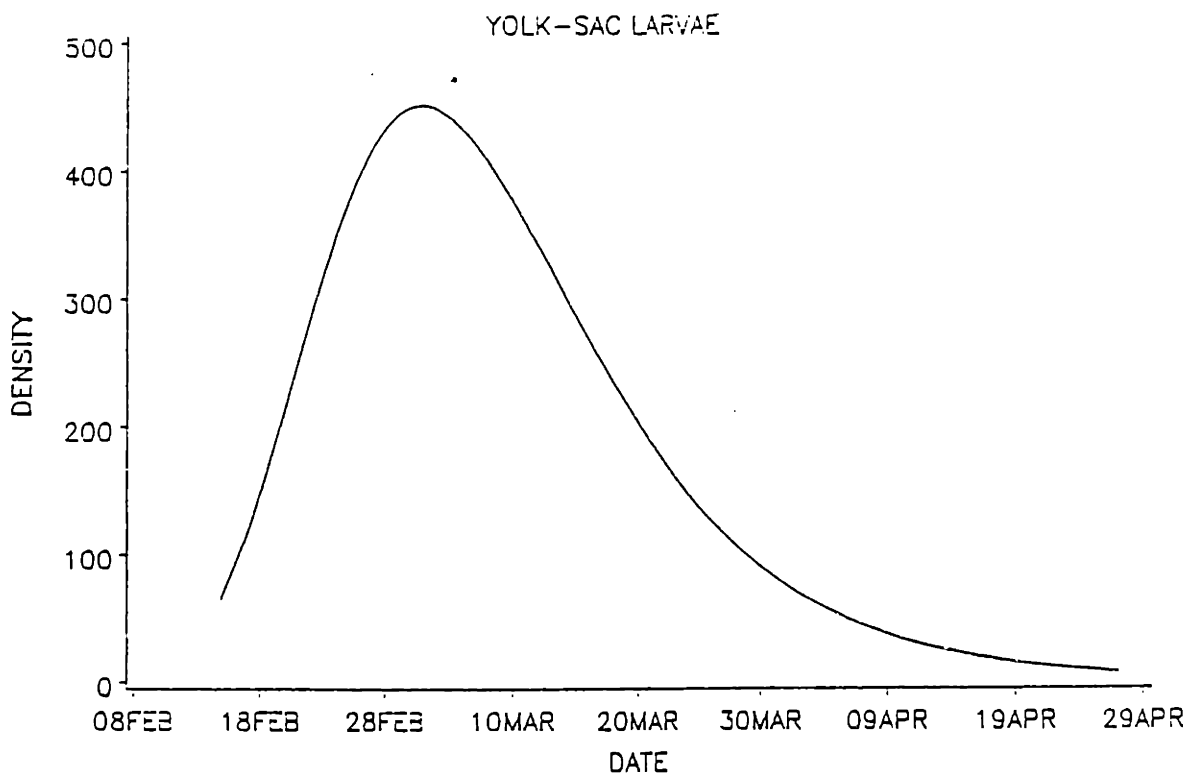

Figure 25 Average temporal abundance of yolk-sac larvae for the period 1984-87 for stations A, B, and C (data from NUEL)

where

B(i-ll) is the number of larvae born on day i - ll

k is the natural mortality rate for larvae less than ten days old. According to data k = $0.105d^{-1}$ (NUEL, personal communication).

If we approximate B(i-ll) in Equation (5.16) by B(i-5) Equation (5.16) becomes

$$N(i,10) = B(i-5)\sum_{ll=1}^{10} e^{-kll} \tag{5.17}$$

and after some algebraic manipulations

$$N(i,10) = B(i-5)\frac{e^{-k} - e^{-11k}}{1 - e^{-k}} \tag{5.18}$$

Solving for B(i) we get

$$B(i) = 0.17N\left[\left[\frac{i}{10} + 1\right]10\right] \tag{5.19}$$

i.e., the daily birth rate is about 17% of the abundance ten days later.

In the simulations a 3-hr timestep is used so according to Equation (5.19) the number of larvae b(t) born in every 3-hr timestep is given by

$$b(t) = 0.0213N\left[\left[\frac{i}{10} + 1\right]10\right] \tag{5.20}$$

Figure 26 shows the average birthrates (number of larvae born per day in 500 m^3) for the period 1984-87 for Stations A, B, and C.

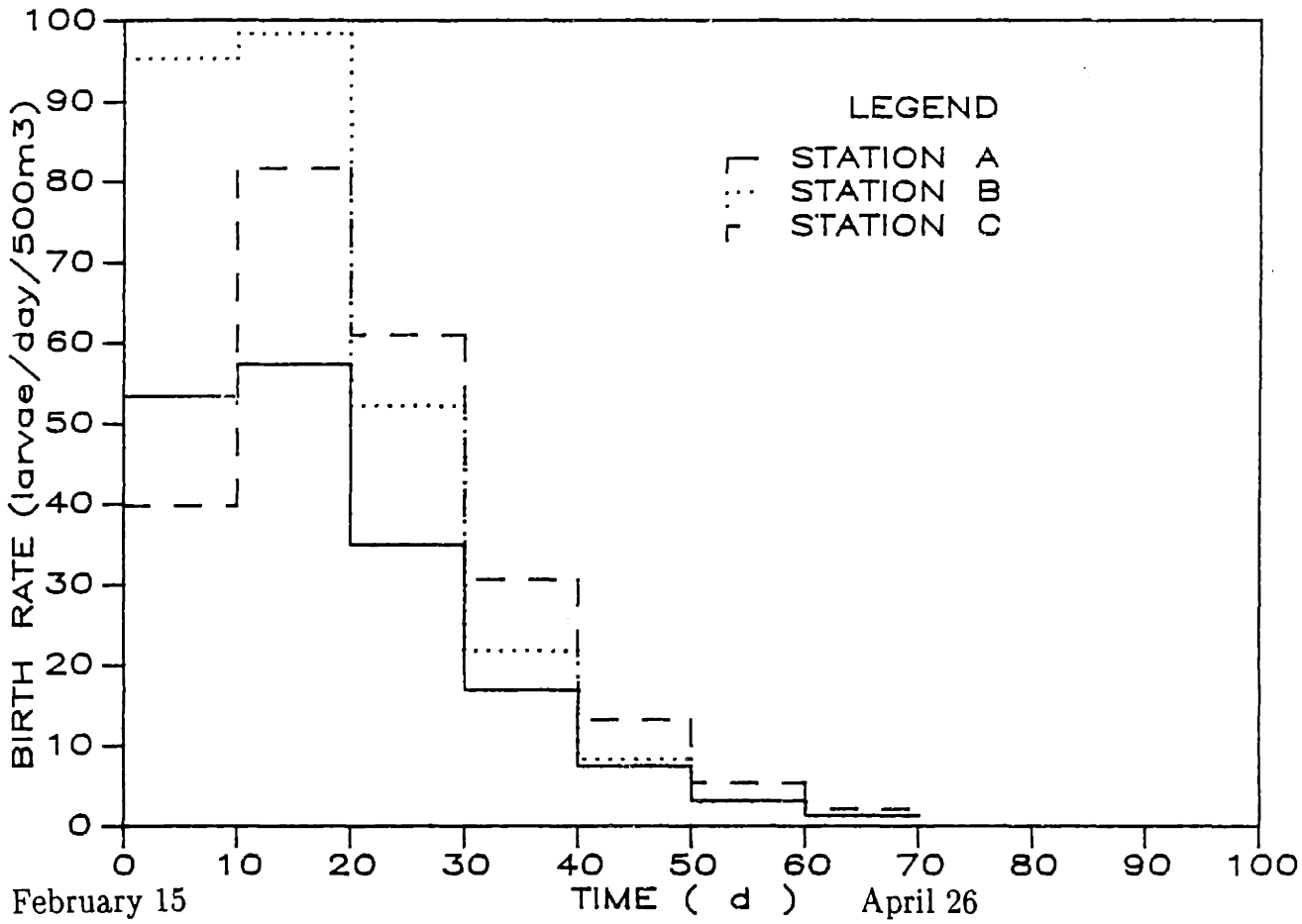

Figure 26 Averaged birthrates (number larvae born per 3 hr in 500 m^3) for the period 1984-87 for Stations A, B, and C

5.6.3 Larval Growth Rate

Annual larval growth rates were calculated by NUEL from twelve years (1976-87) of entrainment data and the annual rates were found to be correlated to seasonal water temperatures. According to these data the growth rate in units of mm/day is given as a function of temperature by the following expression

$$\text{mm/day} = \frac{dL}{dt} = -0.0145 + 0.0134T \tag{5.21}$$

where T is given in ° C.

It was assumed that the length of the larva at the time it is born is 3 mm.

5.6.4 Daily Survival Rates

According to data the average daily survival factor was taken equal to 0.9 for larvae of length between 3-4 mm and 0.97 for longer lengths.

5.6.5 Diel Behavioral Response

According to a comparison of samples collected during daylight and at night, larvae become less available to capture during daylight as they increase in length. Larvae begin to develop this diel behavior at about 5 mm in length. The proportion of larvae (y) available for tidal transport during daylight as a function of length is given by the expressions

$$\begin{aligned} y &= 1.0 \qquad\qquad (L < 5\text{mm}) \\ y &= 0.985 - 0.094 \cdot L \quad (L > 5\text{mm}) \end{aligned} \tag{5.22}$$

This diel behavior was apparent at all stations in the Millstone area except at Station C (Figure 18). Larvae diel behavior was simulated as follows. The displacement for larvae of length more than 5 mm that are located in any area in our domain except near Station C was multiplied by the factor y. So Equations (5.11) and (5.12) become

$$dx = y\left[u + \beta u_0^2 \frac{1}{h}\frac{\partial h}{\partial x} + \frac{\partial(\beta u_0^2)}{\partial x}\right]dt + y\sqrt{2\beta}\, u_0\sqrt{\Delta t}\, p_i \tag{5.23}$$

$$dy = y\left[v + \beta v_0^2 \frac{1}{h}\frac{\partial h}{\partial y} + \frac{\partial(\beta v_0^2)}{\partial y}\right]dt + y\sqrt{2\beta}\, v_0\sqrt{\Delta t}\, p_i \tag{5.24}$$

5.6.6 Tidal Behavioral Response

Larvae in Station C also show vertical migration, but as a function of tidal stage rather than light: they fall to the bottom during ebb and rise within the water column during flood tide. Again larvae begin to develop this behavior at about 5 mm in length. The proportion of larvae y available for transport during an ebb tide is given by the expression

$$\begin{aligned} y &= 1.0 && (L < 5\text{mm}) \\ y &= 1.696 - 0.221 \cdot L && (L > 5\text{mm}) \end{aligned} \tag{5.25}$$

Larvae tidal behavior was simulated by diel behavior, i.e., in the same manner as multiplying the advection and random-walk components by the factor y during ebb for larvae of length more than 5 mm that are located in Station C (Figure 18).

5.6.7 Alternative Solution for Millstone Case Study

Before proceding, it is worth comparing our random walk model with a concentration or "diffusivity" model which could have been used. The question is what "concentration" represents. It can represent mass of larvae per unit volume of water or

number of larvae per unit volume of water. In this case number of larvae per unit volume should be used since we are not interested in the mass of larvae in the domain. The governing equation is Equation (3.28) or its nonconservative form

$$\frac{\partial c}{\partial t} + u\frac{\partial c}{\partial x} + v\frac{\partial c}{\partial y} = \frac{1}{h}\frac{\partial}{\partial x}\left[hD_{xx}\frac{\partial c}{\partial x}\right] + \frac{1}{h}\frac{\partial}{\partial y}\left[hD_{yy}\frac{\partial c}{\partial y}\right] + Q \tag{5.26}$$

The problem using this method, as written, is that larvae behavior can not be modeled. Since larvae show strong behavioral patterns this approach is not appropriate.

Larvae behavior *can* be taken into account using a concentration model if a group of equations of form (5.26) is used

$$\frac{\partial c_i}{\partial t} + u\frac{\partial c_i}{\partial x} + v\frac{\partial c_i}{\partial y} = \frac{1}{h}\frac{\partial}{\partial x}\left[hD_{xx}\frac{\partial c_i}{\partial x}\right] + \frac{1}{h}\frac{\partial}{\partial y}\left[hD_{yy}\frac{\partial c_i}{\partial y}\right] + Q_i \qquad i = 1, \ldots n \tag{5.27}$$

where c_i is the number of larvae of length group i per unit volume of water $L_{li} < L_i < L_{ui}$, L_{li} and L_{ui} being the lower and upper limit of length of group i. As mentioned before we are interested in larvae of length L = 3 mm (length of larvae at the spawning time) to length L = 8 mm. It is enough if we take five groups, i.e., n = 5 (1-mm increments).

The term Q_i is equal to

$$Q_i = k_{i-1}c_{i-1} - k_ic_i + a\cdot\sum_{i=1}^{1} Q_1\cdot c_i\,\delta(x-x_1)(y-y_1) + d_ic_i \tag{5.28}$$

where

$k_{i-1}c_{i-1}$ is a source term and represents the number of larvae per unit volume per time that reach length L_{li}

k_ic_i is a sink term and represents the number of larvae per unit volume per time, that reach length L_{ui}

$a \sum_{i=n}^{l} Q_lc_i\delta(x-x_l)(y-y_l)$ is a sink term and represents the entrainment of larvae through the cooling station

a is equal to 1 if $L_{li} < 5$ mm and equal to 0.2 of $L_{li} > 5$ mm

d_ic_i is a sink term for the natural mortality

The tidal and diel behavior would be simulated in the same way as in the random walk model.

This method was not applied so a comparison can not be made with the random walk method. Generally we could summarize the disadvantages of this method as follows:

- the representation of source and sink terms is easily modeled in the random walk model

- the computational effort increases linearly with n whereas in the random walk model the length of each larvae is computed exactly without any additional computational effort

5.7 Model Simulations

5.7.1 Simulations

Three simulations were made using the 2-D random walk model. These simulated the fate of larvae born in Stations A, B, and C, respectively. The simulation time was equal to 131 days for each simulation covering the period between February 16, when larvae spawning starts, to June 26, when the last larvae spawned have become juveniles.

Particles were released over a two-month period (February 16 to April 26 which equals the spawning period) at a rate of 1 particle per timestep. The timestep was taken equal to 3h. Every particle represented the number or larvae born at that station in a 3-h period per 500 m^3. The birth rate distribution was calculated following the procedure described in Section 4.2 (Figure 26). Every particle was advected and diffused according to the algorithm described in Section 5.5. The diffusion parameter β for Niantic River was calculated according to Equation (2.43) to be equal to

$$\beta = \frac{T}{\pi^2} = \frac{12.4h}{\pi^2} = 1.25h \tag{5.29}$$

5.7.2 Input

The model requires the following input

1 Flow field data. These data are given from the circulation model TEA (Section 5.4).

2 The diffusion parameter β, the simulation time (131 days in this case), and the time over which particles are released which equals the time that larvae are spawned (70 days in this case).

3 Number of larvae/500 m^3 spawned every timestep. Spatially averaged temperature values at every timestep, and data concerning larvae behavior.

5.7.3 Output

The output of every run includes the following information:

At each timestep the position of all particles released through that time is recorded. In addition, at the end of the simulation the following information is summarized for each particle.

- #: number of the particle
- DOB: date of birth
- COHORT: Number of larvae/500 m^3 that are represented by the particle at the time the particle is released
- NSF: NSF of the cohort at the end of the simulation (Equation (5.15))
- FSF: flushing survival factor. FSF can take the following value: 0 if the particle was flushed out of the domain or 1 if the particle was not flushed out
- ISF: intake survival factor. ISF can take the following values: 0 if the particle was entrained when the length of the larvae represented was less than 7 mm, 1 of the particle was not entrained, $(0.8)^n$ if the particle was n times entrained after the larvae reached the length of 7 mm.
- NENT: number if times particles has gone through the entrainment (Figure 21)
- AGE: age of particle at the time when the program stopped tracking it

- LENGTH: length of the particle at the end of its simulation. LENGTH is less than 8 mm
- #LEFT: number of larvae a particle represents at the end of the simulation
- DATE: last date of simulation for the particle
- LOC: location of particle when the program stopped tracking it (Section 4.1)

Figure 27 shows a page of the output file from the simulation of Station A.

After this list of information for every particle, cumulative statistics of larval fate are given. The length distribution is given for larvae entrained, flushed from the domain, and still in the domain at the end of the simulation. Also the number of larvae that died due to natural mortality and the number of larvae that matured are given.

5.7.4 Comparison with Data

Verification of the model was attempted by comparing the length distribution of the larvae entrained resulting from the model simulation to the length distribution data of the larvae entrained provided by the NUEL (personal communication). Table 1 shows the two length distributions. It is clear that the two length distributions are very different: the model simulations for year 1984-87 indicate that about 92% of the entrained larvae have a length between 3 mm and 4 mm, while the data from NUEL show only 12.4% of larvae entrained have a length between 3 mm and 4 mm. There is also a corresponding discrepancy in the times of peak entrainment with model times being much quicker than observed times. (In fact, the agreement between dates of peak abundance and mean larval length is quite good, confirming the growth relationship

#	DOB	COHORT	NSF	FSF	ISF	NENT	AGE	LENGTH	# LEFT	DATE	LOC	
31	18. FEBR	18.	11.90	0.03	0.00	1.00	0	34.13	4.1	0.000	24. MARCH 21.	-1576.20	-1036.63
#	DOB	COHORT	NSF	FSF	ISF	NENT	AGE	LENGTH	# LEFT	DATE	LOC	
32	18. FEBR	21.	11.90	0.04	1.00	0.00	0	30.25	3.9	0.000	21. MARCH 3.	2414.88	2445.98
#	DOB	COHORT	NSF	FSF	ISF	NENT	AGE	LENGTH	# LEFT	DATE	LOC	
33	19. FEBR	0.	11.90	0.07	0.00	1.00	0	25.50	3.7	0.000	16. MARCH 12.	-1191.69	-534.46
#	DOB	COHORT	NSF	FSF	ISF	NENT	AGE	LENGTH	# LEFT	DATE	LOC	
34	19. FEBR	3.	11.90	0.04	0.00	1.00	0	31.13	3.9	0.000	22. MARCH 6.	-1564.43	-1065.91
#	DOB	COHORT	NSF	FSF	ISF	NENT	AGE	LENGTH	# LEFT	DATE	LOC	
35	19. FEBR	6.	11.90	0.09	0.00	1.00	0	23.13	3.7	0.000	14. MARCH 9.	-1492.81	-923.02
#	DOB	COHORT	NSF	FSF	ISF	NENT	AGE	LENGTH	# LEFT	DATE	LOC	
36	19. FEBR	9.	11.90	0.01	1.00	1.00	0	80.38	8.0	0.087	10. MAY 18.	1274.22	6378.43
#	DOB	COHORT	NSF	FSF	ISF	NENT	AGE	LENGTH	# LEFT	DATE	LOC	
37	19. FEBR	12.	11.90	0.79	0.00	1.00	0	2.38	3.1	0.000	21. FEBR 21.	-1036.27	862.33
#	DOB	COHORT	NSF	FSF	ISF	NENT	AGE	LENGTH	# LEFT	DATE	LOC	
38	19. FEBR	15.	11.90	0.81	0.00	1.00	0	2.13	3.1	0.000	21. FEBR 18.	-2544.36	-2516.09
#	DOB	COHORT	NSF	FSF	ISF	NENT	AGE	LENGTH	# LEFT	DATE	LOC	
39	19. FEBR	18.	11.90	0.85	0.00	1.00	0	1.63	3.0	0.000	21. FEBR 9.	-1349.90	574.41
#	DOB	COHORT	NSF	FSF	ISF	NENT	AGE	LENGTH	# LEFT	DATE	LOC	
40	19. FEBR	21.	11.90	0.28	1.00	0.00	0	12.38	3.3	0.000	4. MARCH 6.	2429.71	2382.93
#	DOB	COHORT	NSF	FSF	ISF	NENT	AGE	LENGTH	# LEFT	DATE	LOC	
41	20. FEBR	0.	11.90	0.28	1.00	0.00	0	12.13	3.3	0.000	4. MARCH 3.	2561.23	2261.62
#	DOB	COHORT	NSF	FSF	ISF	NENT	AGE	LENGTH	# LEFT	DATE	LOC	
42	20. FEBR	3.	11.90	0.52	1.00	0.00	0	6.38	3.2	0.000	26. FEBR 12.	2594.93	2229.81
#	DOB	COHORT	NSF	FSF	ISF	NENT	AGE	LENGTH	# LEFT	DATE	LOC	
43	20. FEBR	6.	11.90	0.01	0.00	1.00	1	76.50	7.6	0.000	7. MAY 18.	11.64	-3018.74

Figure 27 Model output

Table 1a

Comparison of Length Distribution of Entrained Larvae by Station (simulation) to Data from NUEL
(percent)

Sta	3-4	4-5	5-6	6-7	7-8
A	85.2	5.4	7.1	2.2	0.1
B	93.5	2.8	2.2	1.6	0.1
C	94.6	3.0	1.2	1.1	0.1
ave.	91.7	3.5	3.0	1.7	0.1
Data	12.4	18.6	24.3	23.1	14.9

Table 1b

Total Number of Larvae Entrained

Sta	Total number ($\times 10^3$)	Percent of larvae hatched
A	305	5.2
B	802	6.0
C	377	8.8
total	1484	6.7
Data	98000	490.

used in the model.) Finally, and importantly, the number of larvae entrained predicted by the model is considerably lower than the number indicated by data (Table 1b).

There appear to be three possibilities for explaining the early entrainment times (and hence "short" lengths) of the model. The first possibility is that the simulated larval residence times within the estuary are too small. This could be due to one or both of the following reasons:

a) The random walk model was calibrated using Ketchum's tidal mixing model. This model is an idealized 1-D model that is based on the assumption of complete mixing of water within every volume segment. It requires validation for complex real estuary mixing.

b) The larval behavior data were not correct.

The second possibility is that some of the entrained larvae were imported from other areas and do not come from Niantic River. Since these other areas are further away, the time of travel would be longer, which could explain why observed entrainment times exceed our simulated times. It would also explain the undersimulation of entrained larvae.

The third possibility is that the mortality rates (see Section 5.6.4) are too high. Larvae mortality would allow older larvae to survive, thus shifting the entrainment distribution to longer lengths. Table 2a shows the length distribution and Table 2b the total number of the larvae entrained for zero mortality rate. In this case the length distribution is more uniform but still there is a maximum (59.8%) at the lower lengths (3-4 mm). From the above we can conclude that a discrepancy in the mortality rates does not explain alone the difference in the resulting length distributions.

Table 2a

Length Distribution of Entrained Larvae by Station (simulation) with *zero* mortality rate (percent)

Station	3-4	4-5	5-6	6-7	7-8
A	44.4	12.3	27.2	14.8	1.3
B	66.2	11.4	9.4	11.2	1.8
C	63.8	14.7	7.9	9.3	4.3
average	59.8	12.8	13.5	11.5	2.5

Table 2b

Total Number of Larvae Entrained with *zero* mortality rate

Station	Total number ($\times 10^3$)	Percent of larvae hatched
A	1507	25.7
B	2728	20.4
C	987	23.0
total	5222	21.0

The first step taken to diagnose the discrepancy was to conduct a dye study within Niantic River. The purpose of this study was to measure the flushing time and hence calibrate the random walk transport model of the estuary. This flushing time could then be compared to the flushing time resulting from Ketchum's model. An additional dye study was also conducted to estimate transport between the estuary mouth and the intake.

5.8 Tracer Studies

Two dye studies were conducted in the Niantic River area during the period November 16, 1988, through January 11, 1989.

5.8.1 Dye Study 1

The motivation for the first study was the estimation of the estuary flushing time. As mentioned in Section 5.7.4, the length distribution of entrained larvae that resulted from the model simulation was different from the actual data. The random walk transport model used for these simulations was calibrated using an idealized model for tidal mixing in an estuary. With data from a dye study, the model could be calibrated from field data.

Dye Study 1 was conducted from November 16 through December 15, 1988. During this period 359 lbs of 20% Rhodamine WT dye solution was injected from a location near the head of the river (Figure 18). So dye was injected at an average rate of 0.0468 kg of pure dye per hour. The following data were measured:

- Continuous concentrations during this period at the Mijoy Dock (Figure 28) and the Millstone Quarry

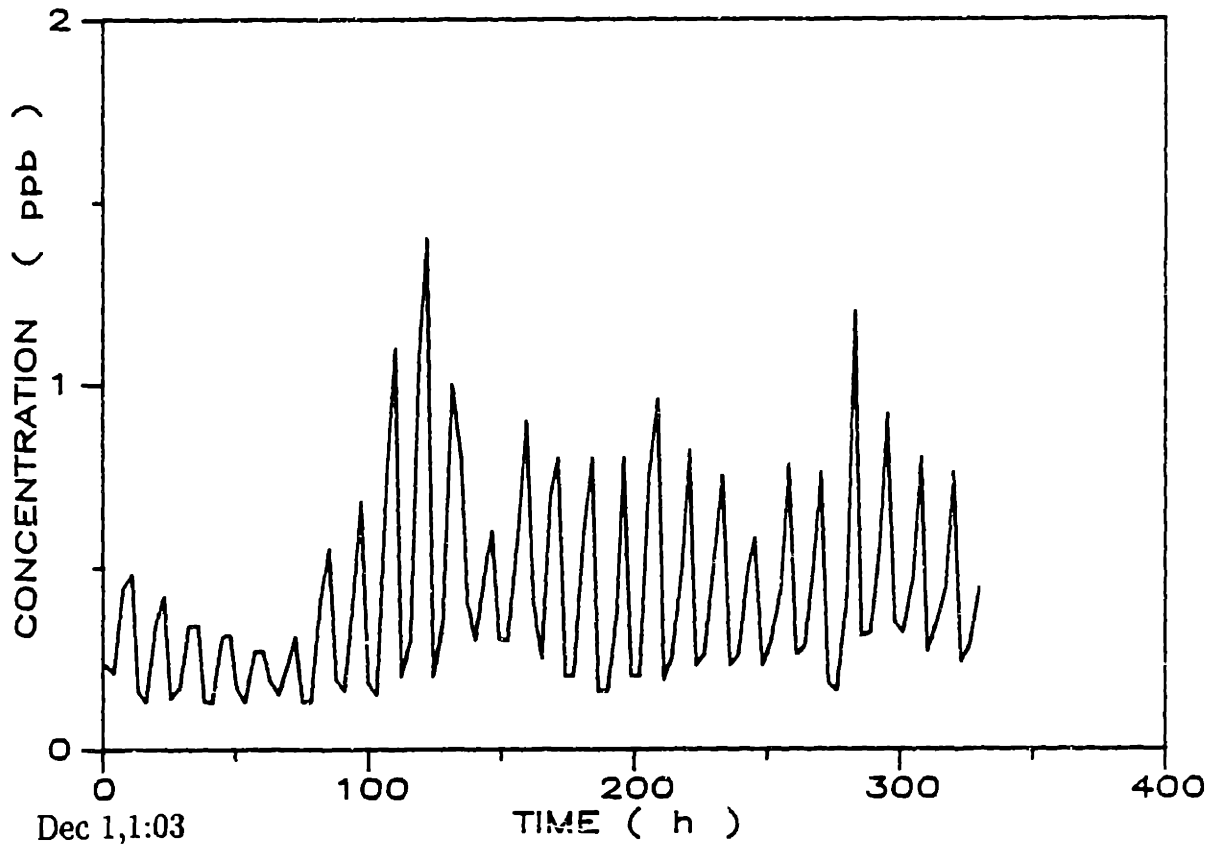

Figure 28 Dye concentrations at the Mijoy Dock in the period from December 1 to December 15

- Transverse concentrations across the river at 2-ft depth on high slack (Figure 29) and low slack (Figure 30) on December 15, 1988
- Vertical profiles of concentration at Stations 1 through 11 (Figures 29, 30) at high slack (Figure 31) and low slack (Figure 32) on December 15, 1988

Figure 28 shows dye concentrations at Mijoy for the period between December 1, 1988, and December 14, 1988. From Figure 28 we can assume that quasi-steady-state conditions were reached after December 5, 1988. As a check, we can perform the following mass balance. If we designate as c the dye concentration at Mijoy and Q the flow at Mijoy then the integral

$$\int_0^T Q \cdot c \cdot dt \tag{5.30}$$

represents the net mean of dye that is flushed out of the river during one tidal cycle T. If dye is conservative this mass should be equal to the mass of dye injected during one tidal cycle m_{in} which is equal to

$$m_{in} = 0.0468 \frac{kg}{h} \cdot 12.4h = 0.58 \text{ kg pure dye} \tag{5.31}$$

We approximate the time variations of dye concentration at Mijoy varies as

$$c = \bar{c} + c_{max}[\sin(\omega t - \phi)] \tag{5.32}$$

and the flow at Mijoy varies as

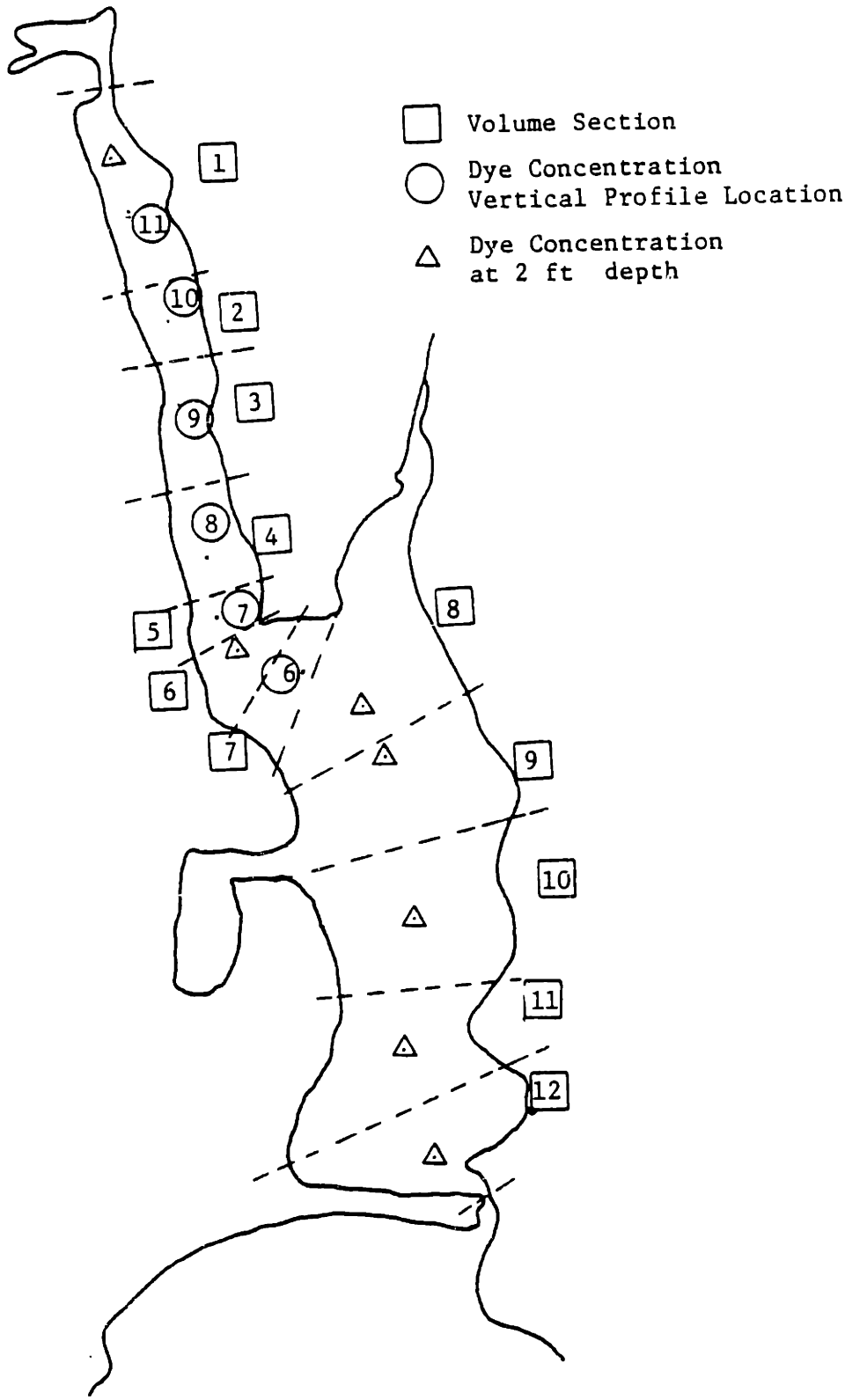

Figure 29 Locations of transverse and vertical concentration measurements at high slack on December 15, 1988

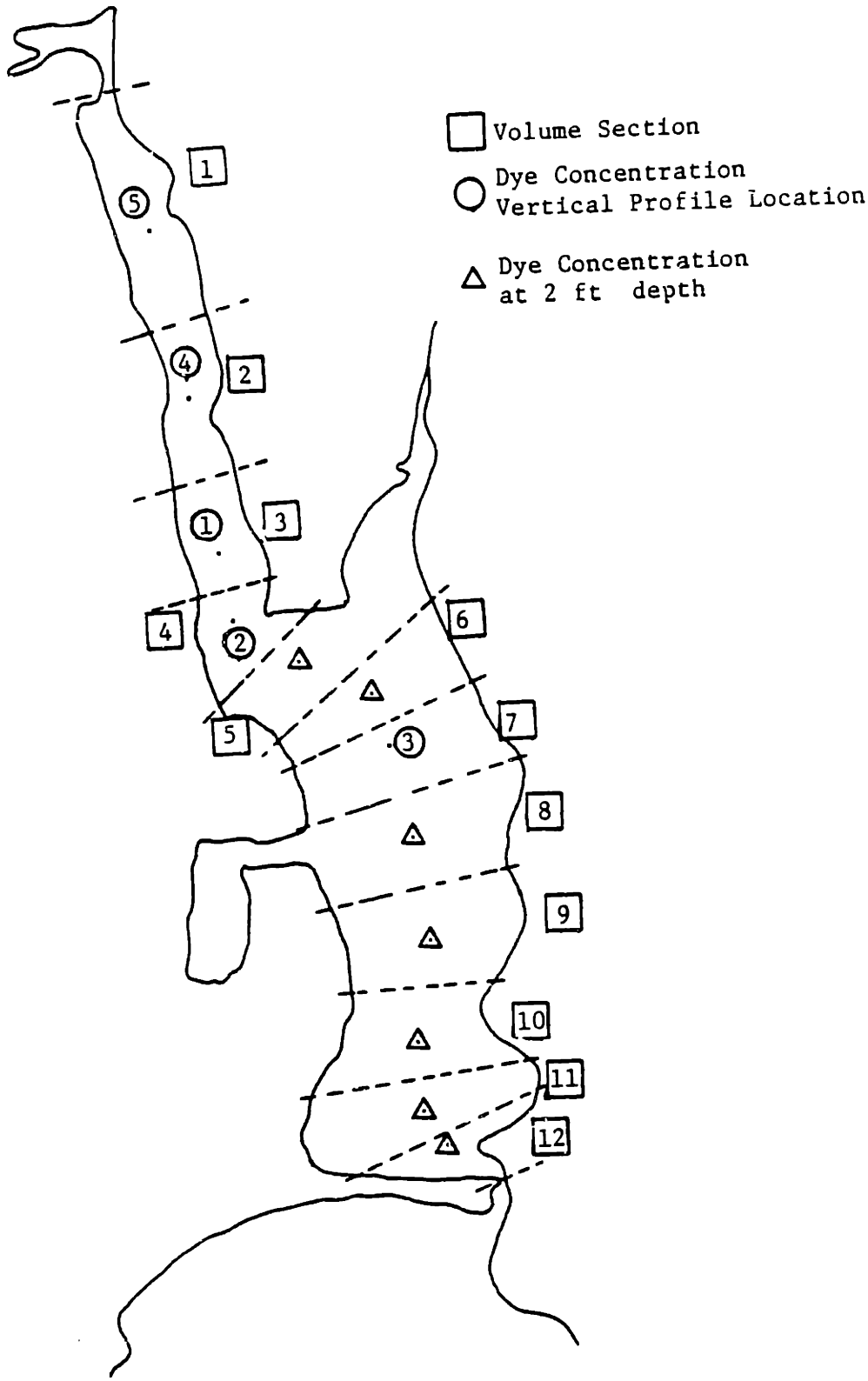

Figure 30 Locations of transverse and vertical concentration measurements at low slack on December 15, 1988

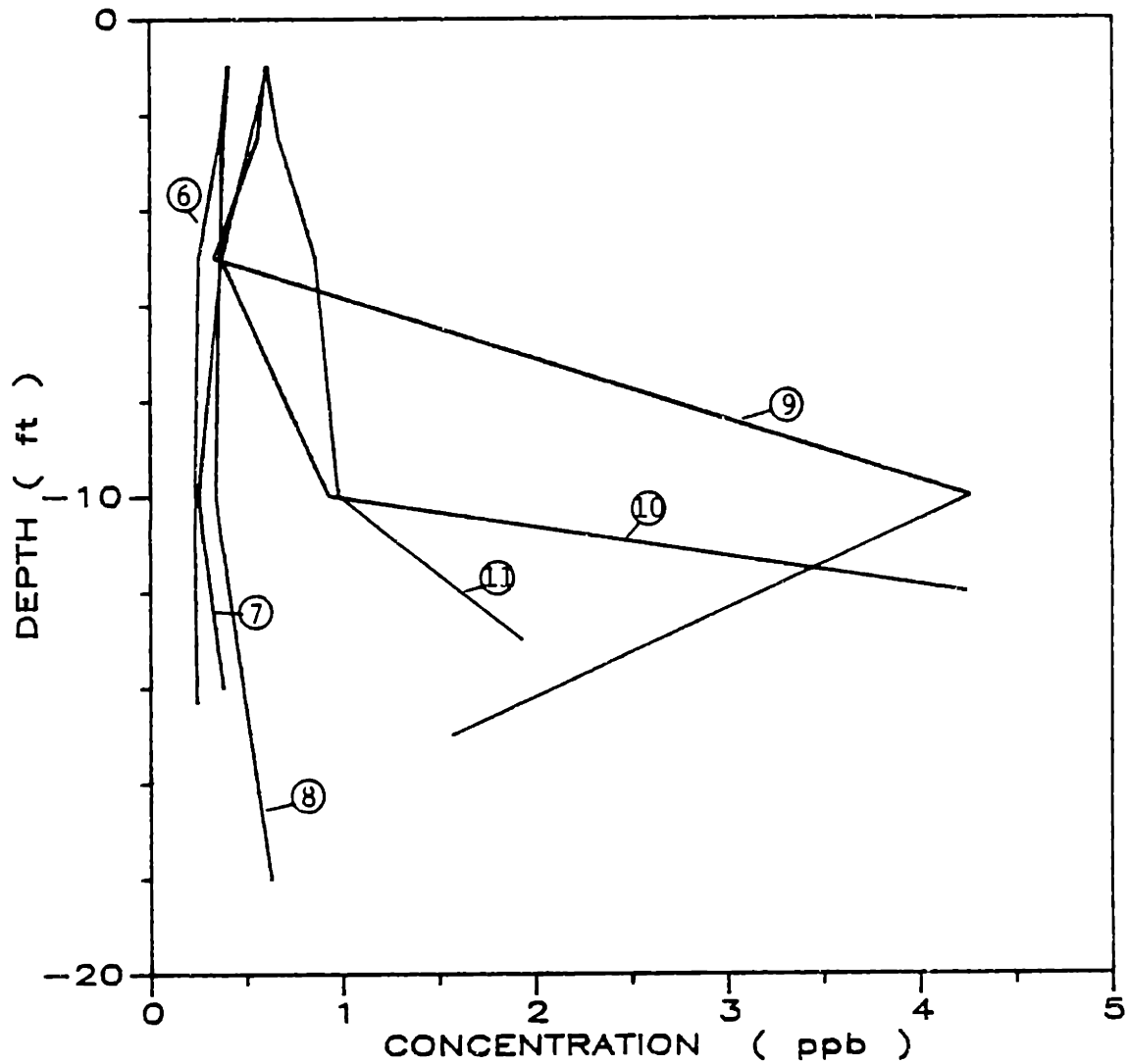

Figure 31 Vertical profiles of concentration at high slack on December 15, 1988

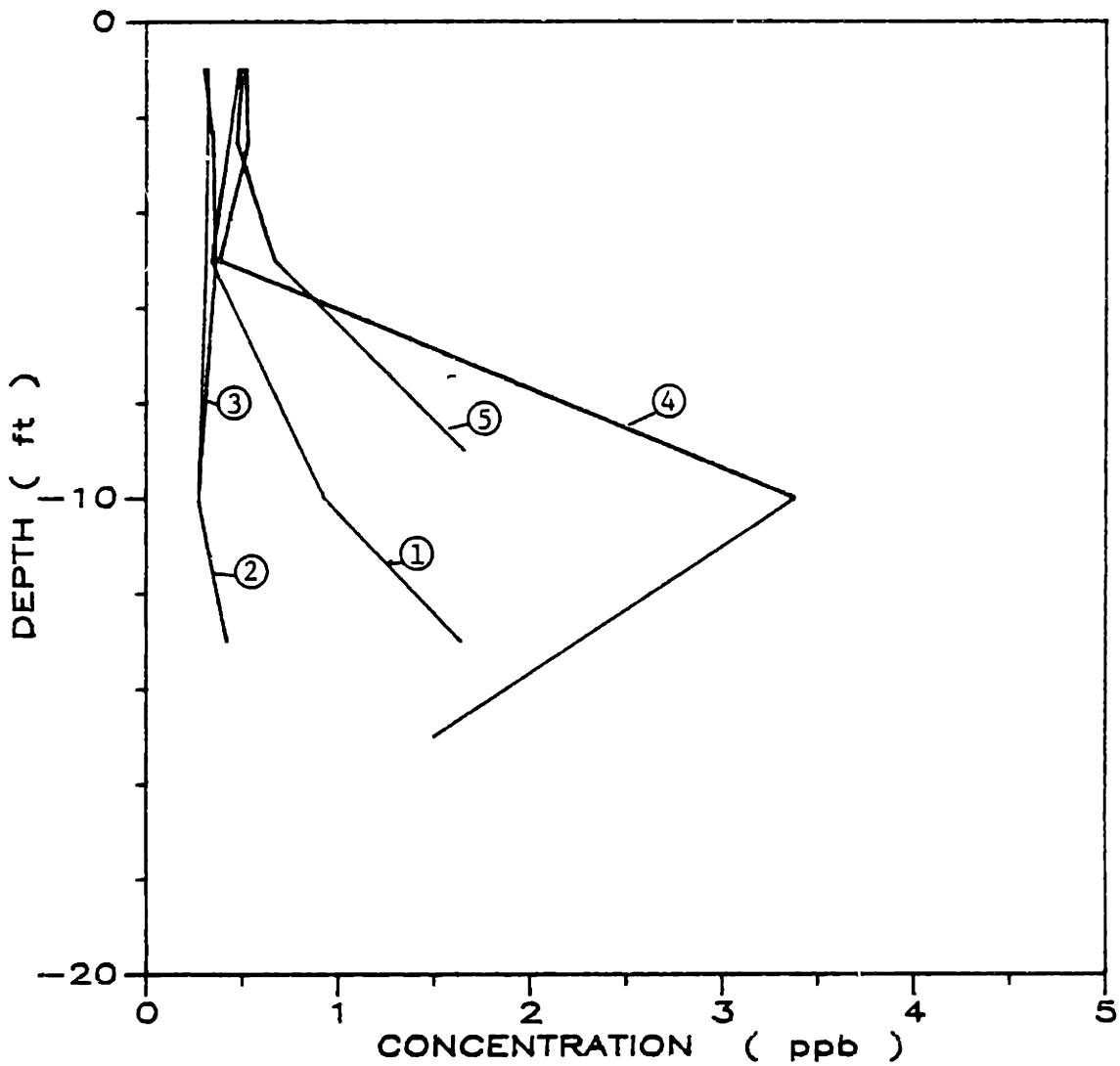

Figure 32 Vertical profiles of concentration at low slack on December 15, 1988

$$Q = Q_{max} \cdot \sin\omega t \tag{5.33}$$

The value of Q_{max} is found by integrating Equation (5.33) over the duration of ebb flow and setting the result equal to the average tidal prism. The unknown parameters of Equation (5.32) are determined by a least squares regression analysis between the theoretical concentration variation described by Equation (5.32) and the observed variation at Mijoy. The result is: $\bar{c} = 0.49$ ppb; $c_{max} = 0.3266$ ppb; $\phi = 0.331$ rad. Equation (5.32) is plotted using these parameters in Figure 33. According to Equation (5.32), in order to find the mass of dye flushed out we have to estimate the integral

$$\int_0^T Q_{max} \cdot \sin\omega t \cdot [\bar{c} + c_{max} \cdot \sin(\omega t - \phi)]dt \tag{5.34}$$

With the above parameters found by the regression analysis, the evaluation of Equation (5.30) equals 0.7 kg which is actually 21% larger than the mass injected. This agreement is not bad for a study of this magnitude and the discrepancy could easily be attributed to:

- discrepancies in the measurements and/or
- background concentrations in the estuary
- tendency for the least squares analysis to overestimate the amplitude of the sinusoidal concentration distribution in arriving at parameters

Using the transverse concentrations across the river and the vertical concentration profiles, the flushing time of the estuary was calculated. Flushing time for our purposes is defined as the mean time required to replace the existing dye in an estuary at a rate

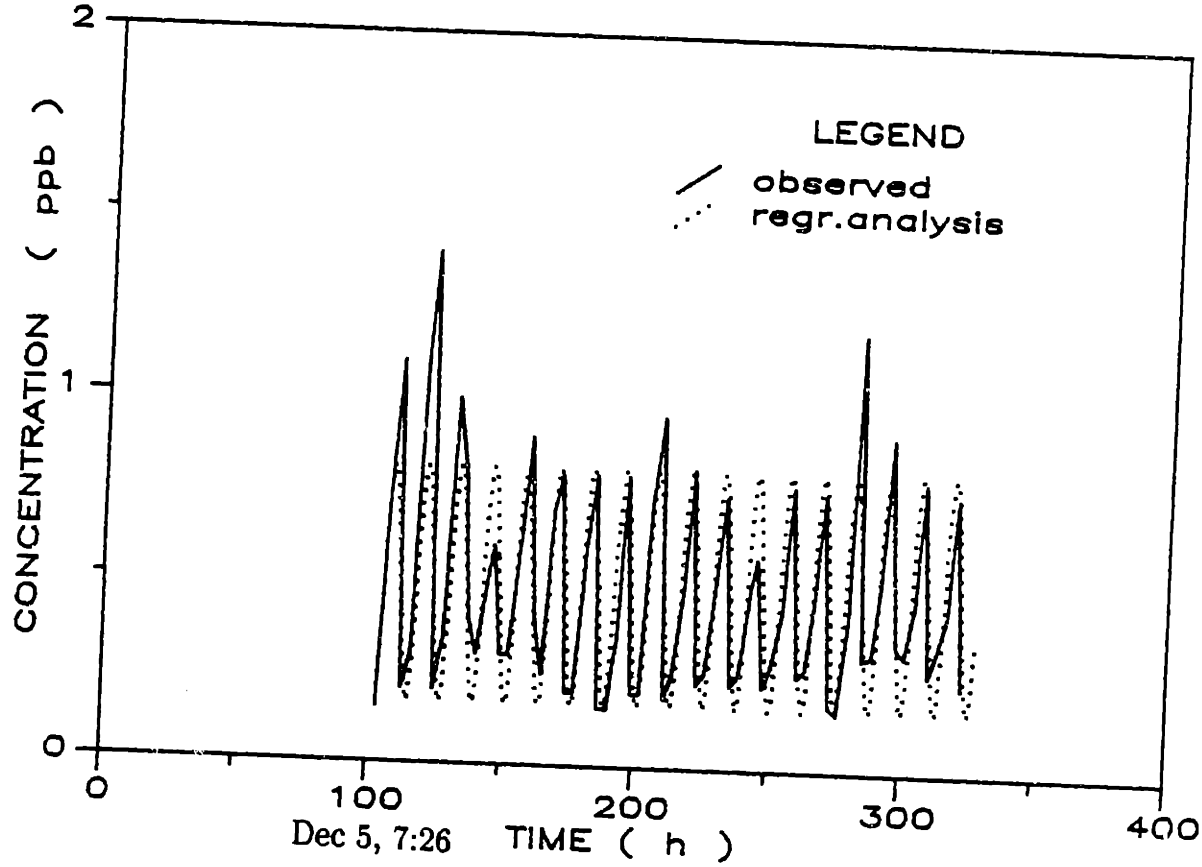

Figure 33 Comparison between steady-state concentration data at Mijoy Dock and results from regression analysis

equal to the dye injection rate. If we designate the dye injection rate by W (mass/time) and the total dye mass in the estuary after a tidal steady state has been reached by V_d the flushing time t_{res} according to Equation (2.18) will be

$$t_{res} = \frac{V_d}{W} \tag{5.35}$$

If we designate the dye concentration at any given location in the estuary as c, the mass of dye in the estuary is given by the integral

$$V_d = \int c \, dV \tag{5.36}$$

where the integral is taken over the entire volume of the estuary.

The following remarks can be made regarding the concentration data used to evaluate Equation (5.36). Concentrations at every cross section show little variation which means that we have complete transverse mixing. In the vertical profiles at sections upstream from Sandy Pt. (Sections 11, 10, 9, 8 for high slack and Sections 5, 4, 1 for low slack), near-bottom concentrations are up to a factor of 10 higher than surface concentrations. This probably occured because the dye is negatively buoyant, so close to the injection point it fell to the bottom. In the sections that are located south of Sandy Point (i.e., Sections 7, 6 for high slack (Figure 29) and Sections 2, 3 for low slack (Figure 30)) concentration is essentially vertically uniform. So we conclude that we have complete vertical mixing in the lower part of the estuary that is located beneath Sandy Point.

The following technique was used to evaluate V_d (Equation 5.36). The river was divided into n sections, corresponding to the measured concentrations, and at every section i the integrated concentration was approximated as $\overline{c_i}V_i$. Different assumptions

were made concerning the segment average concentration $\overline{c_i}$ upstream and downstream from Sandy Pt. Downstream the segments were defined by the location of the lateral transects; the concentrations measured at 2-ft intervals were averaged laterally and assumed to be uniform over depth. Upstream from Sandy Pt. the segments were defined by the vertical profile; concentrations were averaged over the depth and were assumed to be uniform laterally. Figures 29 and 30 show the sections for high and low slack respectively. V_d was then found by summing the mass from each segment and the flushing time was calculated using Equation (5.36).

Using this method the flushing time for the low slack data was 2.6 d, the flushing time for the high slack data was 3 d, and the mean was about 2.8 d.

5.8.2 Salinity

Vertical salinity profiles (Figure 34) at locations indicated in Figure 35 were taken at high tide on December 15. Salinity can be used as an alternative to dye for estimating flushing times of estuaries. If we designate the total river inflow rate by R and the total freshwater volume of the estuary by V_f the flushing time t according to Equations (2.18), (2.19) is given by

$$t = \frac{\int f V}{R} \tag{5.37}$$

where R is the discharge from Lattimer Brook.

R was determined from discharge rates for Pendleton Brook for the period November - December 1988 (Table 3). Using linear regression, the discharge rates of Lattimer Brook are related to the discharge rates of Pendleton Brook by (NUEL, personal communication):

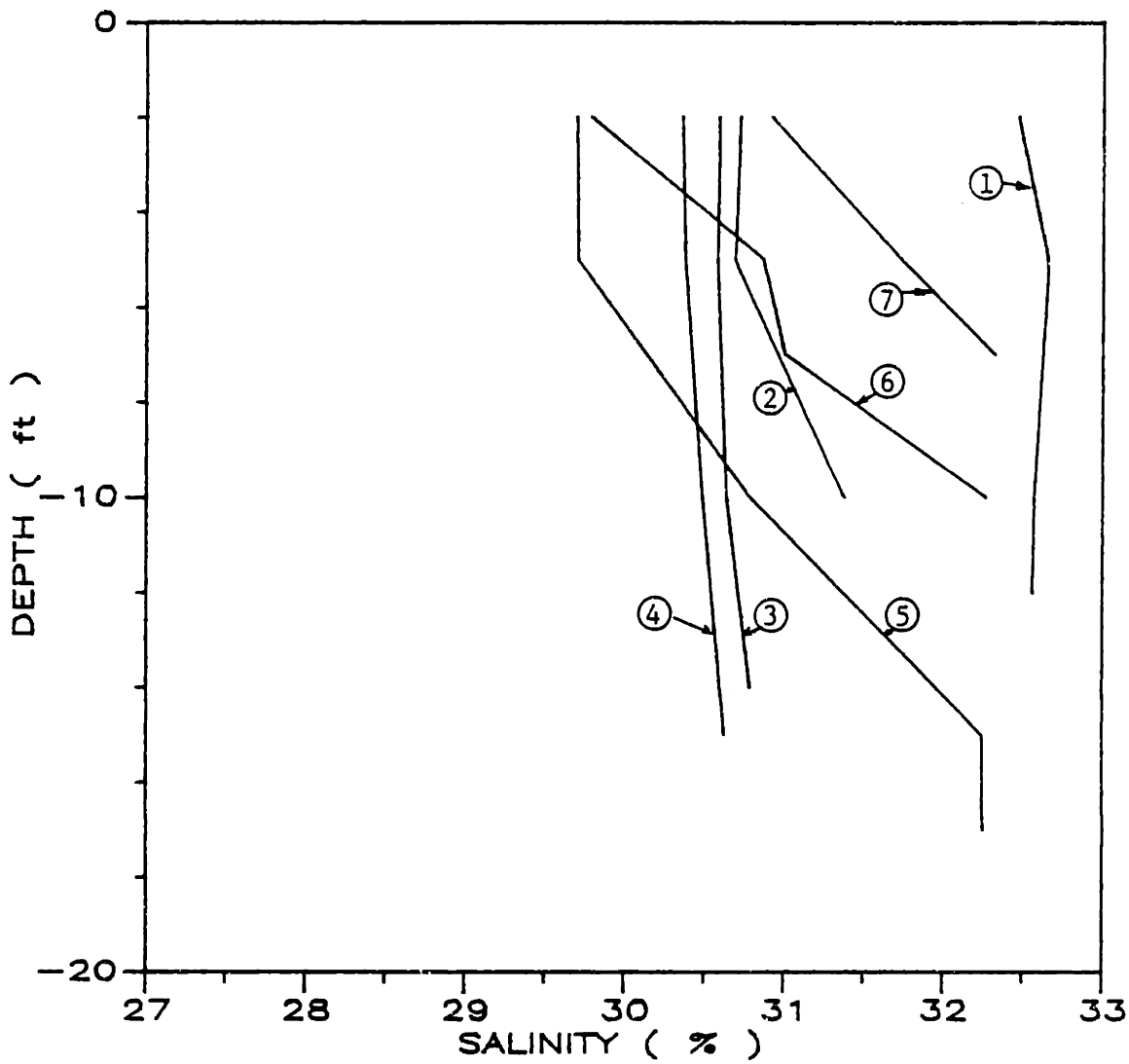

Figure 34 Vertical profiles of salinity at high slack on December 15, 1988

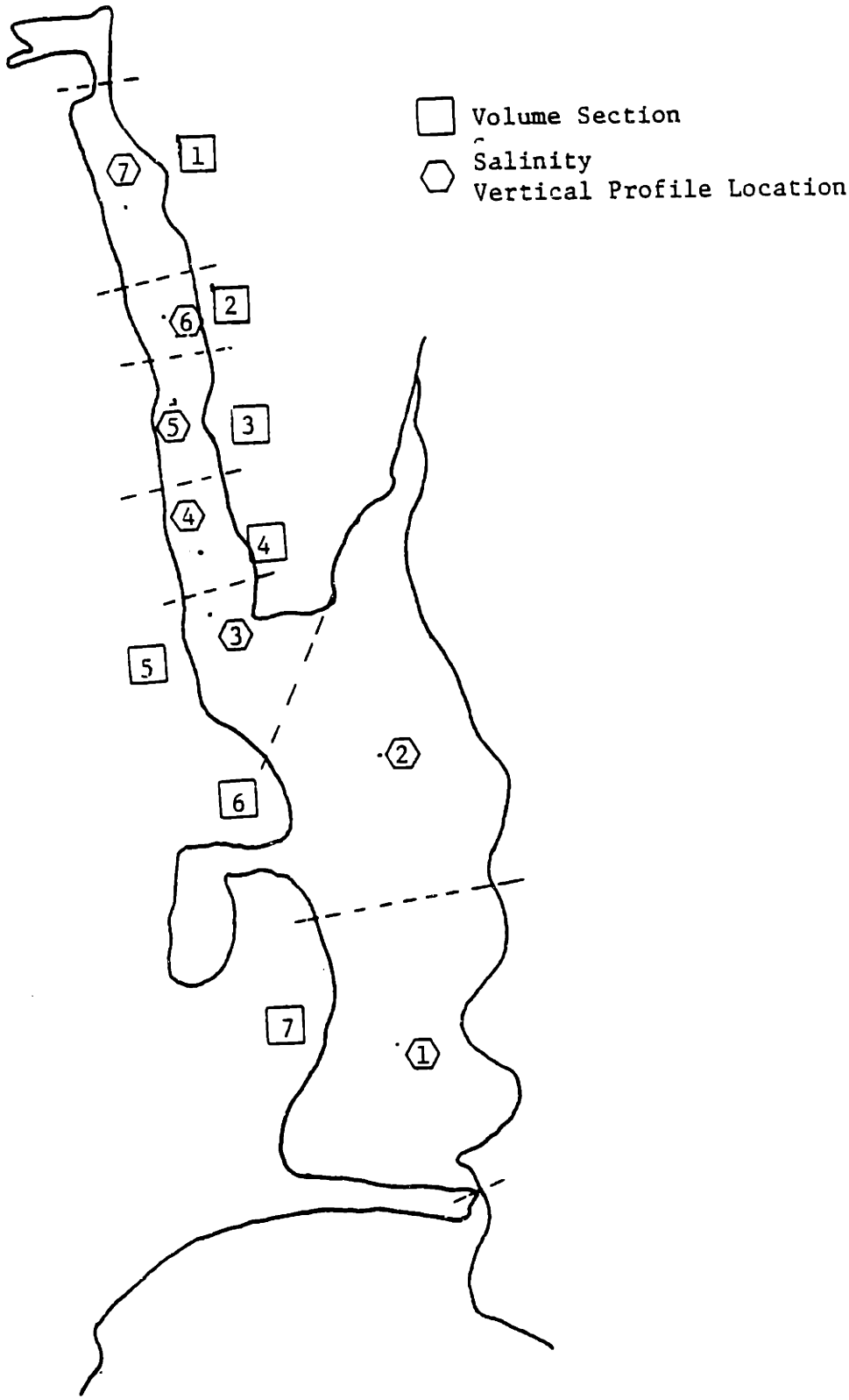

Figure 35 Locations of salinity measurements at high slack on December 15, 1988

Table 3

Flow Data for Latimer Brook

Date	Q Pendleton Brook (cfs)	Q Lattimer Brook (m^3/s)
12/1/88	18	1.53
12/2/88	15	1.27
12/3/88	13	1.11
12/4/88	12	1.02
12/5/88	11	0.94
12/6/88	9.9	0.85
12/7/88	9.6	0.82
12/8/88	9.1	0.78
12/9/88	8.4	0.72
12/10/88	7.7	0.67
12/11/88	7.0	0.61
12/12/88	5.9	0.52
12/13/88	5.9	0.52
12/14/88	12	1.02
12/15/88	11	0.94
12/16/88	8.7	0.75
12/17/88	7.1	0.62
12/18/88	6.2	0.54
12/19/88	5.8	0.51
12/20/88	5.7	0.50
12/21/88	5.8	0.51
12/22/88	5.8	0.51
12/23/88	5.8	0.51
12/24/88	5.8	0.51
12/25/88	5.8	0.51
12/26/88	5.9	0.52
12/27/88	6.0	0.52
12/28/88	6.0	0.52
12/29/88	6.0	0.52
12/30/88	6.0	0.52
12/31/88	6.1	0.53

$$CFS_{latimer} = 0.795 + 2.948 \cdot CFS_{pendleton} \quad (5.38)$$

The flushing time was calculated by dividing the estuary horizontally into seven sections (Figure 35) and the volume V_i of each section was calculated. At each section and depth, values of freshness were computed. The ocean salinity was taken as the salinity of Station 1 (Figure 34). Values at different depths were then averaged to determine a section-average freshness, f_i. The value of R was based on the flow averaged over n days preceding measured salinity. Table 4 shows the sensitivity of the flushing time on the value of n. We see that the values of the flushing time are between 3.9 d and 5.3 d which is a little higher than the flushing time of 2.8 d we get from Dye Study 1.

Flushing times were also determined from earlier salinity data at Stations A, B, C, and Niantic Bay for the period Feb.-April 1985, 86, 87, 88. Salinity data are given at surface, middepth, and bottom, although for some sections the middepth data are missing. The value of R was taken equal to the averaged flow over the week preceding measured salinity. In Table 5 the values of flushing times for different days are shown. We can see that the values of the flushing time are between 1.4 d and 4.5 d which is also consistent with the flushing time of 2.8 d that we get from Dye Study 1.

5.8.3 Comparison between Flushing Time Estimated from Tracer Studies and Model MILL

From Sections 5.8.1 and 5.8.2 we see that the observed flushing times using either dye or salinity are considerably smaller than the theoretical time based on Ketchum's model (and hence the time to which the model MILL has been calibrated). This may be due to vertical stratification, uneven bathymetry (resulting in tidal pumping), or other

Table 4

Sensitivity of Flushing Time on the Number of Days n Used to Average Flow

n (days)	flushing time (days)
1	4.1
2	3.9
3	4.7
5	5.2
6	5.3
7	5.2

Table 5

Flushing Times Using Salinity Data

date	discharge Pendelton Brook (cfs)	discharge R Latimer Brook ($10^3 m^3/d$)	flushing time (days)
21 Mar 85	10.79	79.8	4.4
28 Mar 85	6.87	51.5	3.7
4 Apr 85	7.79	58.1	4.5
12 Apr 85	6.21	46.8	2.1
18 Apr 85	4 39	37.2	5.9
6 Mar 86	8.53	63.5	1.4
20 Mar 86	29.14	21.2	1.5
3 Apr 86	10.17	75.3	3.2
14 Apr 86	8.67	66.6	1.8
24 Apr 86	6.55	49.2	4.5
12 Mar 87	15.14	111.2	1.9
26 Mar 87	7.37	55.1	3.7
7 Apr 87	50.14	363.6	3.0
16 Apr 87	21.00	153.4	2.4
3 Mar 88	9.03	67.1	3.6
17 Mar 88	8.4	62.6	3.6
11 Apr 88	10.81	79.9	3.5
21 Apr 88	6.67	50.1	4.5

effects that allow mixing to take place over distances larger than a theoretically computed tidal excursion. The effect is that the longitudinal dispersion coefficient D_{xx}, and hence the model mixing parameter β should be *increased* in order to match the observed flushing rates. All else equal, this would *decrease* the average time it takes for larvae to be entrained at the intake, leading to a greater discrepancy between the simulated and observed distribution of entrained larval length. As mentioned in Section 5.7.4 the majority (91.7%) of the larvae entrained according to the model simulation had a length between 3-4 mm while the data showed that only 12.4% of larvae entrained having a similar length. This discrepancy is discussed further in Section 5.9.

5.8.4 Dye Study 2

Dye Study 2 was conducted from January 11-17, 1989. The motivation for the second study was to better understand the residence time of larvae between the mouth of the Niantic River and the intake as well as to measure the percentage entrainment. In this regard, dye studies had been done in the past. Specifically Ocean Systems, Inc., conducted four dye experiments during June and July 1975 and a fifth study in March 1976. Figure 18 shows the locations of these studies. The purpose of these studies was to verify the previous concentration models by comparing the percentage of dye entrained to the percentage of larvae entrained.

During ebb tide (1300 to 1700 hrs) on January 11 307 lbs of 20% Rhodamine WT dye solution were injected in the vicinity of the NRRR Bridge (Figure 18). Fluorometers with strip chart recorders measured dye concentrations at the station quarry and at Mijoy. Concentration measurement started one day before the dye release (January 10, 11:20) and continued for 6.5 consecutive days (until January 15, 22:18). During this time the station experienced full operation from all three units.

The concentration of dye at the quarry as a function of time is shown in Figure 36. Time 0 corresponds to the time of the dye release. The background concentration was estimated from measerements on the day before the dye release. According to these data the background concentration changes as a function of the tidal cycle, and ranged from 0 to 0.18 ppb, with an average of 0.12 ppb. The percent of injected dye that passes through the intake is calculated as

$$\frac{Q_0 \int_0^{t_{end}} (c-c_b)dt}{M_0} \cdot \frac{10^{-6}kg}{m^3\text{-}ppb} \cdot 100\% \qquad (5.39)$$

where Q_0 the condenser flow rate = 118 m^3/s, c_b is the background concentration, t_{end} is the end of the survey (6.5 d), and M_0 is the mass of pure dye injected = 28 kg. Using our best estimate of c_b = 0.12 ppb, the percentage recovery is 20.6%. A sensitivity analysis was made in order to estimate the relationship between the background concentration and the amount of dye entrained. The results are shown in Table 6. It can be concluded from Table 6 that a variation in the background concentration between 5% and 15% results in a variation in the percentage of dye passing through the intake of between 25% and 15%.

The results of the second dye experiment were compared with Study No. 5 conducted by Ocean Systems, Inc., on March, 11 1976 (Ocean Systems, Inc., 1976). The earlier study involved 25.9 kg of pure dye discharged over 12.5 hours at the location shown in Figure 18. Concentrations were measured at Mijoy and the quarry for only three days after the dye release because of pump and power supply failures. Assuming a plant flow of 61 m^3/s (only two units were operating at that time) OSI calculated that 6.8% of the dye was entrained. Taking into account that: 1) three units were operating (118 m^3/s) during the second dye experiment and 2) concentrations at

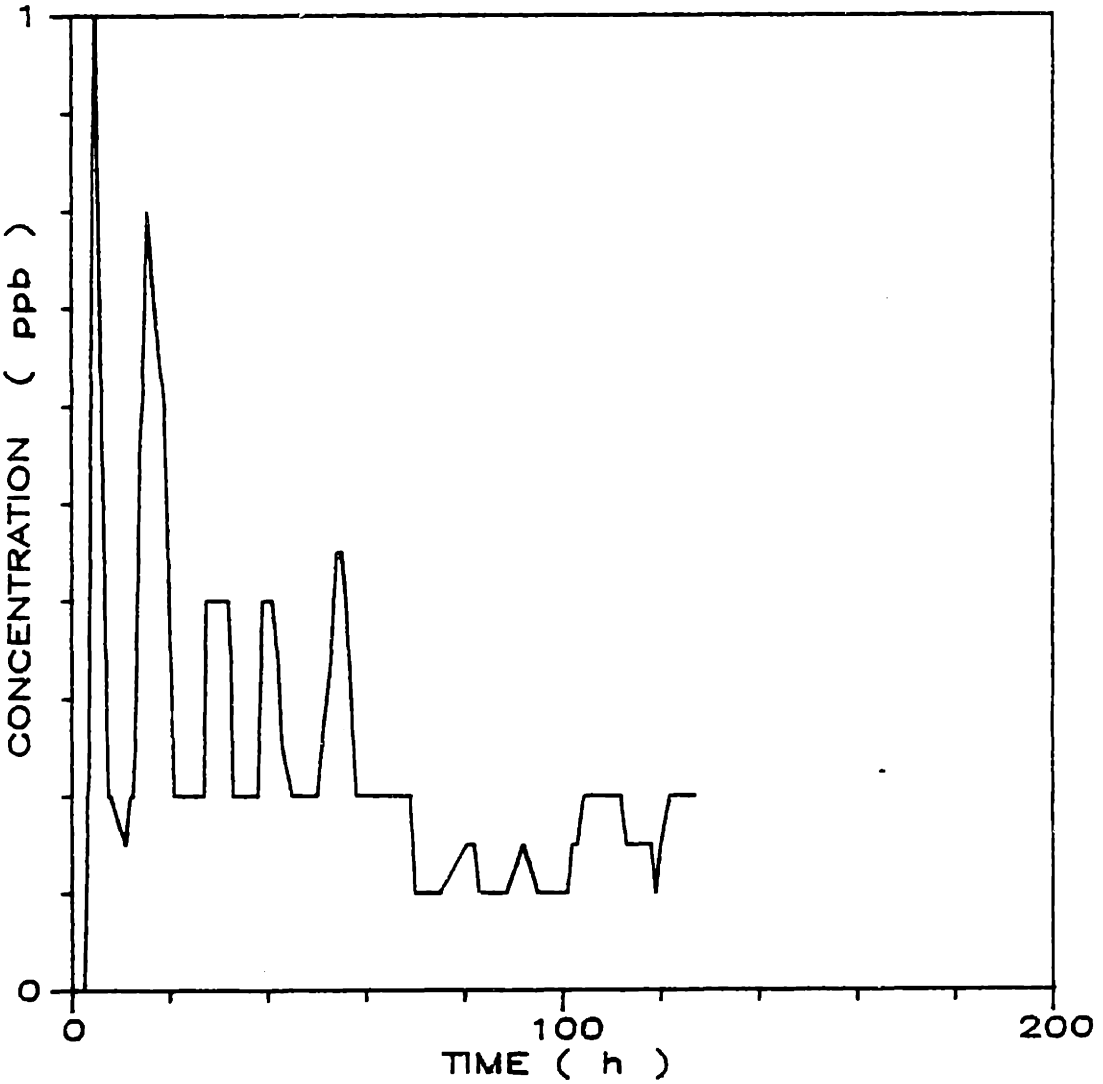

Figure 36 Dye concentration measurements at the Mijoy Quarry during Dye Study 2

Table 6

Sensitivity of Entrainment Percentage of Dye to Background Concentration

Background concentration	% of dye entrained
0.05	34.0
0.08	28.3
0.1	24.4
0.12	20.6
0.15	14.9

the quarry were measured for 6.5 days after the dye release, our estimate of between 34% and 15% entrainment seems reasonable.

5.9 Conclusions of Study

Mathematical model simulations have been performed to simulate the entrainment, at the Millstone Station, of larvae hatched within Niantic River. As discussed previously the simulations suggest that the larvae are arriving significantly earlier, and *in smaller numbers*, than indicated by observations at the intake. The first dye study suggests that the hydrodynamic flushing time is actually less than what was simulated so this does not provide an answer. The other two possibilities--discussed in Section 5.7.4--are that larval behavior has not been adequately taken into account and/or, larvae are being imported from outside Niantic River. These two hypotheses are discussed below.

5.9.1 Import Hypothesis

The import hypothesis is strongly supported by comparing the average total number of larvae born per year during the period 1984-87 to the average number of larvae entrained during the same period (NUEL Annual Report, 1988, p184).

According to the procedure described in Section 5.6.2 the average total number of larvae born per year during the period 1984-87 per 500 m^3 is about equal to 1500. By multiplying with the volume of Niantic River we find the total number of larvae born, i.e.,

$$1477 \text{ larvae}/500m^3 \times 5.58 \times 10^6 m^3 \simeq 20 \times 10^6 \text{ larvae born}$$

According to Table 13 of the NUEL Annual Report 1988 (p184) the average annual number of larvae entrained during the same period is equal to 98×10^6. This number by far exceeds the number of larvae born.

The import hypothesis is also supported by considering the following mass balance equation for larvae in the bay:

$$\frac{d}{dt}c_{bay} = (c_r - c_{bay})\frac{P}{\forall T} - kc_{bay} - \frac{Q_0 c_{bay}}{\forall} \pm s/s \qquad (5.40)$$

where

c_{bay} = density of larvae in bay

c_r = density of larvae in river

P = tidal prism volume of river

$\forall$ = volume of bay

T = tidal period

k = natural mortality rate

Q_0 = flow rate

s/s = source(+)/sink(-) for larvae from/to Long Island Sound

The s/s term has been calculated as the residual term needed to close Equation (5.40) using data provided by NUEL for the remaining terms. Appendix B shows calculations for 1987. It is clearly seen that for late times s becomes a source term. For earlier times s is a sink term. A reasonable explanation for this is that at early times the entrained larvae come from the river. As seen, entrainment begins as soon as spawning starts, which is consistent with the approximate three-day residence time. At later times s becomes a source term which may mean that larvae are imported. A problem that appears in this interpretation is the very large number of larvae entrained during the first forty days after beginning of spawning in 1988.

5.9.2 Hypothesis Explaining Flushing Time Differences

Table 7 shows dates of peak abundance of winter flounder larvae for the years 1983-1988 at the three Niantic River Stations (A, B, and C) and for Niantic Bay. These peak abundances suggest the following average residence times

between Station A and B	5.7 d
between Station B and C	14.5 d
between Station C and Niantic Bay	24.5 d

According to this the average residence time of larvae in Niantic River is equal to 45 d which is about fifteen times bigger than the flushing time of the estuary obtained from the dye study and about three times as large as the time simulated in the model (15 d). The facts that more larvae were entrained than would be expected based on hatching rates, plus the considerably larger residence time of larvae relative to dye, could both be explained if it were determined that the younger as well as the older larvae were found predominantly near the bottom, where they might be undersampled and transported more slowly than dissolved dye.

Table 7

Peak Abundances of Winter Flounder Larvae
(from NUEL, personal communication)

Estimated dates of peak abundance of winter flounder larvae at the three Niantic River stations (A, B, and C) and for Niantic Bay (entrainmenat and mid-Niantic Bay combined).

Year	Sta A	Sta B	Sta C	Niantic Bay
1983	Mar 6	Mar 20	Apr 9	Apr 17
1984	Mar 4	Mar 12	Apr 4	Apr 22
1985	Mar 9	Mar 14	Mar 19	Apr 12
1986	Feb 26	Feb 28	Apr 1	Apr 23
1987	Mar 8	Mar 9	Mar 17	Apr 17
1988	Feb 29	Mar 5	Mar 5	Apr 18

6 SUMMARY AND CONCLUSIONS

Mixing in estuaries is a very complicated phenomenon because of the various mechanisms causing mixing (i.e., wind, tide, internal density variations caused by the river) and the complicated character of each of these mixing mechanisms.

Various models have been used for modeling mixing in estuaries. In our model we use a mixing length approach. According to the mixing length theory mass transport in estuaries can be modeled using a locally one-dimensional model, where all mixing mechanisms are combined into a single longitudinal dispersion coefficient D_x. The main assumption in this theory is that complete mixing is achieved on one tidal cycle over a fraction of the maximum tidal excursion. According to this D_x is given by the expression

$$D_x = \beta u_0^2 \tag{6.1}$$

where

β is a constant

u_0 is the amplitude of the tidal velocity.

The two-dimensional depth-averaged mass transport equation for a conservative substance is given by the expression

$$\frac{\partial(ch)}{\partial t} + \frac{\partial(uch)}{\partial x} + \frac{\partial(vch)}{\partial y} = \frac{\partial}{\partial x}\left[hD_{xx}\frac{\partial c}{\partial x}\right] + \frac{\partial}{\partial y}\left[hD_{yy}\frac{\partial c}{\partial y}\right] \tag{6.2}$$

where

c(x,y,t) is the depth-averaged concentration

u(x,y,t) is the x component of the depth-averaged velocity

$v(x,y,t)$ is the y component of the depth-averaged velocity

$h(x,y)$ is the depth (mean sea level)

D_{xx}, D_{yy} are dispersion coefficients

In an estuary transport model D_{xx} and D_{yy} are chosen so that they are consistent with Equation (6.1)

In a "random walk" model the transported mass m of the conservative substance is represented by N particles. The position $\underline{x}(t)$ of each particle is described by the nonlinear Langevin equation

$$\frac{d\underline{x}}{dt} = \underline{A}(x,t) + \underline{\underline{B}}(x,t)\xi(t) \tag{6.3}$$

where

$\underline{A}(x,t)$ is a known vector representing the deterministic forces that act to change $x(t)$

$\underline{\underline{B}}(x,t)$ is a known tensor that characterizes the random forces

$\xi(t)$ is a random number that represents the microscopic rapidly changing forces that act to change $x(t)$

In our analysis we defined $\underline{A}(x,t)$, $\underline{\underline{B}}(x,t)$, and $\xi(t)$ as functions of u, v, D_{xx}, and D_{yy} so that Equations (6.2) and (6.3) are equivalent:

$$\underline{A} = \begin{bmatrix} \frac{D_{xx}}{h}\frac{\partial h}{\partial x} + \frac{\partial D_{xx}}{\partial x} + u \\ \\ \frac{D_{yy}}{h}\frac{\partial h}{\partial y} + \frac{\partial D_{yy}}{\partial y} + v \end{bmatrix} \qquad \underline{\underline{B}} = \begin{bmatrix} \sqrt{2}\sqrt{D_{xx}} & 0 \\ 0 & \sqrt{2}\sqrt{D_{yy}} \end{bmatrix} \tag{6.4}$$

The random walk model was tested by comparing simulated concentrations and residence times with corresponding analytical solutions for the one-dimensional case of

Equation (6.2) ($v = 0$, $D_{yy} = 0$, h = constant). Excellent agreement was obtained. The following conclusons were drawn:

- As the timestep Δt becomes smaller the concentration distribution curve becomes smoother and resembles in shape the analytical solution. Also the flushing time that results from the integration of the concentration distribution approaches the flushing time resulting from the analytical solution.

- The important factor governing accuracy of the concentration distribution is the number of particles per "cell" or $N_t l_s/u$ where N_t is the number of particles released per time, l_s is the length over which concentration is measured or "cell" length, and u is the advection velocity.

The model was applied to the Millstone Point Case Study in order to predict winter flounder larvae entrainment rates.

It was calibrated using Ketchum's tidal mixing model. Verification of the model was attempted by comparing the length distribution of the larvae entrained resulting from the model simulation to the length distribution data of the larvae entrained provided by the NUEL. In order to explain the early entrainment times and the lower number of entrained larvae predicted by the model three possibilities were examined. The first possibility was that the underestimation of the river flushing time was due to the assumption of estuary mixing in Ketchum's model. In order to investigate this possibility two dye studies were conducted and salinity data were measured along the river. These studies showed that the river flushing time is even less than predicted by the model. The second possibility was that the data concerning larvae abundances and behavior are not correct, which means that either larvae are imported from other parts of the bay or larvae stay longer in the bottom of the estuary. The latter might result in

underestimation of the larvae sampled and higher residence time of the larvae in the river. The third possibility was an overestimation of the mortality rate which would have as result a shift of the length distribution of the entrained larvae to smaller lengths. By setting the mortality rate to zero we concluded that the third possibility does not explain alone the observed inconsistencies but it could be part of the answer.

The main advantages in using a particle model as developed for this study are the representation of sources and sinks and the simulation of larvae behavior. However, two problems were encountered. First, particles had to be reflected several times because of the large lateral random walk displacements close to the mouth of the estuary. A remedy for this is to use small timesteps or use higher-order integration schemes, but these increase the computational effort. A second problem was the number of particles necessary to simulate the behavior. Only one particle per timestep was released. An increase in the number of particles or a repetition of the same simulation, in order to obtain an ensemble average, increases linearly the computational effort so it was avoided.

A useful task for further research would be a comparison, in terms of accuracy and efficiency, between our particle model and an equivalent concentration model.

7 REFERENCES

Ackerer, Ph., and W. Kinzelbach. 1985. Modelisation du transport de contaminant par la methode de march au hasard: Influence des variations de champ d'ecoulement au cours de temps sur la dispersion. Internatinal Symposium on the Stochastic Approach to Subsurface Flow, Proceedings, Montrillargenne, France.

Ahlstrom, S. W., H. P. Foote, R. C. Arnett, C. R. Cole, R. J. Serne. 1977. Multicomponent mass transport model: Theory and numerical implementation. Report BNWL 2127, Battelle, Pacific Northwest Laboratories, Richland, Wash.

Arons, A. B., H. Stommel. 1951. A mixing length theory of tidal flushing. *Transactions of the American Geophysical Union* 32:419-421.

Baptista, A. M. 1987. Solution of advection dominated transport by Eulerian-Lagrangian methods using the backwards method of characteristics. Ph.D. Thesis, Department of Civil Engineering, MIT.

Bowden, K. F. 1967b. Stability effects on mixing in tidal currents. *Phys. Fluids Suppl.* 10:5278-5280.

Bugliarello, G., E. D. Jackson III. 1964. Random walk study of connective diffusion. *Journal of Engineering Mechanics Division, ASCE* 90(Em4):49-77.

Cameron, W. M., D. W. Pritchard. 1965. Estuaries. In *The sea*, Vol. 2, 306-324. New York: John Wiley.

Chorin, A. J. 1973. *Journal of Fluid Mechanics* 57(4):785.

Csanady, G. T. 1972. *Turbulent diffusion in the environment.* D. Reidel Publ.

Dyer, K. R., P. A. Taylor. 1973. A simple segmented prism model of tidal mixing in well mixed estuaries. *Estuarine and Coastal Marine Science* 1:411-418.

Fischer, H. B, et al. 1979. *Mixing in inland and coastal waters.* Academic Press.

Gardiner, C. W. 1985. *Handbook of stochastic methods for physics, chemistry and the natural sciences*, second ed. Springer Verlag

Hansen, D. V., M. Rattray. 1966. New dimensions in estuary classification. *Limnology and Oceanography* 11:319-326.

Jeng, S. W. 1986. Two-dimensional random walk model for pollutant transport in natural rivers. Ph.D. thesis, The University of Texas at Austin.

Ketchum, B. H. 1950. Hydrographic factors involved in the dispersion of pollutants introduced into tidal waters. *J. Boston Soc. Civil Eng.* 37:296-314.

Ketchum, B. H. 1951. The exchange of fresh and salt waters in tidal estuaries. *J. Mar. Res.* 10:18-37.

Ketchum, B. H. 1951a. The flushing of tidal estuaries. *Sewage and Industrial Wastes* 23:198-209.

Kollmeyer, R. C. 1977. A study of the Niantic River estuary, Niantic, Connecticut. U.S. Coast Guard Academy, New London, Connecticut. Report No. RDCGA 18.

Konikow, L. F., J. D. Bredehoft. 1978. *Computer model of two-dimensional solute transport and dispersion in groundwater.* Book 7, Ch. 2, U.S. Geological Survey

Kossik, R. F., et al. 1987. Users' manual for ELA, a two-dimensional Eulerian-Lagrangian transport model. MIT.

Neuman, S. P. 1981. An Eulerian-Lagrangian Scheme for the dispersion-convection equation using conjugate space-time grids. *Journal of Comp. Physics* 41:270-279.

NUEL. 1988. Monitoring the marine environment of Long Island Sound at Millstone Nuclear Power Station. NUEL, Waterford, Conn.

NUEL. 1988-89. Personal communications.

Officer, C. B. 1976. *Physical oceanography of estuaries.* John Wiley and Sons.

Pinder, G. F., H. H. Cooper. 1970. A numerical technique for calculating the transient position of the salt water front. *Wat. Resources Res.* 6(3):875.

Press, W. H., et al. 1986. *Numerical recipes.* Cambridge Univ. Press.

Prickett, T. A., T. C. Naymick, C. G. Lomquist. 1981. Random walk solute transport model for selected groundwater quality evaluations. Illinois State Water Survey Bulletin 65, Champaign, Ill.

Pritchard, D. W. 1967. Observations of circulation in coastal plain estuaries. In *Estuaries*, G. H. Lauff, ed., 37-44. AAAS Publ. No. 83, Washington.

Rattray, M., D. V. Hansen. 1962. A similarity solution of circulation in an estuary. *Journal of Marine Research* 20:121-133.

Saila, S. B. 1976. Effects of power plant entrainment on winter flounder populations near Millstone Point. URI-NUSCO Rep. No. 5.

Stommel, H., H. G. Farmer. 1952. *On the nature of estuarine circulation.* Reference Nos. 52-51, 52-63, 52-88 (3 vols. containing chs. 1-4 and 7). Woods Hole Oceanographic Institution.

Sullivan, P. J. 1971. Longitudinal dispersion within a two-dimensional shear flow. *Journal of Fluid Mechanics.* 49:551-576.

Tompson, A. F. b., E. G. Vomvoris, L. W. Gelhar. 1988. Numerical simulation of solute transport in randomly heterogeneous porous media: Motivation, model development and application. Report No. MIT-316.

Uffink, G. 1987. Modeling of solute transport with the random walk method. NATO Advanced Workshop on Advances in Analytical and Numerical Groundwater Flow and Quality Modeling. Lisbon, Portugal, June 2-6, 1987.

Wang, X., M. L. Spaulding. 1985. A tidal prism flushing model of Narragansett Bay. Dept. of Ocean Engineerng, University of Rhode Island.

Westerink, J. J., et al. 1984. TEA: A linear frequency domain finite element model for tidal embayment analysis. Energy Laboratory Report No. MIT-EL 84-012.

APPENDIX A

Derivation of Displacement Equation for a 2-D Depth Averaged Random Walk Model

In order to find the random walk algorithm

$$d\underline{x} = \underline{A}(\underline{x}(t),t) + \underline{\underline{B}}(x(t),t)\cdot d\underline{W}(t) \tag{A.1}$$

that corresponds to the two-dimensional depth-averaged transport equation

$$\frac{\partial(ch)}{\partial t} + \frac{\partial(uch)}{\partial x} + \frac{\partial(vch)}{\partial y} = \frac{\partial}{\partial x}\left[hD_{xx}\frac{\partial c}{\partial x}\right] + \frac{\partial}{\partial y}\left[hD_{yy}\frac{\partial c}{\partial y}\right] \tag{A.2}$$

where

$\underline{x} = \begin{bmatrix} x \\ y \end{bmatrix}$

represents the displacements in the x and y direction

$\underline{A} = \begin{bmatrix} a_x \\ a_y \end{bmatrix}$

and $\underline{\underline{B}}$ is a diagonal tensor

$\underline{\underline{B}} = \begin{bmatrix} b_x & 0 \\ 0 & b_y \end{bmatrix}$

we must find the coefficients of $\underline{A}$ and $\underline{\underline{B}}$ so that Equation (A.2) is equivalent to the Fokker-Planck equation (see Figure 8, Section 3.3.1)

$$\frac{\partial f}{\partial t} + \frac{\partial}{\partial x}(a_x f) + \frac{\partial}{\partial y}(a_y f) = \frac{\partial^2(\frac{1}{2}b_x^2)}{\partial x^2} + \frac{\partial^2(\frac{1}{2}b_y^2)}{\partial y^2} \tag{A.3}$$

In order to do that we follow this procedure: we set $f = ch$, transform Equations (A.2) and (A.3) using integrations by parts and then set equal the coefficients of c, $\frac{\partial c}{\partial x}$, $\frac{\partial c}{\partial y}$, $\frac{\partial^2 c}{\partial x^2}$, and $\frac{\partial^2 c}{\partial y^2}$. We see that we have to determine four coefficients, a_x, a_y, b_x, b_y, using five equations.

From Equation (A.3) we get

$$\frac{\partial ch}{\partial t} = c\left[\left[\frac{\partial b_x}{\partial x}\right]^2 h + \frac{\partial^2 b_x}{\partial x^2} b_x h + 2b_x \frac{\partial b_x}{\partial x}\frac{\partial h}{\partial x} + \frac{b_x^2}{2}\frac{\partial^2 h}{\partial x^2} - \frac{\partial a_x}{\partial x} h - a\frac{\partial h}{\partial x}\right.$$
$$\left. + \left[\frac{\partial b_y}{\partial y}\right]^2 h + \frac{\partial^2 b_y}{\partial y^2} b_y h + 2b_y \frac{\partial b_y}{\partial y}\frac{\partial h}{\partial y} + \frac{b_y^2}{2}\frac{\partial^2 h}{\partial y^2} - \frac{\partial a_y}{\partial y} h - a\frac{\partial h}{\partial y}\right]$$
$$+ \frac{\partial c}{\partial x}\left[2b_x \frac{\partial b_x}{\partial x} h + b_x^2 \frac{\partial h}{\partial x} - a_x h\right]$$
$$+ \frac{\partial c}{\partial y}\left[2b_y \frac{\partial b_y}{\partial y} h + b_y^2 \frac{\partial h}{\partial y} - a_y h\right]$$
$$+ \frac{\partial^2 c}{\partial x^2}\left[\frac{b_x^2}{2} h\right] + \frac{\partial^2 c}{\partial y^2}\left[\frac{b_y^2}{2} h\right] \qquad (A.4)$$

From Equation (A.2) we get

$$\frac{\partial (ch)}{\partial t} = c\left[-\frac{\partial u}{\partial x} h - u\frac{\partial h}{\partial x} - \frac{\partial v}{\partial y} h - v\frac{\partial h}{\partial y}\right]$$
$$+ \frac{\partial c}{\partial x}\left[\frac{\partial D_{xx}}{\partial x} h + D_{xx}\frac{\partial h}{\partial x} - uh\right]$$
$$+ \frac{\partial c}{\partial y}\left[\frac{\partial D_{yy}}{\partial y} h + D_{yy}\frac{\partial h}{\partial y} - vh\right]$$
$$+ \frac{\partial^2 c}{\partial x^2}[D_{xx} h] + \frac{\partial^2 c}{\partial y^2}[D_{yy} h] \qquad (A.5)$$

By setting the coefficients of c, $\frac{\partial c}{\partial x}$, $\frac{\partial c}{\partial y}$, $\frac{\partial^2 c}{\partial x^2}$, $\frac{\partial^2 c}{\partial y^2}$ in Equations (A.4) and (A.5) we get

$$b_x = \sqrt{2D_{xx}}$$
$$b_y = \sqrt{2D_{yy}}$$
$$a_x = D_{xx}\frac{h_x}{h} + D_x^{xx} + u$$
$$a_y = D_{yy}\frac{h_y}{h} + D_y^{yy} + v$$

APPENDIX B

Calculation of Source/Sink Term in Equation (5.40) (NUEL, personal communication)

1987

YEAR	GROUP	CNB_I	CNB_IO	CNB	CNR	P	V	T	K	Q	CHANGE	FROMNR	TONR	MORTAL	ENTRAIN	SINK
87	0	0.000	0.000	0.000	441.84	5000	100000	0.516667	0.0470568	20338.6	0.000	427.59	0.000	0.000	0.000	-427.6
87	1	0.000	0.000	0.000	827.71	5000	100000	0.516667	0.0470568	20338.6	0.000	801.01	0.000	0.000	0.000	-801.0
87	2	0.000	0.180	0.033	1054.50	5000	100000	0.516667	0.0470568	20338.6	0.180	1020.49	0.032	0.015	0.067	-1020.2
87	3	0.359	22.671	7.202	1045.54	5000	100000	0.516667	0.0470568	20338.6	22.312	1011.81	6.970	3.389	14.640	-964.5
87	4	30.185	149.708	84.917	881.99	5000	100000	0.516667	0.0470568	20338.6	119.523	853.53	82.178	39.959	172.709	-439.2
87	5	164.722	245.649	213.927	670.83	5000	100000	0.516667	0.0470568	20338.6	80.927	649.19	207.026	100.667	435.097	174.5
87	6	247.008	208.858	233.297	477.59	5000	100000	0.516667	0.0470568	20338.6	-38.150	462.19	225.771	109.782	474.493	309.7
87	7	201.271	130.186	165.402	326.00	5000	100000	0.516667	0.0470568	20338.6	-71.085	315.49	160.066	77.839	336.403	187.7
87	8	122.963	70.084	94.864	216.65	5000	100000	0.516667	0.0470568	20338.6	-52.879	209.66	91.604	44.640	192.940	66.8
87	9	65.571	35.206	49.128	141.55	5000	100000	0.516667	0.0470568	20338.6	-30.365	136.98	47.544	23.118	99.920	3.2
87	10	32.792	17.117	24.235	91.49	5000	100000	0.516667	0.0470568	20339.6	-15.675	88.54	23.453	11.404	49.290	-20.1
87	11	15.909	8.194	11.682	58.73	5000	100000	0.516667	0.0470568	20338.6	-7.715	56.83	11.305	5.497	23.760	-24.0
87	12	7.609	3.895	5.570	37.53	5000	100000	0.516667	0.0470568	20338.6	-3.714	30.32	5.391	2.621	11.329	-20.7